Journal of Materials Chemistry A

REVIEW

View Article Online
View Journal | View Issue

Cite this: J. Mater. Chem. A, 2025, 13, 40448

A review on copper-based chalcogenide materials for supercapacitor application: exploring through experimental evidence and machine learning

M. Mohan Ram,[a] R. Sapna,[b] Sachin R. Rondiya *[c] and K. Hareesh *[a]

To unlock the full potential of supercapacitors, it is essential to explore novel materials with tuneable electrochemical properties. Transition metal chalcogenides, in particular copper chalcogenides, have shown immense potential to achieve a next-generation electrode material. This review aims to explore copper-based chalcogenides as promising candidates, highlighting their rich redox activity, high intrinsic conductivity, and structural tunability. We also discuss how variations in morphology, doping effects, and the formation of composites significantly influence electrochemical performance. Along with that the hybridisation of other metallic elements into binary copper chalcogenides, which significantly enhanced conductivity, stability, and redox activity, is addressed. Furthermore, we briefly address few engineering strategies used to amplify the electrochemical performance of copper chalcogenide-based supercapacitors. This review also evaluates the practical applicability of the chalcogenides in a real-world scenario based on the current literature. In addition, it briefly discusses the emerging use of machine learning approaches to predict the electrochemical performance of copper chalcogenide-based systems. Finally, the key challenges associated with scalability, long-term cycling stability, and environmental impact are examined, alongside perspectives for future research directions aimed at overcoming these limitations.

Received 10th June 2025
Accepted 15th September 2025

DOI: 10.1039/d5ta04689k

rsc.li/materials-a

1. Introduction

The progress in science and technology in this modern era has reached new heights day by day. This rapid growth in technology, along with the increase in population, prompted the escalated energy utilisation. The emerging technology-integrated modern life has increased the demand for various forms of energy consumption. It is evident that, along with

[a]Department of Physics, Manipal Institute of Technology Bengaluru, Manipal Academy of Higher Education, Manipal 576104, India. E-mail: hareesh.k@manipal.edu
[b]Manipal Institute of Technology Bengaluru, Manipal Academy of Higher Education, Manipal 576104, India
[c]Department of Materials Engineering, Indian Institute of Science, Bengaluru 560012, India. E-mail: rondiya@iisc.ac.in

M. Mohan Ram

Mr Mohan Ram M. received his BSc in Physics from Sri Ramakrishna Mission Vidyalaya College of Arts and Science, India, in 2021 and MSc in Physics from Manipal Academy of Higher Education, India, in 2023. He is currently pursuing his PhD in Physics, Manipal Institute of Technology Bengaluru, Manipal Academy of Higher Education, Manipal, India. His research interests include 2D chalcogenide-based electrode materials for supercapacitor and energy storage applications.

R. Sapna

Dr Sapna R. is an Assistant Professor in the Department of Information Technology, Manipal Institute of Technology Bengaluru, Manipal Academy of Higher Education, Manipal, India. She got her PhD from Visvesvaraya Technological University. Her areas of interest include semantic web, machine learning, IoT, cloud computing and green computing. She has around 8 years of teaching experience. She has published many papers in international journals and international conferences.

technological advancements, the consumption of different forms of energy has evolved with time. Electricity is the core source of energy for all the technologically advanced systems. Therefore, it has become a necessity in this modern era. Currently, the generation of electricity is still dependent on conventional sources such as coal and fossil fuel. Nevertheless, the exhaustion of these non-renewable energy sources, along with growing ecological concerns, calls for the shift to renewable energy sources.[1–3] Thus, the advancement of the sustainability of renewable energy sources is just as crucial to the cutting-edge energy storage systems.[4] Among the energy storage systems, batteries and supercapacitors (SCs) have become prominent electrochemical energy storage devices as a result of their effective energy storage and delivery.[5] Fig. 1 displays the Ragone plot of various energy storage systems. The Ragone plot is intended to assess the performance of various energy storage systems such as fuel cells, batteries, capacitors and supercapacitors by plotting their energy density *versus* power density. This plot simplifies the process of selecting the most suitable device for the desired application based on the requirements of energy density and power density.

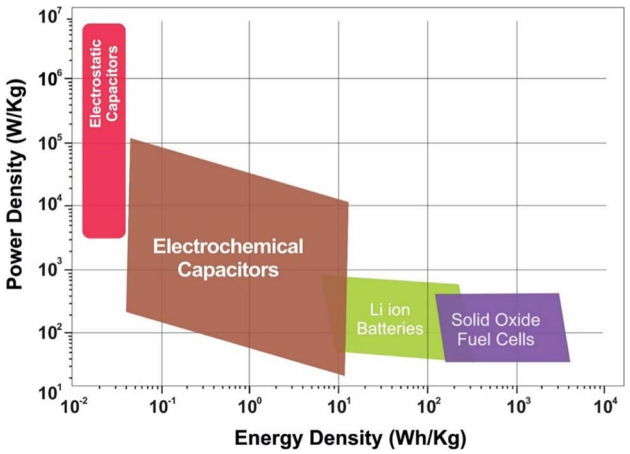

Fig. 1 Ragone plot comparing various energy storage systems. Reproduced with permission[5] copyright 2018, Elsevier.

In comparison with batteries, supercapacitors provide superior performance in numerous ways, including high power density, high stability, fast charging and discharging, and superior safety. This makes them suitable for particular applications that demand a quick energy burst, including regenerative brake systems in electric vehicles and power backup systems.[6] Based on their charge storage mechanism, supercapacitors can be broadly categorised into three types: electric double-layer capacitors (EDLCs),[7] pseudocapacitors (PCs),[8] and hybrid capacitors (HCs).[9] SC performance can be highly influenced by the choice of electrode materials, which determines the device's redox activity, energy and power density. Among the various electrode materials, carbon-based materials, conducting polymers, and transition metal oxides have received significant interest due to their high surface area, flexibility and rich redox activity. These materials are well studied, and a few of them are already commercialised.[10] Even though these materials exhibit good performance, they still face significant challenges such as limited energy density, low charge storage capacity and structural degradation over prolonged usage.[11]

To overcome these challenges, research has been shifted towards transition metal chalcogenides (TMCs). TMCs are gaining due to their inherent outstanding electron mobility, rich redox activity, and improved structural integrity. These characteristics make them the most suitable candidates for high-performance supercapacitor electrodes.[12] TMCs are a class of materials composed of transition metal atoms and chalcogen atoms (S, Se and Te). Based on the chalcogen element, TMCs can be differentiated into three main groups: metal sulphides, metal selenides, and metal tellurides. Each material possesses

Sachin R. Rondiya

Dr Sachin R. Rondiya is the principal investigator of the "Energy Materials and Devices" research group in the Department of Materials Engineering at the Indian Institute of Science, Bengaluru. He joined IISc as an Assistant Professor in 2022. From 2018 to 2022, he was a Postdoctoral Fellow at School of Chemistry, Cardiff University, UK, and Department of Materials, Imperial College London. At IISc, Dr Rondiya's group develops organic and inorganic semiconductors, focusing on chalcogenides and two-dimensional perovskites, covering fundamental studies using advanced spectroscopic and microscopic tools through to prototype development for energy storage and optoelectronic applications.

K. Hareesh

Dr Hareesh K. received his PhD (2014) from Mangalore University, India, followed by Post-Doctoral Fellowship (2013–2017) from Savitribai Phule Pune University, India, and University of Western Australia, Australia. Currently, he is an Assistant Professor–Senior Scale in Physics in the Department of Physics, Manipal Institute of Technology Bengaluru, Manipal Academy of Higher Education, Manipal, India. His research interest includes the applications of 2D materials to sensors, field emission, supercapacitors, hydrogen production and photovoltaic applications.

its unique edges and shortcomings that modulate the supercapacitor's performance.

In the family of transition metal chalcogenides such as MoS_2, WS_2, CoS, and $NiSe_2$, copper chalcogenides have gained specific interest because of their unique intrinsic properties. The high electrical conductivity is attributed to the mixed valency of Cu and its band structure that favours rapid charge transfer. Its multiple oxidation states (Cu^+/Cu^{2+}) offer active sites for fast, reversible redox reactions, favouring the pseudo capacitance mechanism for high specific capacitance. The crystal structure and morphology of copper chalcogenides are highly tunable compared to the other TMCs, allowing for both the optimisation of ion transport channels and accessibility of electrochemically active sites, including the improvement of the mechanical stability over charge–discharge cycles. Along with these properties, their abundance, lower toxicity and ease of synthesis make them strong contenders for a high-performing electrode material for a supercapacitor application.[13,14]

Copper chalcogenides are classified into three main groups based on the chalcogen atoms: copper sulphides (CuS), copper selenides (CuSe) and copper tellurides (CuTe). Copper chalcogenides consist of various phases from stoichiometry to nonstoichiometry. The comparison of various phases of copper chalcogenides (CuX (X = S, Se, and Te)) is displayed in Table 1. Among the various phases, main crystal phases such as CuS, CuSe and CuTe exhibit a layered structure, which facilitates the rapid intercalation of ions and results in rapid charge transport. Various non-stoichiometric copper chalcogenides such as $Cu_{2-x}S$, $Cu_{2-x}Se$ and $Cu_{2-x}Te$ hold rich copper vacancies, resulting in the growth of complex crystal structures with mixed valence states and defects. Intrinsic properties such as electrical conductivity, charge carrier concentration and ion diffusion rates are directly related to the phase and crystal structure. This phase diversity enables tailoring the properties of the materials by varying the copper content. The crystal structures of three major copper chalcogenide phases are displayed in Fig. 2. The crystallographic data for Fig. 2 were obtained from the Materials Project database[23] and visualised using the VESTA software.[24]

When we notice the crystal structure of major copper chalcogenide phases, the structure of CuTe is entirely different from those of CuS and CuSe due to the primary factors: atomic size, bonding effect, electronegativity, electronic structure, orbital hybridisation, crystal field effect and thermodynamic stability. Compared to sulphur (100 pm) and selenium (115 pm), the atomic radius of tellurium (140 pm) is significantly larger. Along with that, the electronegativity differs significantly between S (2.58), Se (2.55) and Te (2.1), which plays a crucial role by creating different charge distributions and bonding covalencies in CuTe, making it more ionic than CuS and CuSe.[25,26] This atomic size and electronegativity fundamentally influence the bonding geometry; the vulcanite CuTe structure consists of $CuTe_4$ tetrahedra and two distinct anisotropic Cu–Te bonds.

Table 1 Comparison of various copper chalcogenide crystal phases and their key properties

Copper chalcogenide	Phase type	Crystal structure	Key properties	Ref.
CuS	CuS (covellite)	Hexagonal	Common phase; high conductivity due to high hole density, layered structure promotes fast ion intercalation	15 and 16
	Cu_2S (chalcocite)	Monoclinic	Good electronic mobility, stability	
	$Cu_{1.8}S$ (digenite)	Cubic	Electronic tuning, high pseudocapacitive redox activity	
	$Cu_{2-x}S$ (non-stoichiometric)	Monoclinic, orthorhombic, triclinic	Defect rich phase which enhances charge storage	
CuSe	CuSe (klockmannite)	Hexagonal	High intrinsic conductivity, layered lattice facilitates ion diffusion	15 and 17–19
	Cu_2Se (berzelianite)	Cubic (high T), orthorhombic (low T)	High electronic conductivity, structural disorder facilitates rapid ion transport	
	Cu_3Se_2 (umangite)	Tetragonal	Unique layered motifs enhance electrochemical reversibility	
	$Cu_{2-x}Se$ (non-stoichiometric)	Cubic, orthorhombic	Copper vacancies create defect states, improved redox and ion transport dynamics	
CuTe	CuTe (vulcanite)	Orthorhombic	Anisotropic electrical properties, layered structure boost charge carrier mobility	20–22
	Cu_2Te (novotny)	Hexagonal	Tunable electronic band structure	
	$Cu_{2-x}Te$ (non-stoichiometric)	Hexagonal, FCC	Mixed electronic–ionic conduction, compositionally driven structural variability	

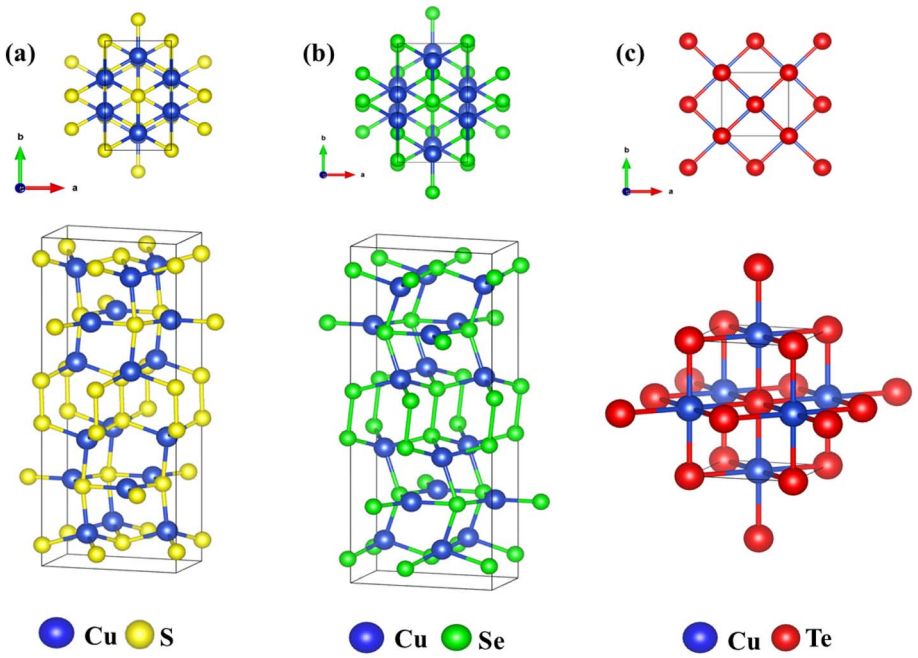

Fig. 2 Crystal structure of copper chalcogenides: (a) CuS, (b) CuSe and (c) CuTe.

This more covalent Cu–Te interaction and tetrahedral coordination is mainly due to the Te 5p orbital hybridisation, which facilitates a different crystal effect than the S 3p and Se 4p orbital hybridisation. When comparing the structural difference, we can observe that the layered structure of CuS and CuSe benefits them in ion intercalation and boosts their electrochemical properties. However, CuTe's distinct orthorhombic structure facilitates anisotropic electrical and charge transport properties, which make it more suitable for hybrid composites.[27,28]

Apart from the crystallographic phase, a few amorphous phases of copper chalcogenides are also reported, which are synthesised under non-equilibrium synthesis conditions, rapid quenching or other chemical routes to prevent their crystallisation. Amorphous CuS can be synthesised at low temperatures (10 °C), but over time it will eventually turn into crystalline covellite. Therefore, the amorphous forms are considered as metastable intermediate states formed during synthesis.[29,30] In this review, we will mainly focus on the crystalline phases of copper chalcogenides.

By considering properties such as excellent electrical conductivity, rich redox activity, and cost-effectiveness, it is evident that copper-based chalcogenides (CuS, CuSe, and CuTe)[15] can be potential electrode materials for next-generation supercapacitors.[24,26] However, challenges such as structural instability, low intrinsic energy density, and limited cycle life hinder their practical applications. In this review, we will discuss about the research carried out on copper chalcogenide materials. This review also highlights some strategies that are implemented by the research to mitigate the limitations. Along with that, we will briefly discuss about the machine learning approach and how efficient it can be to predict the performance of the electrode.

2. Copper chalcogenide materials as electrode materials for supercapacitors

2.1 Electrochemical evaluation methods of electrode materials

To understand the electrochemical performance of copper chalcogenides and the values, a brief overview of the fundamental methods that are employed to evaluate the specific capacitance (C_s), energy density (E_D) and power density (P_D) is discussed below. The electrochemical characterisation is carried out by three- or two-electrode configurations, among which the three-electrode configuration consists of a working electrode (active material), a counter electrode (platinum foil), and a reference electrode (Ag/AgCl or Hg/HgO). A two-electrode system consists of only a working and a counter electrode. The two-electrode configuration is mainly employed to study the device's practical performance, whereas the three-electrode configuration provides the fundamental insights about the electrode's intrinsic properties, which make it a widely reported method to fundamentally study the copper chalcogenides.

The electrochemical performance of an electrode is primarily assessed by cyclic voltammetry (CV), galvanostatic charge–discharge (GCD) and electrochemical impedance spectroscopy (EIS). In CV, by varying the potential sweep rate, it provides insights into the charge storage mechanism and redox peak potentials, and by analysing the potential–current profile, the specific capacitance, operating potential window, rate capability and stability can be evaluated.[31]

From the cyclic voltammetry, the specific capacitance (C_s) of an electrode can be calculated by integrating the current response over the applied potential:

$$C_s = \frac{\int_{V_1}^{V_2} I(V)\mathrm{d}V}{m\Delta V v}$$

'$I(V)$' is the current response of electrode at voltage 'V', 'm' is the mass of active material on the electrode, 'ν' is the scan rate, '$\Delta V = V_2 - V_1$' is the working potential window, V_2 is the upper potential of the CV curve and V_1 is the lower potential of the CV curve. This equation directly relates to the current response to ion intercalation kinetics, which relates that at a high scan rate, the full specific capacitance cannot be measured.

GCD provides the voltage–time profile under constant current, which enables the calculation of the specific capacitance, rate capability and coulombic efficiency. Additionally, the equivalent series resistance (ESR) can be measured from the initial potential drop (IR drop) of the GCD curve. However, the capacitance can also be measured from the slope of the GCD discharge curve, when compared to CV in this method, the specific capacitance is measured at steady-state ion transport, which offers more reliable values for practical applications.[32]

$$C_s = \frac{I\Delta t}{m\Delta V}$$

'I' is the applied current and 'Δt' is the discharge time.

Further, the energy density (E_D) is a critical factor that determines the practical application of supercapacitors, which can be calculated using the following relation, and it is usually expressed in Wh kg^{-1}:

$$E_D = \frac{1}{2}C(\Delta V)^2$$

This equation also emphasises the role of voltage window, which clearly indicates that tuning the electrolyte with a wide operating potential window is equally important to optimising the electrode. The power density (P_D) is calculated using the following relation:

$$P_D = \frac{E_D}{\Delta T}$$

P_D is expressed in W kg^{-1}, which shows the ability of an electrode to deliver a rapid energy output. The trade-off between E_D and P_D can be easily visualized in the Ragone plots.

Electrochemical impedance spectroscopy (EIS) is an essential tool to understand the intrinsic properties of an electrode and correlates with its electrochemical performance. EIS provides the frequency-dependent response of the electrode–electrolyte interface. It provides complete information of all the processes that occur in the system, from the conduction of electrons in the electrode to the diffusion of ions in the electrolyte. EIS enables us to break down the contribution of resistive, capacitive and diffusive mechanisms that determine the overall performance of an electrode.[33] The EIS technique effectively differentiates the equivalent series resistance (ESR), charge transfer resistance (R_{ct}) and diffusion resistance. In this technique, an AC signal of small amplitude is applied over a wide range of frequency from MHz to mHz. The corresponding response of the electrode is a complex impedance '$Z(\omega)$', which can be expressed as follows:

$$Z(\omega) = Z'(\omega) + jZ''(\omega)$$

where '$Z'(\omega)$' is the real component in this expression, which represents the impedance of the entire system; '$Z''(\omega)$' is the imaginary component, which corresponds to the capacitive behaviour or inductive behaviour. While interpreting an EIS data, we can observe an intercept with real axis in the high-frequency region that provides insights into the intrinsic resistance of the electrode material, ionic resistance and contact resistance. A semicircle in the mid-frequency range gives insights into the R_{ct} value of the faradaic redox reaction. An elevated slope line in the lower frequency region provides information about the diffusion of ions into the porous electrode and electrolyte interface.[34] By understanding the above-mentioned evaluation techniques, the following section will focus on the electrochemical performance of copper chalcogenides.

2.2 Copper sulphides

Copper sulphide (CuS) is an extensively studied material for supercapacitor applications compared to other copper chalcogenides due to its structural versatility, defect chemistry and electrochemical activity. CuS belongs to the $P6_3/mmc$ space group with a hexagonal crystal structure. It is a p-type semiconductor with a narrow band gap of 1.2 eV to 2.0 eV. The covellite phase of CuS is one of the most stable phases; the layered structure with S–S bonds and Cu–S coordination facilitates the anisotropic charge transport.[16,35–37] Copper with mixed valence states (Cu^+/Cu^{2+}) provides the redox-active sites, which drive the pseudocapacitive charge storage. The layered architecture, which facilitates the ion intercalation and surface adsorption, and defect-rich chemistry of CuS, combining these properties, makes it an effective electrode material for prolonged cycling stability. Even though Cu–S have a strong covalency compared to CuSe and CuTe, it still has stability concerns such as polysulphide dissolution during continuous charge–discharge cycling. However, CuS offers a balance of abundance, cost-effectiveness and rich electrochemical activity, making it the benchmark for supercapacitor applications.[38–40] The following sections provide an in-depth analysis of how morphological tuning, composite engineering, and metal hybridisation collectively influence the capacitive behaviour of CuS.

2.2.1 CuS with different morphologies. The electrochemical performance of copper sulphides can be significantly impacted by the morphology. By modifying the morphology, the specific surface area (SSA), diffusion of ions, and charge transport can be tailored. Intrinsic properties such as electrical conductivity and electron mobility are also interlinked with the phase, crystallinity and grain boundaries. By fine-tuning the morphology, the electrochemical characteristics of the material can be tailored. The following section reviews the impact of various morphologies and their influence on the electrochemical behaviour of CuS.

In a comparative study, Goswami and team[41] investigated how the structural architecture of the material significantly governs the charge storage capability. They synthesised different CuS structures such as nanoparticles (NPs), nanotubes

(NTs), hexagonal coins (HCs), cross-linked nanotubes (CLNTs), and nanoworms (NWs). Comparing the capacitance performances of the various CuS structures that were synthesized, CuS CLNTs delivered an excellent specific capacitance of 275 F g^{-1} at a current density of 0.5 A g^{-1}; this better performance compared to the other structures is due to their hollow architecture, which facilitates the electrolyte Na^+ ion interface with the redox active sites. Along with high electrochemical performance, it also retained 99% of the initial charge storage capacity after 500 cycles, which displays its exceptional cycle life performance. In Fig. 3(a), the CV profiles of different morphologies of CuS clearly indicate that the crosslinked nanotube outperforms all the other nanostructures by enclosing the large area; this unique architecture provides abundant edge active sites which increase surface-based ion storage, short ion diffusion distance and continuous pathways for electron transport. This study reveals that the hierarchical porous and hollow morphologies can be employed to mitigate the limitations of transportation of ions.

Similarly, Liu *et al.*[42] have successfully synthesized and investigated various hierarchical CuS nanostructures including tubular (T-CuS), spherical (S-CuS) and microflower (H-CuS), by altering the solvent conditions during synthesis. Among the synthesized structures, the H-CuS electrode demonstrated an outstanding electrochemical performance, delivering a charge storage capacity of 536.7 F g^{-1} when tested with a current load of 8 A g^{-1} and preserving 83.6% of its charge storage capacity after 20 000 cycles, demonstrating its excellent stability. Fig. 3(b) displays the electrochemical impedance spectra for various hierarchical CuS structures. The EIS studies revealed that H-CuS exhibits lower R_{ct} values than its counterparts. The small semicircle region in the high-frequency region indicates the rapid electron transfer, and the linear steep line at a lower

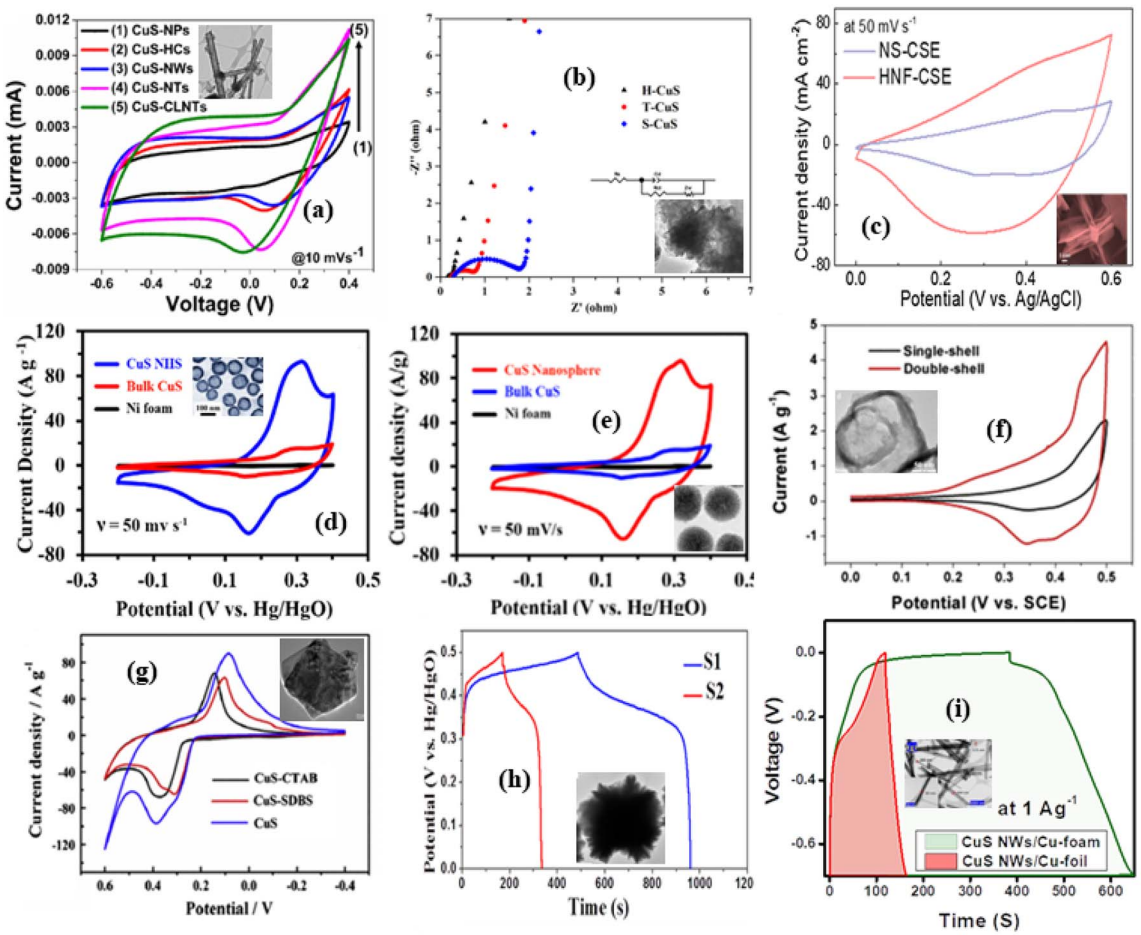

Fig. 3 Electrochemical studies with TEM images: (a) Comparative CV plot of CuS: NPs, NTs, HCs, CLNTs, and NWs; inset: TEM image of CuS (CLNTs). Reproduced with permission.[41] Copyright 2023, American Chemical Society. (b) Comparative EIS graph of different CuS structures; inset: TEM images of hollow microflower. Reproduced with permission.[42] Copyright 2018, Elsevier. (c) Comparison of the electrochemical performance of NS-CSE and HNF-CSE; inset: TEM image of HNF-CSE. Reproduced with permission.[43] Copyright 2022, Elsevier. (d) Cyclic voltammetry curves of CuS NHS, Bulk CuS and Ni foam; inset: TEM image of CuS NHS. Reproduced with permission.[44] Copyright 2017, Elsevier. (e) Copper sulphide nanosphere's CV curve; inset: TEM image of nanospheres. Reproduced with permission.[45] Copyright 2017, Elsevier. (f) CV curve of double- and single-shell nanocages; inset: TEM image of a double-shell nanocage. Reproduced with permission.[46] Copyright 2017, Elsevier. (g) Cyclic voltammetry curves of CuS and CuS with surfactant CTAB, SDBS and inset morphology analysis *via* TEM of CuS-SDBS. Reproduced with permission.[47] Copyright 2015, Elsevier. (h) Galvanostatic charge–discharge cycle curves; inset: TEM image of 3D hierarchical CuS microspheres. Reproduced with permission.[48] Copyright 2015, American Chemical Society. (i) GCD profiles of CuS nanowires; inset: TEM images of CuS NW. Reproduced with permission.[50] Copyright 2023, Elsevier.

frequency reveals the efficient diffusion of ions and reflects almost like an ideal capacitive behaviour. H-CuS with microflower-like architecture provides a high surface-to-volume ratio with interconnected porous channels. This architecture combines the advantages of 2D nanosheets with abundant active edge sites with the 3D porosity, which eventually reduces the impedance between the electrode and electrolyte interface. This microflower architecture helps to mitigate the limitations of spherical and tubular architecture, which suffer from low surface area exposure and high interfacial resistance.[42]

Kim *et al.* developed a hierarchical flower-like CuS (HNF-CSE) electrode composed of 1D nanorods integrated with 2D nanosheets (NS-CSE).[43] It delivered a C_s of 1.35 F cm^{-2} at 2 mA cm^{-2}. Further studies after 20 000 charge and discharge cycles show that it achieved 93.2% of capacitance retention, which portrays high stability of this unique structure. Fig. 3(c) displays the electrochemical performance of HNF-CSE and NS-CSE, where it clearly depicts that the hierarchical structure shows better performance, by enclosing the large area. This study primarily emphasises the structural robustness and its effectiveness in boosting the electrochemical performance. In another study by Heydari *et al.*,[44] they synthesised three different morphologies, namely nanoplates, nanowires and CuS nanohollow spheres, which were also associated with porous structures. CuS nanohollow spheres have porous structures with a high active SSA of 97 m^2 g^{-1}, and these combined properties resulted in a higher electrochemical capacitance of 948 F g^{-1} tested at a specific current of 1 A g^{-1}. The cyclic voltammetry profiles of the synthesised nanohollow spheres (NHS-CuS) and bulk CuS are displayed in Fig. 3(d). We can observe that the performance of directly grown CuS nanosheets on a Ni foam is better than that of bulk CuS, due to the short ion diffusion pathways and high edge sites provided by the ultrathin nanosheets. When coupling it with the Ni foam further boosts the conductivity and stability, whereas the bulk CuS is constrained by poor charge transport and low ion accessibility. This study highlights that by tailoring the morphology and dimension, diffusion barriers and redox-active interface can be tuned.

Heydari and team[45] continued their studies further with a different approach by synthesising a nanoporous CuS nanosphere with a diameter ranging from 90 to 110 nm with thin walls (>10 nm) and nanopores (~7 nm). This unique architecture exhibits an SSA of 65 m^2 g^{-1}, and it displayed an excellent specific capacity of 814 F g^{-1} when tested at a specific current of 1 A g^{-1}. Its exceptional performance was evaluated by CV, which is displayed in Fig. 3(e). The CV profiles of bulk CuS and nanoporous CuS clearly indicate that it outperforms the bulk CuS. This performance boost is mainly due to the thin walls, and interconnected pores, which enable rapid ion diffusion and facilitate a highly penetrable architecture for efficient electrolyte penetration and accessible redox-active channels. Along with performance boost, it exhibited an excellent stability of 95.9% over 5000 cycles. This study specifically highlights the unique approach to overcome the limitations by inducing porous architecture.

Furthermore, Guo *et al.*[46] synthesized hollow nanocage-structured CuS utilizing nanocubic Cu_2O as a framework. The hollow CuS nanocages were synthesised by repeated vulcanization in a Na_2S solution and etched using HCl. At a tested current density of 1 A g^{-1}, the resulting electrode achieved a high C_s of 843 F g^{-1} and even after 4000 consecutive cycles, it maintained 89.2% of its capacity retention. This enhanced electrochemical performance can be clearly seen in Fig. 3(f), in comparison with the single shell, double-shell configuration additionally provides active surface area and internal electrolyte reservoirs, which eventually enhance the performance, and this hollow nanocage architecture also serves as a buffer region that prevented the dimensional change during charging and discharging, hence enhancing the electrode's structural integrity.

Apart from the various architectures, the study conducted by Huang and team[47] on CuS nanosheets, which were synthesised with and without surfactants (CTAB & SDBS), revealed a few insights. These surfactants are crucial in tuning the microstructures of the material. From Fig. 3(g), we can understand that CuS nanosheet morphology synthesised without any surfactant provides better performance. This is owing to the nanosheet structure, which facilitates better charge transport and electrolyte ion diffusion. The results suggest that surfactants can be a double edge sword: they might help in optimising the morphology but might affect the performance. Surfactants have the ability to modulate the surface termination and sulphur vacancy, which directly affect the diffusion of ions and conductivity. This study highlights that surfactant engineering is underexplored, yet it can be an effective method to tailor the structural and electronic properties.

Zhang[48] and his team synthesised three-dimensional CuS spherical architecture, exhibiting a unique structural design, including a mesoporous structure and thin nanosheet subunits. Fig. 3(h) unveils the GCD plots of CuS with two different morphologies, namely nanosheet (S-1)-like and thick plate-like structures (S-2). From the GCD plots, it is evident that the nanosheet architecture exhibits a longer discharge time, indicating its high specific capacitance and small IR drop, which reflects low equivalent series resistance and efficient electron transport. The nanosheet morphology exhibited an excellent electrochemical performance by achieving a charge storage capacity of 237 F g^{-1} at a specific current of 0.5 A g^{-1}. It eventually preserved 75.9% of its capacitance even at 8 A g^{-1}, indicating its impressive rate capability and stability. This study highlights the combined advantages of nanosheets, which facilitate rapid charge kinetics, and nanospheres, which provide mechanical stability over charge–discharge cycles.

The research carried out by Justin Raj[49] and his team mainly focused on the impact of heat treatment. They synthesised and explored the heat-treated CuS (H-CuS) nanoplatelets and their counterpart bare CuS (B-CuS). Their motive is to enhance the electrochemical performance by tuning the morphology. The characterisation results displayed that the crystallinity and morphology of CuS have improved after the heat treatment. It also achieved a charge storage capacity of 72.85 F g^{-1} under a potential sweep rate of 5 mV s^{-1}, in a 1 M $LiClO_4$ electrolyte. It is observed that the pseudo-capacitance behaviour was

primarily due to lithium-ion insertion/extraction processes, which were more effective in the heat-treated samples. Furthermore, the study noted that the cyclic retention of the heat-treated copper sulphide (H-CuS) electrode was approximately 86.09% after 100 cycles, while the other electrode (B-CuS) maintained approximately 63.71% of its original capacitance, underscoring the enhanced stability of H-CuS in supercapacitor applications. The findings from this study highlight the importance of morphology engineering, and the synergistic interplay between crystallinity and electronic properties is crucial for enhancing the performance.

In a study by Goswami and team,[50] a self-supported, binder-free CuS nanowire array on porous copper foam electrodes was developed to boost the electrochemical efficiency of Na-ion capacitors (NICs). When tested at 1 A g^{-1} current density, it revealed a significant improvement in C_s of 380 F g^{-1}, which is significantly higher than that of CuS nanowires on Cu-foil (70 F g^{-1}). The findings shown in Fig. 3(i) reveal that replacing the traditional Cu-foil with a porous Cu-foam significantly boosted the performance. This is due to the porous architecture of the Cu-foam. This binder-free technique eventually reduced the ion diffusion pathways, suppressed the volumetric change and enhanced the reaction kinetics. When a symmetric device is fabricated using CuS nanowires, when tested at a current density of 1 A g^{-1}, the measured capacitance value is 400 F g^{-1}. After 5000 consecutive charge–discharge cycles, it displayed 79% of capacity retention, which shows its excellent stability. This study highlights that the interplay between the substrate and morphology also plays a crucial role in performance and practical applications.

A study by Samdhyan and team[51] investigates an innovative approach to synthesis a unique marigold flower-like morphological architecture of CuS. The electrochemical studies revealed a remarkable charge storage capacity of 631.2 F g^{-1} when tested under an applied current of 1 A g^{-1}. This exceptional performance is due to the structural advantage, which provides a high specific surface area, enabling the ions to access more redox active sites. The reduced ion diffusion pathways eventually contribute a good rate capability. It also displayed its long-term durability, by retaining 80% of its initial capacitance after 2500 consecutive charge–discharge cycles. The overall studies emphasise that the morphology of the active material always plays a crucial role in its performance and practical application. Among the various morphologies, rational nanostructures such as crosslinked nanotubes, hallow microflowers, nanohallow spheres and nanocages exhibited an excellent specific capacitance, rate capability and structural integrity. This clearly highlights that this unique design is a powerful strategy to unlock the full potential of CuS.

2.2.2 Doped copper sulphides. Doping is a well-known approach to tailor the intrinsic properties of CuS, and when a hetero atom is introduced into the CuS lattice, it significantly alters the electronic band structure, by introducing localized states within the band structure, and acts as additional redox active sites. The substitution of Cu with a hetero atom induces a lattice distortion effect due to the variation in ionic radius between copper and the dopant, creates strain to enhance the electron transport kinetics and creates defect site for charge accommodation. Apart from this, doping influences the morphology and surface area because it acts as a nucleation center and influences the growth of particles and nanostructures. In the following section, we will discuss about the doped copper sulphides with various elements.

Bushra Qasim *et al.*[52] prepared CuS and Ni-doped CuS hydrothermally and investigated the effect of doping at various Ni concentrations of $Ni_{0.003}$, $Ni_{0.005}$ and $Ni_{0.007}$. The results demonstrate that the $Ni_{0.007}$-CuS electrode delivered an exceptional performance by delivering a storage capacity of 1485.35 F g^{-1}. This result outperforms the pristine and many other reported electrode materials. The EIS studies revealed a decrease in the charge transfer resistance of 1.68 Ω, and it also demonstrated excellent stability by retaining its initial capacity of 92.96% after 5000 GCD cycles. These results suggest that Ni doping improves the charge transfer pathways and stabilizes the CuS framework. Additionally, it achieved a high E_D value of 94.27 Wh kg^{-1}, along with that, maintaining a high P_D of 338 W kg^{-1}. These findings show that the substitution of Cu^{2+} ions (0.73 Å) with Ni^{2+} ions (0.69 Å) creates a minimal lattice strain and introduces additional d-orbitals, which notably enhance the overall performance and stability of CuS.

Brown and his team[53] successfully developed Fe-doped CuS nanostructures using a mild hydrothermal method with CTAB as a cationic surfactant as a stabilizer. This study highlights the incorporation of Fe ions, which induces the formation of interconnected flake-like mesoporous nanostructures. The electrochemical characterisation reveals the improved performance of Fe-doped CuS compared to pristine CuS, Fe-doped CuS exhibited a higher electrochemical capacitance of 516.39 F g^{-1} than pure CuS (328.26 F g^{-1}). This boosted performance is attributed to the combined effect of Fe doping and the mesoporous structure. The substitution of Fe induces a significant lattice distortion and defects which act as the charge storage sites; additionally, the mesoporous structure facilitates better ion transport, which further enhances the redox activity and conductivity.

In the other research carried out by Jeyabanu *et al.*,[54] La@CuS was synthesized using a microwave irradiation method. In this, they studied the effect of La doping at different concentrations such as 0%, 1%, 3%, and 5%. The electrochemical studies demonstrated that the addition of lanthanum into the CuS lattice remarkably improved the charge storage capacity of CuS. At 5% La-doping, it delivered a superior charge storage capacity of 1040 F g^{-1}. Fig. 4(a) shows that the Nyquist plots illustrate the reduction of charge-transfer resistance by increasing the La doping concentration. The results indicate that La doping not only introduces additional active sites and structural defects into the CuS lattice, but also contributes to improved conductivity and ion transport kinetics. This confirms that doping with La, a rare earth element, will enhance the materials' overall performance.

Podili and team[55–57] conducted a comprehensive study on the effect of Ni, Co and Zn doping on the CuS nanostructure at different concentrations (0.05, 0.15, and 0.30 mM).

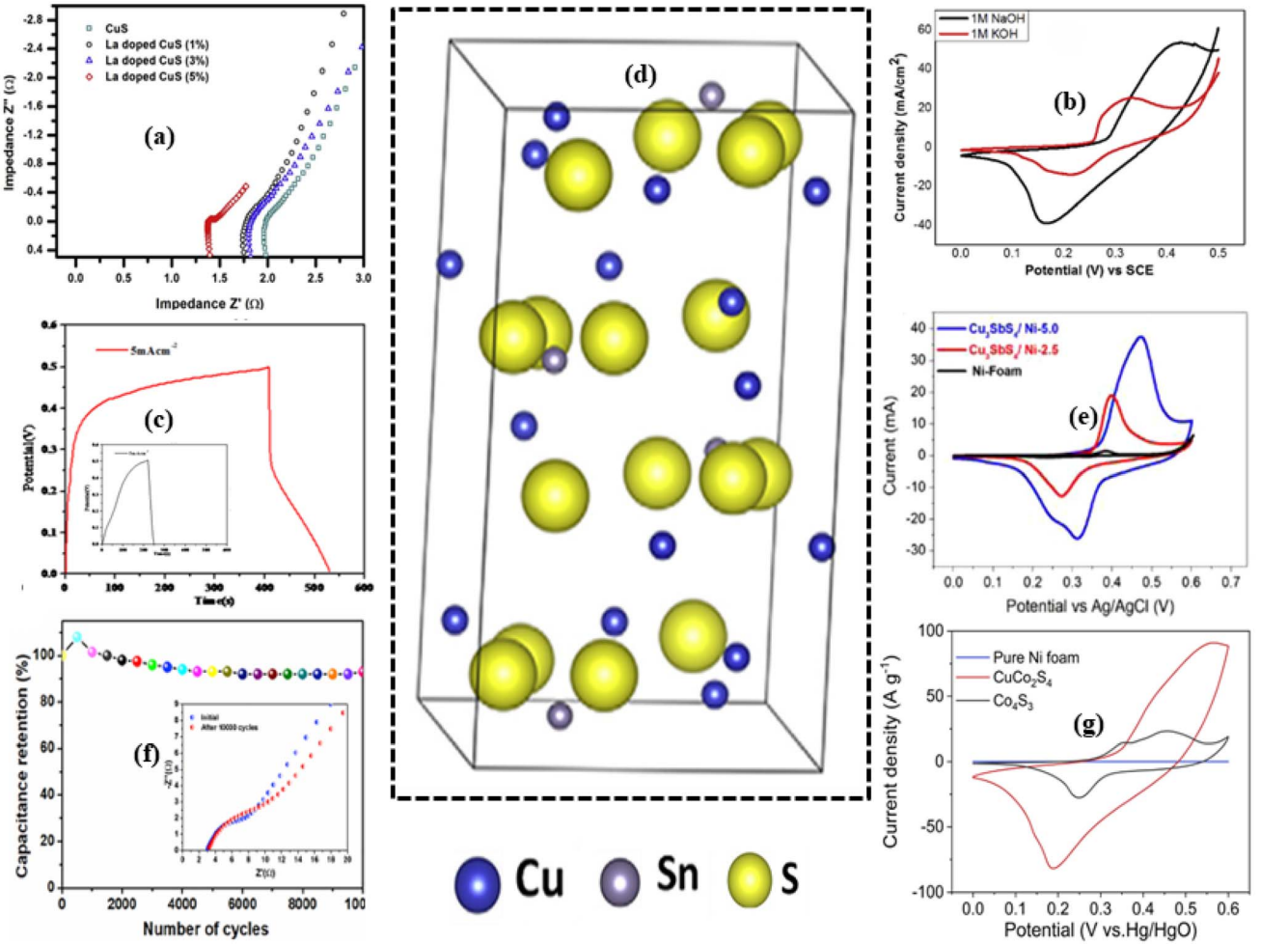

Fig. 4 (a) EIS plots of La-doped CuS. Reproduced with permission.[54] Copyright 2019, Elsevier. (b) CV curves of the CTS electrode at 5 mV s^{-1} scan rate in 1 M KOH and 1 M NaOH electrolyte. Reproduced with permission.[58] Copyright 2018, Elsevier. (c) CTAB–Zn (0.05 mM)-doped CuS electrode at a constant current density; inset: charge–discharge curve of CTAB-CuS. Reproduced with permission.[57] Copyright 2020, Springer Nature. (d) Crystal structure of copper tin sulphide. Reproduced with permission.[58] Copyright 2018, Elsevier. (e) Comparative cyclic voltammetry (CV) curves of the bare Ni foam, Cu_3SbS_4/Ni-2.5, and Cu_3SbS_4/Ni-5 electrodes were obtained at a scan rate of 5 mV s^{-1}. Reproduced with permission.[59] Copyright 2019, Elsevier. (f) CWS/Ni//Graphene asymmetric supercapacitor (ASC) device demonstrated excellent cycling stability over 10 000 charge–discharge cycles. The inset illustrates the Nyquist plots recorded before and after the 10 000 cycles, highlighting the device's electrochemical durability. Reproduced with permission.[60] Copyright 2019, Elsevier. (g) CV curves of the pure Ni foam, Co_4S_3, and $CuCo_2S_4$ electrodes measured at a scan rate of 20 mV s^{-1} within a potential window of 0–0.6 V *versus* Hg/HgO. Reproduced with permission.[61] Copyright 2018, Elsevier.

Co-doped CuS at 0.15 mM promoted a uniform particle growth, achieved a surface area of 13.59 m^2 g^{-1} and a specific capacitance of 586.45 F g^{-1}, lower than those of the other dopants, whereas Ni doping at 0.30 mM favoured the formation of Cube-like nanostructures with a higher surface area of 19.631 m^2 g^{-1} and achieved a specific capacitance of 753 F g^{-1}. This better performance is due to the well-defined faceted surface, which facilitates the intercalation of electrolytic ions for the faradaic redox reaction. Among the other dopants, Zn-doped CuS favoured the growth of mesoporous flower-like nanostructure with a surface area of 18.23 m^2 g^{-1}. The nearly triangular GCD profile displayed in Fig. 4(c) illustrates the good capacitive behaviour and less internal resistance. It also highlights the rapid, reversible redox reaction of Zn-doped CuS. This unique mesoporous flower-like nanostructure enhances the accessibility of electrochemically active sites and ion transport kinetics by providing efficient ion transport pathways. This study highlights the first utilisation of mesoporous flower-like Zn-doped CuS nanostructures as supercapacitor electrodes.

The studies highlight that doping a hetero atom has significantly boosted the performance. When a hetero atom was introduced into the CuS lattice, it eventually altered the band structure, improved the number of redox active sites and facilitated an efficient transport mechanism. Among the transition metal dopants, Ni exhibited the highest specific capacitance and excellent stability, which is primarily due to the reduced charge transfer resistance. Along with the transition metal elements, La doping resulted in high performance, and this highlights that doping with rare earth elements can also be an

effective approach to enhance the performance along with the stability.

2.2.3 Ternary and quaternary copper sulphides. Binary copper chalcogenides with their intrinsic properties such as high electronic conductivity, rich redox reactivity and tunable redox chemistry were set apart from the other pseudocapacitive materials. However, it still faces limitations such as fundamental compositional constraints, electronic band structure tuning and limited redox active sites, which opened new research areas towards ternary and multinary systems. The multinary copper chalcogenides provide compositional tunability, which enables precise control over the band structure and electronic transport properties. The presence of multiple cations increases the density of states near the Fermi level by facilitating an improved charge transfer kinetics and specific capacitance. In recent years, ternary and quaternary copper sulphides are considered as advanced electrode materials, gaining researchers' interest due to their superior electrical conductivity, structural stability and presence of multiple fast redox active sites. The synergistic effect of multiple metal cations introduces abundant redox active sites, improves ion transport by providing efficient charge transport pathways and improves the structural integrity over charge discharge cycles. In the following section, we will discuss about various ternary and quaternary copper chalcogenides and their properties.

This study mainly focuses on the binder-free synthesis of the Cu_4SnS_4 (CTS)[58] electrode. In Fig. 4(d), it displayed the incorporation of Sn into the CuS crystal matrix. This ternary component exhibits an exceptional electrochemical capacity of 704 F g^{-1} compared to the other counterparts such as Cu_2SnS_3 (406 F g^{-1}) and Cu_2ZnSnS_4//RGO (591 F g^{-1}). This improvement is mainly due to the synergistic effect of Cu, Sn and Se, and their superior electrochemical activity. CTS provides a large number of reversible redox Cu sites compared to $Cu_2SnS_3$and Cu_2ZnSnS_4, additionally in the presence of Sn^{4+}, which improves the stability of the lattice, whereas Cu_2SnS_3 provides fewer active sites, which limit the charge storage capacity, and the presence of electrochemically inactive Zn^{2+} in Cu_2ZnSnS_4 hinders its performance by minimising the redox activity. In CTS, the hybridization of Cu-3d and Sn-5s orbitals modifies the intrinsic electronic structure and provides an enhanced ion transport pathway. This facilitates rapid electron transport compared to localized inactive 3d orbitals of Zn. When CTS properties were coupled with the binder-free synthesis approach, it significantly boosted the specific capacitance by providing a direct interface between the active material's and the electrode. From Fig. 4(b), we can notice that the electrochemical activity is better suited in NaOH electrolytes than KOH. This result shows the material affinity toward the Na^+ ion interaction. The EIS studies also revealed its enhanced ionic conductivity and mobility. CTS cycling stability was studied after 2000 consecutive GCD cycles, which resulted in an impressive 81% capacity retention. This is primarily due to the tetragonal crystal structure with strong Cu–S and Sn–S bonds.

In this research, they synthesised a $CuCo_2S_4$ nanosheet array,[61] and they used NF as the substrate. A binder-free technique is employed to further refine the functionality of $CuCo_2S_4$. This improved performance of CCS in comparison with its counterparts is due to the presence of rich redox activity and superior conductivity, whereas in this research, this performance enhancement is also attributed to the nanosheet morphology. This morphology facilitates high specific surface area, which eventually leads to increased interaction between the ions and electrochemically active sites and facilitates an efficient ion diffusion pathway. These properties elevate the performance of $CuCo_2S_4$, and when the material was studied at 1 A g^{-1}, it delivered an outstanding electrochemical capacitance of 3132.7 F g^{-1} depicted in Fig. 4(g).

This clearly indicates that they manufactured a symmetric supercapacitor, and its studies reveal that it delivered 46 Wh kg^{-1} of maximum energy density coupled with an impressive power density of 991.6 W kg^{-1}. Along with the enhanced electrochemical activity, it also exhibited an exceptional stability of 70.8% capacity retention even at 2 A g^{-1}. This result conveys that it possesses an exceptional rate capability and suitability for energy storage applications.

In this research, they explored copper tungsten sulphide (CWS)[60] nanostructures developed *via* a binder-free method. They synthesised CWS directly on a Ni-foam by a binder-free technique. The CWS achieved an electrochemical capacitance of 2666.6 F g^{-1}. This enhanced performance can be attributed to the binder-free synthesis method. To check the practical applicability, an ASC was made using CWS/Ni and graphene as the electrodes. This device achieved an E_D of 48.5 Wh kg^{-1}. Fig. 4(f) illustrates the synthesised material's cycling stability, which remains at around 92.1% even after 10 000 cycles. The inset in Fig. 4(f) provides the results of EIS before and after 10 000 cycles, which reveals the increase in R_s (from 2.96 to 3.07 Ω) and R_{ct} (from 3.84 to 5.92 Ω). In the other study, a copper antimony sulphide (Cu_3SbS_4) nanowire was synthesised *via* a binder-free approach.[59] The electrochemical studies show an extraordinary specific capacitance of 835.24 mA g^{-1}. To demonstrate its practical applicability, they fabricated an asymmetric supercapacitor using Cu_3SbS_4 and Cu_2MoS_4, which delivered 58.15 Wh kg^{-1}, a notable energy density coupled with an exceptional power density of 6363.63 W kg^{-1}. These results out-perform the graphene-based supercapacitors by three times. Fig. 4(e) displays the CV graphs of the synthesised material recorded at a scan rate of 5 mV s^{-1}, from which we can clearly see the superior performance of Cu_3SbS_4//Ni-5. Intercalation or displacement of the lithium ion with copper in Cu_3SbS_4 during the charging and discharging cycle is the cause of the redox peaks displayed in the profile. The CV profiles of both Cu_3SbS_4/Ni-2.5 and Cu_3SbS_4/Ni-5 electrodes exhibited Faradaic-dominated characteristics, corresponding to Type C curves. By emphasizing the importance of morphology in governing electrochemical behaviour, this research advances the fundamental understanding of charge storage mechanisms in complex nanostructures while paving the way for high-energy-density supercapacitor systems.

In a study, researchers synthesised and explored chalcopyrite ($CuFeS_2$)[62] platelets as a high performing electrode for symmetric supercapacitors. This synthesised material, when studied at a scan rate of 5 mV s^{-1}, exhibited an electrochemical

capacitance of 95.28 F g^{-1}. The study further extended after 2000 consecutive charge–discharge cycles, and it showcased an excellent stability of 94.38% capacity retention. This enhanced performance can be attributed to the unique open-pore microflower-like morphology, which facilitates high surface area and reduced diffusion pathways, making it a potential candidate. They fabricated a SSC device with $CuFeS_2$ electrodes. When tested at a specific current of 1 mA g^{-1}, it delivered peak C_s of 34.18 F g^{-1}, along with that it delivered about 4.74 Wh kg^{-1} of E_D coupled with P_D of 166 W kg^{-1}, and these insights show how efficiently it can be applied in advanced energy solutions. While comparing, the ternary and quaternary copper chalcogenides demonstrate exceptional performance compared to the binary counter parts. This indicates the synergistic effect of multiple metal cations and facilitates a large number of redox-active sites and surface area. The above-mentioned studies show that the introduction of various metal cations into the CuS matrix significantly boosts the performance. From the analysis, we can observe that the incorporation of Co (Co^{2+}/Co^{3+}) and Sb (Sb^{3+}/Sb^{5+}) provides rich multivalence redox chemistry and enhanced electronic conductivity. Sn and W incorporation improves ionic transport, stabilises the Cu–S lattice and maintains the structural integrity. However, Fe incorporation induces stable redox activity with less capacitance but provides long-term retention, which is primarily due to its porous morphology and reduced diffusion pathways.

2.2.4 Copper sulphide composites. The integration of CuS with a suitable composite is a promising approach to overcome its limitations of low intrinsic conductivity, volume expansion during charging/discharging and limited cyclic stability, which hinder its practical applicability. To overcome these challenges, CuS has been integrated with various composites that lead to a significant increase in conductivity, stability and specific capacitance. Integrating CuS with carbon-based materials like CNT and graphene improves the electrical conductivity by lowering the internal resistance and facilitates fast redox reaction. Additionally, coupling CuS with conductive polymers and other metal oxides provides additional charge storage active sites and improves the charge storage capability. This composite strategy eventually improves overall performance and structural integrity. In the following, we will discuss about the outcomes of various CuS-based nanocomposite strategies.

In the study by Luxmi Rani *et al.*,[63] CuS/Cu_2S nanostructures and multi-walled carbon nanotube (MWCNT)/CuS/Cu_2S nanocomposites were synthesised by a hydrothermal method. The CuS/Cu_2S nanoparticles yielded a C_s value of 356 mAh g^{-1}, while MWCNT/CuS/Cu_2S nanocomposites delivered a high capacitance of 427.38 mAh g^{-1} when examined under a specific current of 1 A g^{-1}. This shows that the integration of MWCNTs improved the charge storage capacity, which is primarily due to the unique architecture, providing low internal resistance pathways for effective ion diffusion during fast redox reactions. This MWCNT network induces a uniform distribution of nanoparticles, provides a high surface area and facilitates more active sites. It also buffers the volume expansion and enhances the stability. An aqueous ASC developed with MWCNT/CuS/Cu_2S nanocomposites and activated carbon (AC) displayed an impressive E_D value of 70 Wh kg^{-1} and a P_D value of 750 W kg^{-1}. The g-CuS/carbon cloth (*Cc*) composite synthesised and studied by Jin *et al.*[64] *via* galvanostatic electrodeposition method exhibited a specific capacitance of 4676 mF cm^{-2} and a stability of 91.8% after 2000 cycles. The fabricated symmetric supercapacitor delivered a high energy density of 0.96 Wh cm^{-2} and a power density of 4.36 W cm^{-2}. This is primarily due to the high specific surface area of 450.76 m^2 g^{-1}. The carbonised cotton fabric, which is used as a substrate, not only provides high surface area but also offers high flexibility and light weight. Lu *et al.*[65] synthesised 3D hierarchical CuS and CuS/CNT microspheres *via* a simple PVP-assisted reflux method. This approach facilitated the development of a stable porous structure with enhanced structural integrity. The composite achieved a peak charge storage capacity of 2221 F g^{-1} and showcased outstanding rate capability, maintaining a substantial capacity of 1770 F g^{-1} even at a high scan rate of 100 mV s^{-1}. As illustrated in Fig. 5(d), the CV profiles of the CuS and CuS/CNT electrodes showcase distinct redox peaks, suggesting that the composite made up of CuS/CNT possessed a greater enclosed area under the CV curve relative to pure CNTs and bare Ni foam, confirming their superior charge storage capability. The composite displayed a capacitance retention of 89%, which is primarily due to the integration of CNTs, which buffer the volumetric strain and enhance the stability. In another study by Ravi *et al.*,[66] polyimidazole-coated CuS was synthesised over a CNT network (CuS@CNT) on a nickel foam. The resulting composite PIM/CuS@CNT was studied under a specific current of 1.2 A g^{-1} and achieved 1.51 F cm^{-2} as electrochemical capacitance. However, the specific capacitance of the previously reported CuS@CNT is significantly higher. After 1000 charge–discharge cycles, the electrode showed exceptional cycling stability and 92% capacity retention. No observable sulphonate peak in the analysis indicates that the CuS material has high stability. The introduction of CuS into the CNT matrix resulted in a unique pore structure and reduced the particle size, which enhanced the ion diffusion pathways. This study highlights the interlink between the charge transport dynamics and the porous structure of the materials. This result indicates the significance of optimising the structure to improve the number of accessible active sites and enhance the ion diffusion pathways, which will eventually boost the performance.

Pan *et al.*[67] studied the composite of MXenes and copper sulphide (Ti_3C_2/CuS) studied at a specific current of 1 A g^{-1} and demonstrated a remarkable C_s value of 169.5 C g^{-1}. This incorporation of CuS into the MXene significantly increased the C_s value of Ti_3C_2 five times. The GCD curve of Ti_3C_2, CuS, and Ti_3C_2/CuS composites displayed in Fig. 5(b) clearly indicates that the composite offers superior performance. This enhanced performance is attributed to the combined effect of Ti_3C_2 sheets, which provide high electrical conductivity, and CuS, which facilitates exceptional electrochemical activity. The intercalation of CuS facilitates faster ionic and electronic transport by increasing the distance between Ti_3C_2 sheets, which is substantial for high-performance supercapacitors. The composite delivered an energy density of 15.4 Wh kg^{-1}, combined with a power output of 750.2 W kg^{-1}. It also exhibited

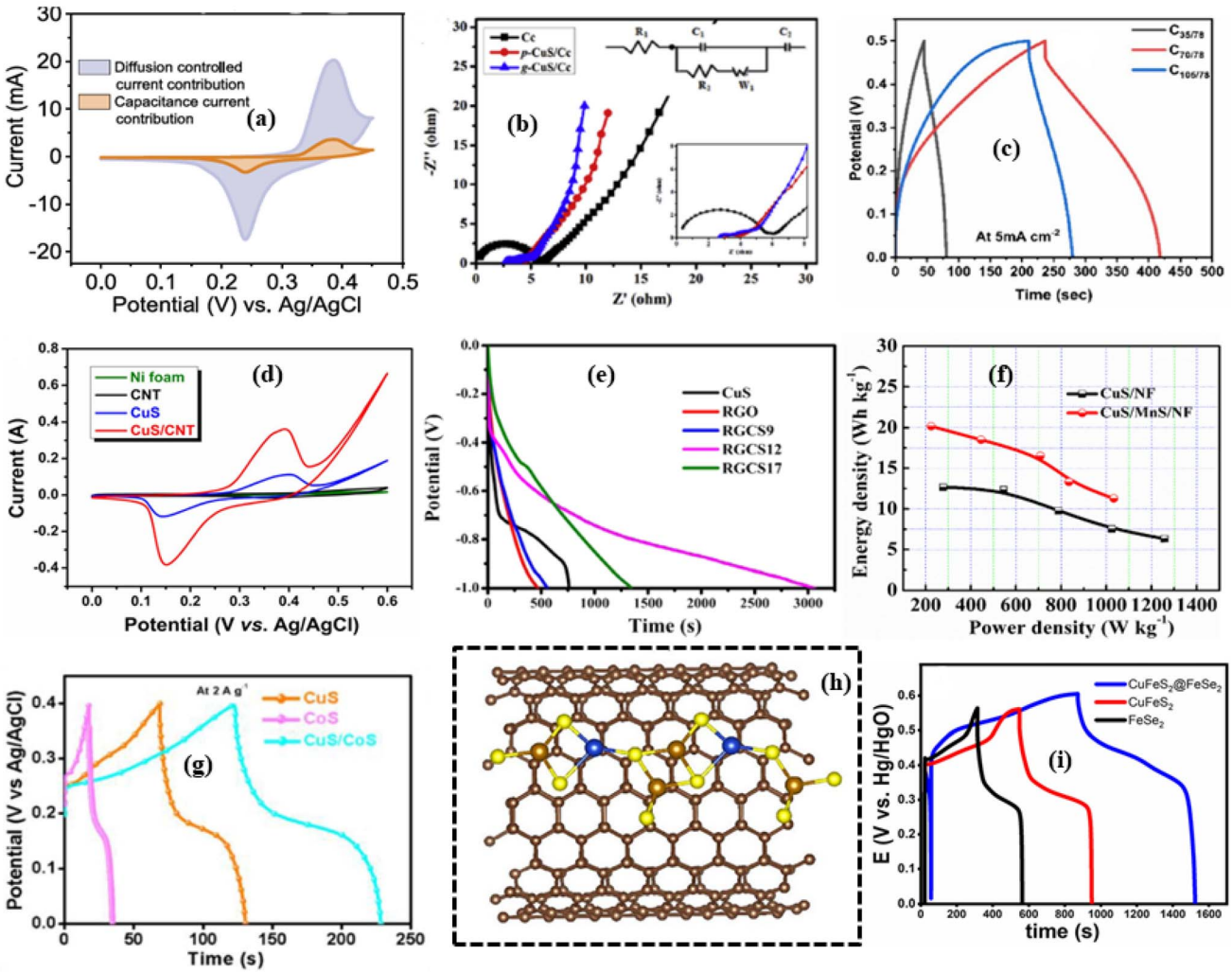

Fig. 5 (a) CV profiles of CTS-rGO/NF and CTS/NF electrodes recorded for comparative electrochemical performance evaluation. Reproduced with permission.[75] Copyright 2024, American Chemical Society. (b) GCD profiles of Ti_3C_2, CuS, TC-6, TC-9, and TC-12 electrodes measured at a current density of 1 A g^{-1} for performance comparison. Reproduced with permission.[67] Copyright 2019, Royal Society of Chemistry. (c) Comparison of the GCD curves for $C_{35/78}$, $C_{70/78}$, and $C_{105/78}$ at a current density of 5 mA cm^{-2}. Reproduced with permission.[70] Copyright 2024, American Chemical Society. (d) CV curves of CuS, CNT, and CuS/CNT composites. Reproduced with permission.[65] Copyright 2015, Nature. (e) Discharge curve of CuS/RGO nanocomposites, RGO and CuS at 1 A g^{-1} current density. Reproduced with permission.[68] Copyright 2021, American Chemical Society. (f) Ragone plots of CuS and CuS@MnS/NF composite-based supercapacitors. Reproduced with permission.[71] Copyright 2019, Elsevier. (g) Comparative GCD plot of CuS, CoS, and CuS/CoS samples studied under a specific current of 2 A g^{-1}. Reproduced with permission.[72] Copyright 2021, Elsevier. (h) Top view of the optimized structure of the CFS/CNT composite. Reproduced with permission.[73] Copyright 2020, Elsevier. (i) GCD plots of $CuFeS_2$, $FeSe_2$ and $CuFeS_2$@$FeSe_2$. Reproduced with permission.[74] Copyright 2024, Royal Society of Chemistry.

excellent stability by retaining 90.5% capacitance after 5000 cycles.

Ghosh *et al.*[68] investigated CuS quantum dots embedded on reduced graphene oxide (RGO) sheets at different concentrations of 9, 12 and 17 wt% of CuS quantum dots. Fig. 5(e) illustrates the GCD profiles of CuS, RGO, and the composites RGCS9, RGCS12, and RGCS17 at a current density of 1 A g^{-1}, which clearly indicates that RGCS12 achieves an excellent specific capacitance of 3058 F g^{-1}. The quantum dot architecture provides a large number of redox active sites, when hybridised with highly conductive RGO, facilitates low charge transfer resistance and improves ion diffusion dynamics. Compared to the Ti_3C_2/CuS system, this study highlights the influence of dimension on charge storage efficiency.

Chandini Behera[69] and team reported a facile and simple method for developing copper sulphide with a morphology of hierarchical flower, a nanosheet-like morphology of thickness 30–40 nm and Ni–CuS nanocomposites with Ni nanoparticles anchored on CuS at different molar ratios. This report demonstrates the influence of precursors' chemistry on modifying the morphology. The electrochemical studies reveal that a Ni-decorated CuS hierarchical flower delivered a specific capacitance of 464 F g^{-1} at a current density of 2 A g^{-1}, which is higher than that of pristine CuS (132.89 F g^{-1}). This enhanced

performance is due to the decoration of Ni nanoparticles, which provides additional active sites, and the EIS study reveals the lower R_{ct} (8.094 Ω) for Ni–CuS, showcasing its enhanced conductivity.

Lu *et al.*[70] studied CuS nanosheets synthesised by an *in situ* chemical reaction method at a fixed temperature of 78 °C, at different treatment times of 35, 70, and 105 minutes. The resulting electrodes were labelled $C_{35/78}$, $C_{70/78}$, and $C_{105/78}$. Fig. 5(c) clearly indicates the excellent performance of $C_{70/78}$ compared to its counterparts by achieving an aerial capacitance of 1814.0 mF cm^{-2}. This can be attributed to the morphology with an increased number of redox-active sites. An ASC was constructed with a reduced GO as the cathode and a CuS nanosheet as the anode. This device delivered a C_s value of 256 mF cm^{-2} at 2 mA cm^{-2}, achieving a peak energy output of 0.05 mWh cm^{-2} and a power delivery capability of 12.15 mW cm^{-2}. By retaining 74% of its capacitance after 1000 cycles, with a coulombic efficiency consistently above 96%, it also exhibited exceptional cycling stability while showcasing its reliable long-term performance. The composite structure of nanosheet/nanoparticle enhances the surface area and facilitates ion transport, resulting in improved electrochemical performance. Himasree *et al.*[71] in their research studied the synergic effect of CuS and MnS composites, which were hydrothermally prepared on an NF. This study highlights the unique cone-shaped morphology formation of CuS@MnS. The CuS@MnS/NF composite showed superior electrochemical performance compared to CuS and MnS due to its efficient ion diffusion pathways and improved charge transfer dynamics. It achieved a remarkable specific capacitance of 89.77 mAh g^{-1} at 1 A g^{-1} and displayed an excellent stability by retaining 95.9% capacity retention after 3000 charge/discharge cycles, proving its excellent long-term stability. This is due to the combined effects of its unique cone-like structure, enhanced surface area, and binder-free approach on a highly conductive nickel foam substrate. The Ragone plot displayed in Fig. 5(f) confirms the material's capability to achieve a peak energy output of 20.17 Wh kg^{-1} at a power delivery capability of 224.67 W kg^{-1}. A three-dimensional (3D) hierarchical porous nanostructure of CuS/CoS nanocomposite was synthesized by a hydrothermal approach by Raghavendra *et al.*[72] and investigated. The GCD profiles at 2 A g^{-1} of CuS, CoS, and the CuS/CoS composite, shown in Fig. 5(g) reveal the improved performance of the composite compared to its individual counterparts. It delivered an electrochemical capacitance of 138.75 mAh g^{-1} and retained 87.56% of its initial value after 4000 cycles, showcasing its reliability. This enhanced electrochemical performance is mainly attributed to the morphology, which offers an efficient ion diffusion pathway between the electrode/electrolyte interface, thereby minimising interfacial resistance. The composites developed by integrating chalcopyrite and CNT[73] harnessed an efficient electrochemical performance. The novel structural design of this composite system is shown in Fig. 5(h). This distinctive structure enhanced the available electroactive surface, which prompted redox activity, simultaneously facilitating the diffusion of ions by a well-defined diffusion channel. In addition to that, the robust interfacial bonding with the sodium ions further contributes to the enhanced charge storage. Besides, there are some limitations, such as low energy density and poor cyclic stability. In another study, $CuFeS_2$ spherical nanoparticles encapsulated within $FeSe_2$ ($CuFeS_2$@-$FeSe_2$)[74] *via* a binder-free hydrothermal method achieved an electrochemical capacitance of 1306 A g^{-1}. The GCD profiles of $CuFeS_2$ and $CuFeS_2$@$FeSe_2$ displayed in Fig. 5(i) indicate that the specific capacitance of $CuFeS_2$@$FeSe_2$ is superior to that of $CuFeS_2$. This remarkable performance can be attributed to the synergistic effect, which amplified the charge transfer kinetics and increased the availability of electrochemically active sites. Moreover, it displayed a capacity retention of 91.03% after consecutive 3000 charge–discharge cycles, thereby confirming its stability and long-term reliability.

Researchers investigated a copper tin sulphide-reduced graphene oxide composite, developed on a nickel foam (CTS-rGO//NF).[75] It delivered an outstanding charge storage capacitance of 820.83 F g^{-1} under a potential sweep rate of 5 mA cm^{-2}, surpassing pristine CTS/NF (516.67 F g^{-1}). This framework effectively overcomes its internal drawbacks of copper tin sulphide, such as lower conductive behaviour and poor cycling stability. The incorporation of reduced graphene oxide imparts remarkable conductive properties and increased surface area, which collectively enhance the charge transport dynamics and facilitate rapid ion diffusion. Furthermore, the electrode demonstrates impressive rate capability, maintaining 73.1% of its capacitance even at various current densities increasing from 5 to 12 mA cm^{-2}, and exhibits superior cycling stability with 92.7% retention over 1000 cycles. Fig. 5(a) shows the CV profiles of the composite, where the redox peaks are associated with $Cu^{+} \rightarrow Cu^{2+}$ and $Sn^{2+} \rightarrow Sn^{4+}$ oxidation, while the reduction corresponds to $Sn^{4+} \rightarrow Sn^{2+}$. The boosted electrochemical performance of CTS-rGO/NF highlights the potential of metal sulphide–graphene hybrids and how rGO integration can enhance the electrode durability by maintaining the structural durability during prolonged operation while offering high capacitance, excellent stability, and efficient charge transport. These findings reveal that integrating CuS with materials like graphenes, MXenes and other metal sulphides can significantly boost the performance by mitigating the intrinsic limitations like poor conductivity and stability. They also emphasise that CuS is a promising candidate for next-generation supercapacitor applications.

2.3 Copper selenides

Copper selenide (CuSe) inherits distinct physical and chemical properties, due to the large ionic radius and lower electronegativity of Se (2.55). The bond strength between Cu and Se is weaker than that of Cu–S, which eventually lowers the band gap, while the indirect and direct band gaps of CuSe lie between 1.05 eV and 2.7 eV. This narrow bandgap facilitates the faster redox reaction of mixed valence states of copper (Cu^{+}/Cu^{2+}) and also reduces the coulombic barrier during ion intercalation, which enables efficient charge storage.[70,76] Additionally, CuSe has emerged as a distinct copper chalcogenide due to its unique ion-electron transport characteristics, whereas the ionic

conductivity is the result of the high mobility of Cu^+ ions present within the Se framework. The synergy of both electronic and ionic conductivity eventually boosts the charge transfer kinetics compared to CuS, and the high free caries density further enhances the electrochemical activity.[77] However, CuSe faces structural instability due to its weaker bonding under prolonged cycling. Overcall properties like enhanced ionic mobility, electronic conductivity and mixed-valence redox chemistry make it a highly promising candidate for supercapacitor applications, but it is less explored than CuS. In this section, we will delve into the electrochemical behaviour of CuSe and how the morphology, doping and integration of composites impact its electrochemical properties.

2.3.1 CuSe with different morphologies. The electrochemical behaviour of CuSe is closely related to the morphology of the material. CuSe exhibits a strong anisotropic change due to its unique layered structure. By optimising the morphology, we can control the directional ion diffusion. Morphologies like nanosheets and nanoflakes provide more active sites, which eventually improve the accessibility of ions and the surface redox reaction. Hierarchical structures like nanoflowers and hollow spheres will facilitate electrolyte penetration and suppress the volume expansion. In the following, we will assess how various morphologies impact the performance of CuSe.

The study carried out on mesocrystal $Cu_{2-x}Se$ nanoplates[78] reveals its unique mesocrystal architecture and significantly boosts the charge storage efficiency. The electrochemical studies resulted in a notable pseudo capacitance of 495.6 F g^{-1} at a specific current of 1 A g^{-1} with 81% of capacity retention after 2000 cycles. This performance boost is attributed to the mesoporous structure, facilitating an enhanced interfacial interaction between the electrode and the electrolyte. This led to an increase in ion diffusion kinetics, additionally mitigating the volume expansion, ensuring a long cycling stability.

In this research, $CuSe_2$ nanoneedles were directly developed on a copper foil, *via* a binder-free approach.[79] It achieved an impressive charge storage capacity of 1037.5 F g^{-1} at a specific current of 0.25 mA cm^{-2}. This is primarily due to the hierarchical needle-like architecture of CuSe. This nanoneedle morphology significantly increased the surface area, exposing abundant active sites and promoting the interaction of the electrolyte. This led to a boost in charge storage, and the study revealed that $CuSe_2$/Cu energy density is about 51.85 Wh kg^{-1}, which is superior to its counterparts of CuO and CuS. Furthermore, this research highlights the increase in specific capacitance of 118% over 1000 cycles. This can be due to the activation process that occurred over time, which enhanced this increase in electrochemical activity. With the intrinsic properties like exceptional electronic conductivity and enhanced redox activity, transition metal selenides can be considered efficient materials for supercapacitor applications.

Similarly, in another research study, Cu_2Se nano-dendrites[80] were synthesised *via* an electrochemical deposition method. It also highlights that the electrochemical performance can be optimised by tailoring the nanostructure morphology. Various structures were developed at different deposition potentials, among which nanodendrite-like Cu_2Se was obtained at −0.75 V s^{-1} CE that exhibited the highest C_s value of 688 F g^{-1}, attributed to its high surface area, improved conductivity, and improved ion transport. This study also discusses about tailoring the morphology by varying the deposition potential, where cauliflower-like structures were formed at −0.65 V s^{-1} CE and nanoparticles at −0.85 V s^{-1} CE. Each morphology demonstrates a different impact on electrochemical behaviour. Further, electrochemical impedance spectroscopy studies confirmed that the nano-dendrite structure facilitates rapid ion and electron transport by minimising charge transfer resistance. By demonstrating the potential of the electrochemical synthesis approach, they also pointed out the importance of nanostructure design in enhancing the supercapacitor efficiency.

In this research, they studied two-dimensional CuSe nanosheets[81] for SHICs. It is expected that to deliver a superior performance, due to its inherent properties like remarkable conductivity and rich redox behaviour. The electrochemical study results showcase that it achieved its peak capacity of 425 mAh g^{-1}. It also exhibited its durability by maintaining 96.7% of its initial capacitance. This result surpasses the previous reported values of CuSe. Fig. 6(a) shows the GCD profile of the fabricated SHIC. Remarkably, these nanosheets (inset in Fig. 6(a) displays the morphology) undergo a unique activation process, facilitating an enhanced capacity of 330 mAh g^{-1} after 70 cycles, which is unusual for conventional electrode materials. It also revealed an exceptional stability by retaining 91.2% of its initial capacitance at a current density of 5 A g^{-1}, even after 3300 cycles. When further studies were carried out, it demonstrated its rate capability by achieving a specific capacitance of 211 mAh g^{-1} even at a current density of 10 A g^{-1}. The kinetic analysis indicates that this exceptional performance is due to the synergistic effect of diffusion-controlled and pseudocapacitive contributions.

In another study, CuSe nanosheets were synthesised by a one-pot colloidal synthesis method.[82] This study also emphasises the influence of the controlled synthesis process. These nanosheets were examined at a potential sweep rate of 2 mV s^{-1}, which delivered a notable charge storage capacitance of 718 F g^{-1} (322 mF cm^{-2}), calculated from the CV profile shown in Fig. 6(b). This performance is attributed to the hexagonal nanostructure (inset of Fig. 6(b)). This unique structure provides a high SSA and promotes the diffusion of electrolyte ions, leading to enhanced electrochemical energy storage. Along with the performance, its durability was studied after 3500 cycles; it showcased an excellent stability of 96% capacity retention. A symmetric solid-state supercapacitor was developed with CuSe and PVA-NaOH gel electrolytes. The study after 10 000 cycles revealed its robust stability with 74% capacitance retention. The fabricated device achieved an E_D of 14 Wh kg^{-1} coupled with an impressive P_D of 1.1 kW kg^{-1}.

In this study, they employed an innovative synthesis approach to develop vertically aligned CuSe nanosheet films. It is synthesised *via* a bottom-up electrodeposition method. The developed material offers key advantages for flexible solid-state supercapacitors.[83] Unlike conventional top-down methods, which often result in poor structural control, this approach

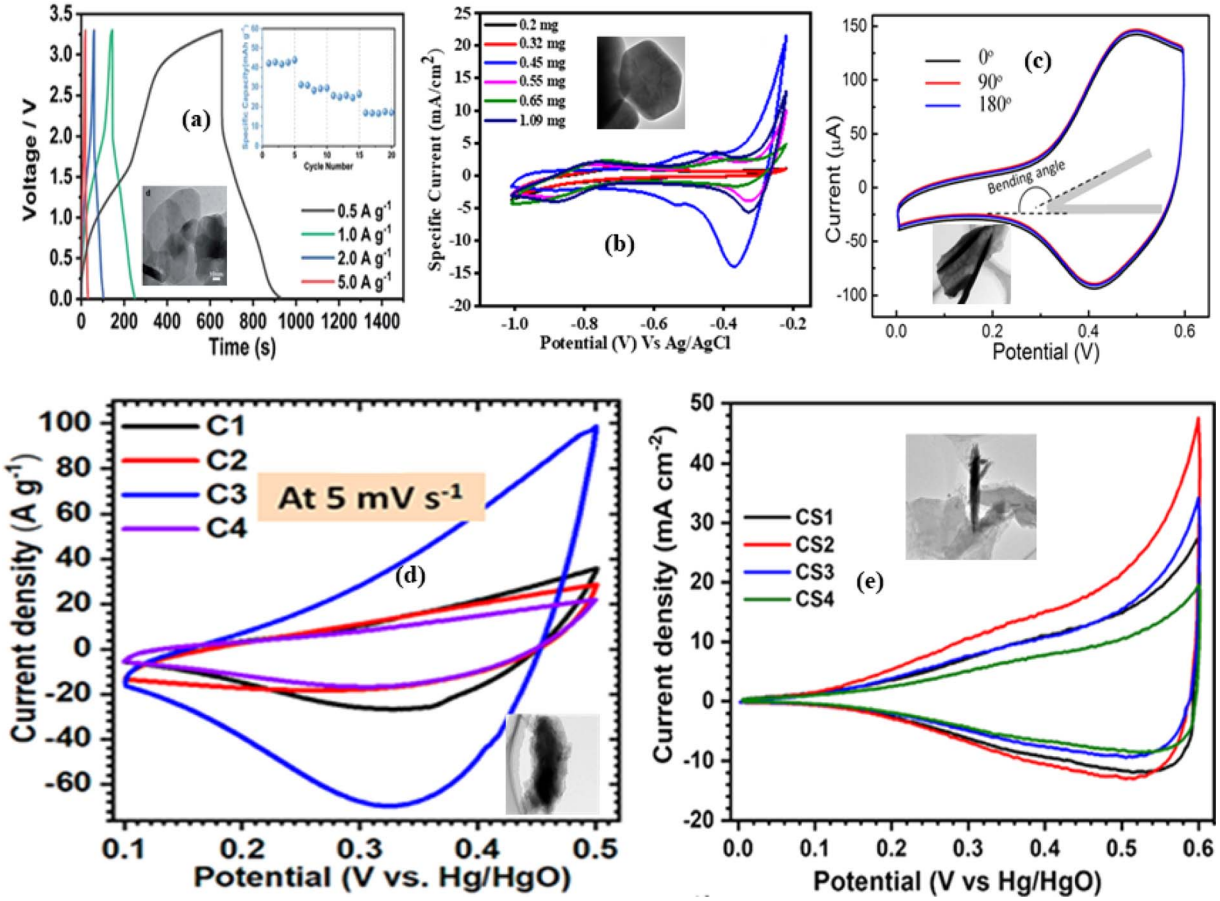

Fig. 6 (a) GCD profiles of the CuSe//$Ti_3C_2T_x$ MXene SHIC at various current densities; inset: TEM image reveals the nanosheet morphology of CuSe. Reproduced with permission.[81] Copyright 2022, Royal Society of Chemistry. (b) CuSe CV profile at various scan rates; inset: TEM image. Reproduced with permission.[82] Copyright 2024, Royal Society of Chemistry. (c) Flexibility and electrochemical stability of the CuSe NS-based solid-state supercapacitor (SSC) device assessed through CV measurements under various bending angles. The inset shows the TEM image of the CuSe nanosheets, highlighting their structural features. Reproduced with permission.[83] Copyright 2017, American Chemical Society. (d) Comparative cyclic voltammetry (CV) curves recorded at a scan rate of 100 mV s^{-1}, illustrating the electrochemical behaviour of different electrode samples; inset: morphology analysis *via* TEM of Cu_3Se_2. Reproduced with permission.[85] Copyright 2020, Royal Society of Chemistry. (e) CV curves of the CS series electrodes recorded at a scan rate of 20 mV s^{-1}, highlighting their electrochemical response, with the inset showing the TEM image of the C2 sample. Reproduced with permission.[86] Copyright 2023, Elsevier.

enables precise tuning of nanosheet orientation and morphology. The synthesised CuSe nanosheets were prepared under an optimised deposition condition at −0.15 V at 60 °C for 30 minutes. It offered a notable electrochemical capacitance of 209 F g^{-1} and a volumetric capacitance of 30.17 mF cm^{-3}. From Fig. 6(c), we can see the flexibility and stability of the device when bent at 0°–180°. This superior performance is mainly attributed to the open channel architecture provided by this vertical alignment, which increased the SSA and enhanced the ion diffusion. These results establish CuSe nanosheets as a compelling electrode material for future energy storage systems.

The study presents a distinct approach for the development of copper selenide with 3D micro-flower (CuSe-MF)[84]-like morphology. The hierarchical structures were synthesised *via* a low-temperature, wet-chemical method. This is primarily due to the high intrinsic conductivity, which facilitates rapid charge transport and significantly improves the overall performance. The CuSe-MFs were examined under 1.5 A g^{-1}, which exhibit a high electrochemical capacitance of 490 F g^{-1}. The CuSe-MF retained 88% of its initial capacity after 11 090 cycles at 10 A g^{-1}, which display its exceptional stability and rate capability.

This research showcased the significant role of synthesis conditions in optimising the materials electrochemical performance. They synthesised Cu_3Se_2 [85] films *via* a chemical bath deposition approach, by controlling the reaction bath temperature, and studied within the range of 323 K to 353 K. This approach contributes to enhancing the crystallinity, pore size, and surface morphology, which lead to elevated electron and ion kinetics. The electrochemical studies shown in Fig. 6(d) display the CV profiles examined at a potential sweep rate of 100 mV s^{-1} of the synthesised samples C1, C2, C3, and C4, throughout the operating voltage range of +0.1 to +0.5 V. Notably, C3 exhibits superior capacitive behaviour compared to its counterparts. The nature of the CV graphs displays its

pseudocapacitive nature. A flexible solid-state symmetric supercapacitor (SSC) was fabricated, which describes its significant advancement in supercapacitor technology. The fabricated SSC delivered an impressive C_s value of 132 F g^{-1}. In addition to that, the measured SSA showed 5.32 m^2 g^{-1}, which validates the correlation between the surface morphology and charge storage efficiency. This device has achieved 91% of cycling stability after consecutive 5000 cycles, highlighting its durability, which is attributed to its structural integrity and gel electrolyte stability. This study further emphasises the broader applicability of transition metal chalcogenides in energy storage technology and their commercial viability due to their abundance, eco-friendliness and scalability.

This study presents the development of a self-supported Cu_3Se_2@Cu electrode[86] using a simple yet effective self-growth method. The films prepared at deposition times of 1, 2, 4, and 6 h were denoted as CS1, CS2, CS3, and CS4, respectively. Fig. 6(e) presents the comparative CV curves of CS1, CS2, CS3, and CS4 electrodes recorded at a potential sweep rate of 20 mV s^{-1}. When the synthesised samples are examined at a potential sweep rate of 2 mV s^{-1}, sample CS2 attained a substantial electrochemical capacitance of 928 F cm^{-2}. Its durability was studied after 5000 charge–discharge cycles, which showcased its stability of 87% capacity retention. This outstanding electrochemical performance is primarily contributed to its distinctive nanosheet-like architecture, which offers a high density of active sites. It not only enhances the charge efficiency; along with that, the open cage-like structure also plays a key role in reducing the internal resistance, which leads to efficient ion transport. This work demonstrates that the optimization of the immersion time during synthesis is a critical factor for developing a material with balanced structural integrity and electrochemical performance. These findings offer a solid foundation for future energy storage technology. The studies highlight that the morphology of Cu–Se nanostructures directly dictates their electrochemical performance by influencing ion diffusion, surface accessibility, and charge transfer kinetics. Controlled synthesis strategies such as solvothermal, electrodeposition, and colloidal methods enable fine-tuning of porosity, crystallinity, and structural integrity, leading to superior stability and capacitance. From my perspective, the rational design of nanostructures combined with scalable fabrication approaches will be key in advancing Cu–Se materials from laboratory research toward practical energy storage applications.

2.3.2 Ternary and quaternary copper selenides. Ternary and quaternary copper selenide chalcogenides have emerged as potential electrode materials' for supercapacitors due to their tuneable electronic structures, increased conductivity, and rich redox chemistry. When additional metal cations are introduced into the materials crystal matrix of copper selenides, it becomes more electrochemically stable, offers high specific capacitance, and improves the rate capability. The synergistic interaction between these elements optimizes the charge storage capacity, enables low-resistance diffusion pathways, and accelerates faradaic redox reactions. Their excellence in electrochemical performance makes them interesting candidates for future energy storage applications.

This study particularly focused on copper-antimony chalcogenides, and they synthesised $Cu_3Sb(S/Se)_4$, Cu_9S_5, and $Cu_{2-x}Se$ and studied their electrochemical behaviour.[87] The Fig. 7(e) displays the successful integration of Sb into the crystal structure of Cu_3Se_4, the crystal structure of $Cu_3Sb(S/Se)_4$ offers better stability, and when studied under a potential sweep of 5 mV s^{-1}, it delivered an electrochemical capacitance of 397 F g^{-1}, which is depicted in Fig. 7(a). It validates that the incorporation of a third element in ternary chalcogenides enhanced the materials' structural integrity and electrochemical performance. It is also noted that it provided consistent performance even at different high current densities. Furthermore, this research emphasises that predominant faradaic charge storage is exhibited by chalcogenide materials, which makes them more suitable for supercapacitor applications.

This work focuses on copper–cobalt selenide hollow spheres (CCSe-HSs).[88] This ternary copper selenide with its unique structure emerged as highly promising battery-type positive electrodes for hybrid supercapacitors, when compared to the other chalcogenides. In this study, it exhibited a mesoporous hollow architecture, which facilitated a high SSA of 73.4 m^2 g^{-1}. This morphology facilitates superior charge storage and ion diffusion. This structural advantage not only enhances electrolyte accessibility but also increases the density of electroactive sites, resulting in impressive cyclic durability and rate capability. When assembled with activated carbon in a hybrid supercapacitor configuration, the CCSe-HSs achieved an electrochemical capacitance of 151.5 F g^{-1} and a notable energy density of 53.86 Wh kg^{-1} at a power density of 800 W kg^{-1}. It also showcased its remarkable rate capability by delivering E_D of 34.63 Wh kg^{-1} even at high current density. This overall functionality boost is attributed to the synergy of high SSA, porosity and rich redox activity.

This research discussed the development of nanowire-structured Cu–Co selenide.[89] The cyclic voltammetry displays the pseudocapacitive behaviour and exceptional performance of the fabricated device using CuCoSe, and the woven carbon fibre (WCF) is displayed in Fig. 7(b). It recorded a peak electrochemical capacitance of 28.63 F g^{-1}. The integration of nanowires with WFC eventually increased the tensile strength by 89.38% and the modulus by 70.41%. The device eventually achieved 191.64 mWh kg^{-1} of E_D which is coupled with a PD of 36.65 W kg^{-1}. In this study, they have optimised the Cu/Co ratio of 0.63/0.37 which promoted the expected nanowire formation. This nanostructure offers a high SSA and availability of a large number of active sites. Whenever the optimal ratio was not reached, we must compromise with the mechanical properties of the nanowires. The integration of an ionic liquid and lithium salts eventually facilitated enhanced electrolytic conductivity by forming a microchannel. It also displayed remarkable stability by maintaining 96.5% of capacitance after 2000 cycles.

In this study, the hollow spheres of bimetallic copper–cobalt selenide (CCSe)[90] were synthesised by a self-templating method. This hollow architecture contributes to a remarkable surface area increase to 70.2 m^2 g^{-1} far exceeding the 19.4 m^2 g^{-1} of

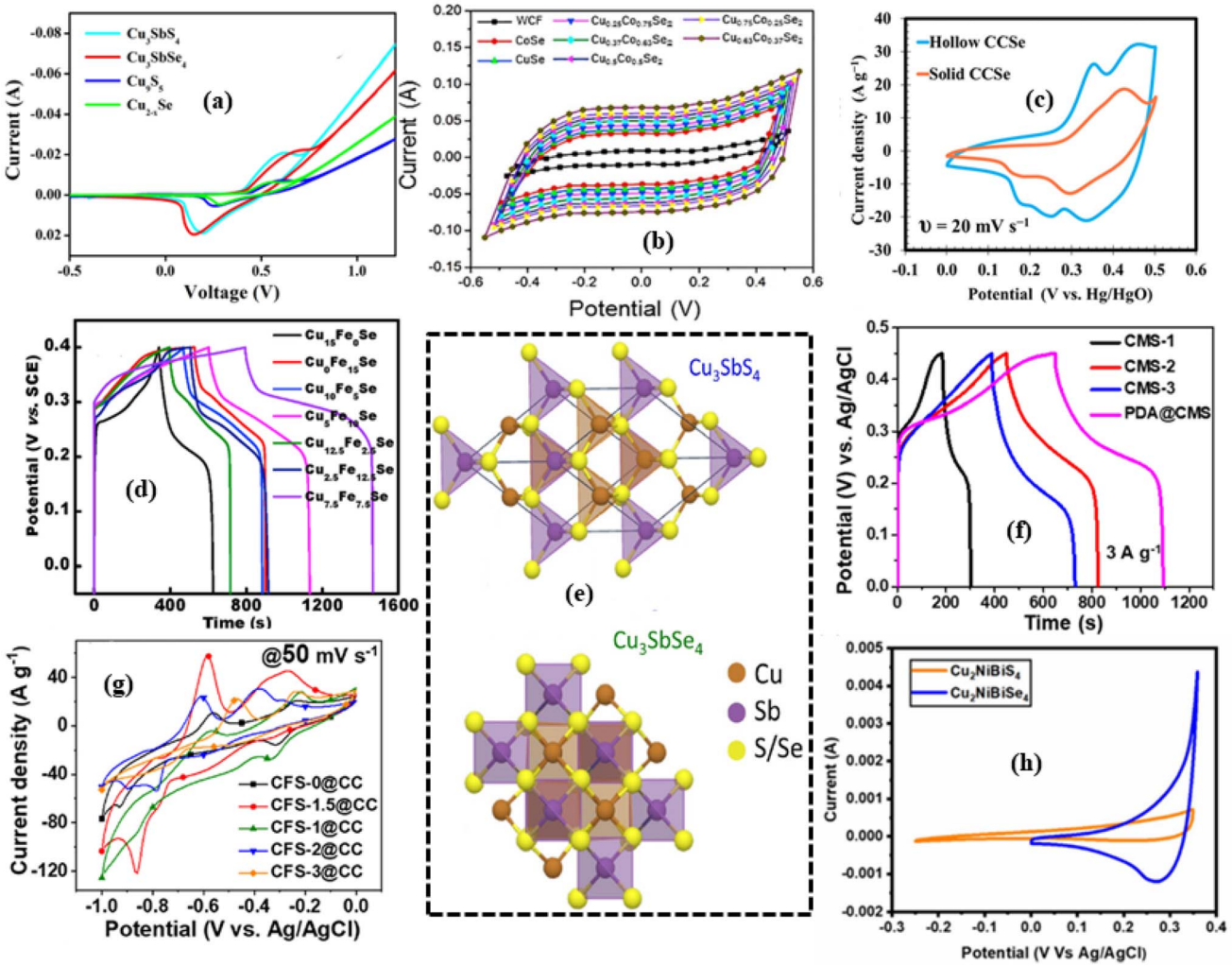

Fig. 7 (a) CV curves of $Cu_3Sb(S/Se)$, Cu_9S_5 and $Cu_{2-x}Se$. Reproduced with permission.[87] Copyright 2023, Elsevier. (b) Cyclic voltammograms of nanowire-coated WCF supercapacitors recorded at a scan rate of 10 mV s^{-1}, highlighting the electrochemical performance and charge storage behaviour of the electrode system. Reproduced with permission.[89] Copyright 2019, Elsevier. (c) CV plots of solid and hollow CCSe electrodes. Reproduced with permission.[90] Copyright 2020, Royal Society of Chemistry. (d) GCD profiles of prepared Cu_xFe_ySe. Reproduced with permission.[91] Copyright 2021, Elsevier. (e) Crystal structure of Cu_3SbS_4 and Cu_3SbSe_4. Reproduced with permission.[87] Copyright 2023, Elsevier. (f) GCD curves of the synthesised copper manganese selenide. Reproduced with permission.[92] Copyright 2025, Elsevier. (g) Cyclic voltammetry (CV) curves of various CFS@CC array cathodes recorded at a scan rate of 50 mV s^{-1}, illustrating their distinct redox behaviour and electrochemical response. Reproduced with permission.[93] Copyright 2023, Elsevier. (h) Cyclic voltammograms of Cu_2NiBiX_4 electrodes recorded in 1 M KOH electrolyte at a scan rate of 5 mV s^{-1}. Reproduced with permission.[94] Copyright 2023, American Chemical Society.

solid counterparts, thereby improving accessibility to active sites and minimizing ion transport pathways for superior charge storage and electrochemical efficiency. The CV plots of solid and hollow CCSe electrodes (Fig. 7(c)) within a 0.0–0.5 V potential window at a potential sweep rate of 20 mV s^{-1} reveal similar curves with redox peaks from Co^{4+}/Co^{3+} and Cu^{+}/Cu^{2+} pairs, indicating battery-type behaviour. Notably, CCSe hollow spheres delivered an impressive electrochemical capacitance of 562 C g^{-1} under a current density 2 A g^{-1}, along with exceptional cyclic stability by maintaining 94.5% of its capacity even after 5000 cycles. This extraordinary performance is owing to the thin shell-like structure distributed uniformly, which provides a high SSA and a high density of electroactive sites. However, this CCSe achieved an E_D value of 32.4 Wh kg^{-1} coupled with a P_D value of 800 W kg^{-1}. From this, we can understand its suitability for the next-generation energy storage device, and this study highlights the impact of structural design on electrochemical properties.

This research assessed hierarchical mesoporous Cu_xFe_ySe,[91] synthesised on a nickel foam *via* a one-step chemical deposition method. The integration of Cu and Fe into the matrix of electrode significantly tailored the electronic structure, which boosted the electron mobility and diffusion of electrolytic ions. Fig. 7(d) displays the GCD curves of the $Cu_{7.5}Fe_{7.5}Se$ electrode, from which we can see that when studied under 1 A g^{-1} it delivered a charge storage capacitance of 186.1 mAh g^{-1} and displayed its durability by retaining 63.7% of its capacity under the elevated specific current of 50 A g^{-1}. From these results we

can conclude it robust electrochemical property which can be used for high energy requirements. An ASC with AC as the anode was developed, which delivered an E_D value of 74.2 Wh kg^{-1} coupled with a P_D value of 1058.3 W kg^{-1}.

This study introduced a polydopamine (PDA)-coated copper manganese selenide ($CuMn_2Se_4$) nanocomposite electrode,[92] developed to enhance the electrochemical performance of quasi-solid-state hybrid supercapacitors (QSS-HSCs). The GCD curves at 3 A g^{-1} are presented in Fig. 7(f) which show that the synthesised material delivered an electrochemical capacitance of 3140 F g^{-1}, and this is mainly contributed to the fine tuning of copper and manganese ratios. This ratio plays an integral part in controlling the morphology and its electrochemical activity. Most importantly, the binder-free synthesis method enhanced the electrode–electrolyte interface and improved the charge transfer kinetics by eliminating the inactive mass. PDA coating enhanced the conductivity and promoted the cycling stability, after 10 000 cycles, the device retained 96.5% of its initial capacitance. This PDA coating opened up a new stage in improving the performance of supercapacitors.

This study synthesised $Cu_xFe_{3-x}Se_4$ (CFS)[93] nanoheterostructure arrays on carbon cloth *via* a binder-free strategy. Its electrochemical performance can be analysed from the CV profiles examined under a potential sweep rate of 50 mV s^{-1}, which is showcased in Fig. 7(g). The pseudocapacitive behaviours can be attributed to the reversible redox reaction, which is due to the presence of redox active species (Fe^{2+}/Fe^{3+} and Se^0/Se^{2-} or Se^{2-}/Se^0), which facilitate the efficient charge storage. To be noted, it delivered an extraordinary 84.8 Wh $kg^{-1}$of E_D coupled with a P_D of 664 W kg^{-1}. It displayed an exceptional cycle life of 86.4% of capacity retention over 10 000 charge–discharge cycles. This excellent performance is mainly due to the binder-free approach and the synergy between Cu and Fe ions which improved the conductivity, electrochemical activity, stability and facilitated more efficient ion diffusion pathways.

This study comparatively investigates Cu_2NiBiX_4 (X = S, Se) [94] and assesses its novelty as a quaternary chalcogenide. The cyclic voltammetry profiles of Cu_2NiBiS_4 and $Cu_2NiBiSe_4$ are displayed in Fig. 7(h) from which we can distinctively compare the electrochemical behaviour of the two materials. From that we can see that $Cu_2NiBiSe_4$ delivered the better capacitance of 1443 F g^{-1} than Cu_2NiBiS_4 (1221 F g^{-1}). This study focused on the synergistic interaction between the Cu and Ni, Bi which contributed to this excellent electrochemical performance.

The study is on yolk-shelled $CuCo_2Se_4$ (YS-CCS) microspheres,[95] synthesised *via* a two-step hydrothermal method. When compared to metal oxides and metal sulphides it possesses a superior electrical conductivity. The studies revealed that when the material was tested under a specific current of 1 A g^{-1}, it attained an electrochemical capacitance of 512 F g^{-1}. The YS-CCS outperformed its counterpart S-CCS. The electrode displayed a cycling stability of about 12% loss after 6000 charge–discharge cycles. This notable boost in performance can be due to the yolk-shelled structure, which also facilitated enhanced ion transport due to its hollow interiors, which eventually boosted the electrochemical kinetics. These studies suggest that ternary and quaternary copper selenides exhibit enhanced electrochemical activity. This is primarily due to its synergistic effect and optimised hierarchical nanostructures. These studies provide key insights to understand metal selenides and also open a new stage for next-generation energy storage solutions. This makes it a potential candidate for a high-performance electrode for supercapacitor applications.

2.3.3 Copper selenide composites. To overcome the conductivity constraints of CuSe and also to improve its electrochemical stability, composite frameworks will eventually provide exceptional outcomes. Here, the CuSe composites target the conductivity and Se framework stabilisation, and this will eventually optimise ion diffusion pathways. Carbon-based CuSe composites like CuSe/graphene and CuSe/CNT hybrids offer better charge transport along with reduced structural degradation. Simultaneously, the incorporation of CuSe within MXenes or conductive polymers enables synergistic charge storage through combining surface redox reaction with fast reaction rates and durable long-term cyclability. Compositional flexibility of CuSe composites allows the engineering of HSC electrodes with controlled E_D and P_D. The following sections will explore how various composite fabrication strategies influence the electrochemical behaviour of CuSe-based electrodes.

The investigation of the $NiSe_2$–CuSe nanocomposite offers valuable insights into its electrochemical behaviour, highlighting its promise as a high-efficiency material for advanced energy storage systems.[96] A key finding is the remarkable capacity of 376 C g^{-1}, which exceeds that of its individual components, $NiSe_2$ and CuSe, emphasizing the synergistic effect of their integration. This superior performance can be credited to the composite's distinctive architecture in which the cubic $NiSe_2$ is integrated with CuSe nanoparticles. This resulted in an increased porosity of the structure, promoted efficient ion diffusion pathways and facilitated abundant electroactive sites. It also achieved a cyclic stability of 71% across a wide range of current densities and demonstrated its excellent rate capability. This is due to the synergy effect of $NiSe_2$ and CuSe, which facilitated interconnected electron pathways, decreased the resistance and improved the charge transfer kinetics. Additionally, it was used to fabricate a battery-hybrid supercapacitor configuration at an operating voltage of 1.8 V. It delivered a specific capacitance of 148 F g^{-1} and also excellent durability by retaining 91.7% of its initial capacitance. Further EIS also confirmed its superior performance is due to the reduced charge transfer resistance (R_{ct}). This boost in performance is attributed to the synergy of efficient ion transport pathways by acting as an ion-buffering network, better rate capability, and better stability provided by the unique structure.

In this research we will discuss the development of TiO_2/CuSe[97] nanocomposites, which showcased its electrochemical performance and also provided a structural advantage. From the Fig. 8(a) we can see the CV graphs of the synthesised material in which CuSe ZT-3 demonstrated an excellent result by delivering a specific capacitance of 184 F g^{-1} (2 A g^{-1}). This enhanced performance is due to the synergistic effect of TiO_2 and CuSe. The integration of TiO_2 eventually prevented the

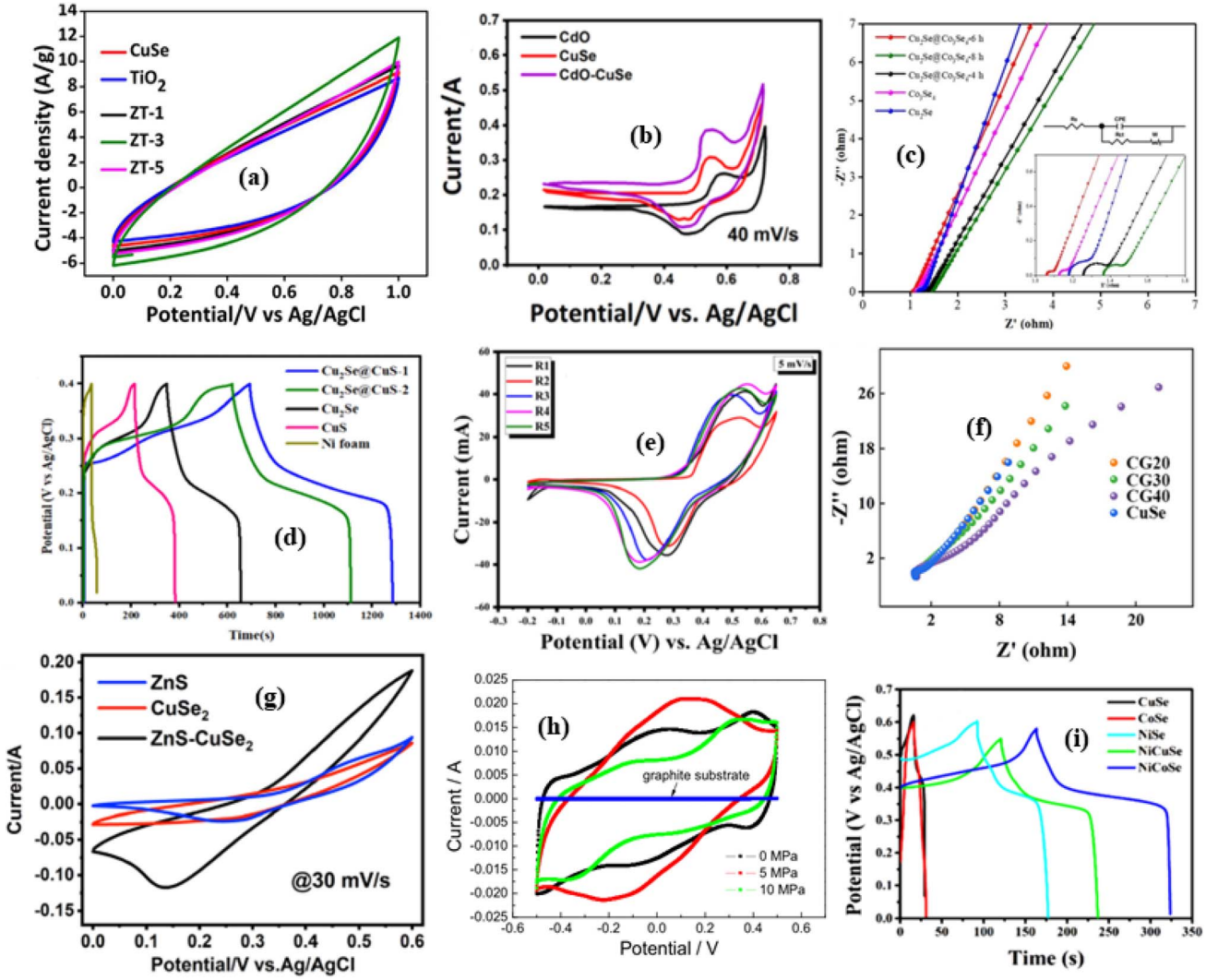

Fig. 8 (a) Comparison CV curves of CuSe, TiO_2, ZT-1, ZT-3 and ZT-5. Reproduced with permission.[97] Copyright 2022, Elsevier. (b) Comparative CV plots of CdO, CuSe, and CdO–CuSe nanocomposite electrodes. Reproduced with permission.[98] Copyright 2023, Elsevier. (c) Comparative Nyquist plot of NF, Cu–Co precursor, Cu_2Se, Co_3Se_4 and Cu_2Se@Co_3Se_4-6h. Reproduced with permission.[99] Copyright 2021, Wiley. (d) Galvanostatic charge–discharge curves compared at 2.5 mA cm^{-2}. Reproduced with permission.[100] Copyright 2020, Elsevier. (e) Comparison of CV responses at a scan rate of 5 mV s^{-1}. Reproduced with permission.[101] Copyright 2024, Elsevier. (f) Comparison EIS graph of CuSe and CuSe/GO composite. Reproduced with permission.[102] Copyright 2024, Springer Nature. (g) Combined CV curve comparison of ZnZ, $CuSe_2$ and ZnS–$CuSe_2$ at fixed scans. Reproduced with permission.[103] Copyright 2023, Elsevier. (h) CV curves of KCu_4Se_8-based supercapacitors fabricated under 0 MPa, 5 MPa, and 10 MPa pressures, along with a graphite substrate capacitor without KCu_4Se_8, studied at a potential sweep rate of 50 mV s^{-1}. Reproduced with permission.[104] Copyright 2014, Elsevier. (i) Galvanostatic charge–discharge curves of CuSe, CoSe, NiSe, NiCuSe, and NiCoSe. Reproduced with permission.[105] Copyright 2022, Elsevier.

restacking and improved the stability of the material, and CuSe facilitated fast electron transport and efficient diffusion of ions. The fabricated ASC with the composite achieved a wide voltage window of 2.2 V. This device offered a high E_D value of 27 Wh kg^{-1} and a P_D value of 7125.5 W kg^{-1}. Along with the excellent performance, it provided an excellent cycling stability of 90% capacity retention after 20 000 GCD cycles, which showcased its excellent durability.

A recent study on CdO–CuSe nanocomposites[98] revealed its strong potential as an energy-efficient electrode for hybrid supercapacitors. The synthesised composite delivered a charge storage capacity of 385 C g^{-1}, which is superior to its individual parts CdO (210 C g^{-1}) and CuSe (255 C g^{-1}). These composites provided a unique morphology inherited high surface area, which also facilitated an optimised ion diffusion and rapid electron transport. Overall, this synergy boosted the performance of the composite. The integration of CuSe nanoparticles acts as a conductive pathway that connect with CdO. It also provides abundant active sites, which enhanced the overall performance. To be noted the composite displayed an exceptional cyclic stability by retaining 94.8% after consecutive 9000 cycles at an elevated specific current density of 15 A g^{-1}. This showcases its excellent rate capability and stability required for future energy storage applications.

The synthesis of Cu_2Se hexagonal nanosheets decorated on Co_3Se_4 nanospheres[99] revealed its excellent potential for supercapacitor application. The hybrid structure demonstrated an excellent electrochemical performance, which facilitated rapid ion transport and resulted in high ionic conductivity. This unique structure takes advantage of the high ionic conductivity of Cu_2Se and the robust structural stability of Co_3Se_4, which eventually improved the overall performance. Fig. 8(c) shows the comparative EIS graph. The synergistic interaction between Cu_2Se and Co_3Se_4 results in an outstanding specific capacitance of 1005 F g^{-1} at a specific current density of 1 A g^{-1}, significantly surpassing the performance of individual materials. The comparative CV graph is shown in Fig. 8(b). Notably, the composite demonstrates outstanding rate capability, retaining 56% of its initial capacitance even at an elevated current density of 10 A g^{-1}. This efficiency is primarily ascribed to the uniformly distributed Cu_2Se nanosheets, which inhibit particle agglomeration and improve electrolyte penetration. Apart from the performance, it displayed its extraordinary durability by showcasing its loss of only 5.8% of its initial capacitance after 10 000 GCD cycles. This unique architecture made the composite $Cu_2Se@Co_3Se_4$ to deliver an impressive ED of 30.9 Wh kg^{-1} while maintaining a high-power density of 21.0 W kg^{-1}. This makes it a promising candidate for supercapacitor applications.

In this research, we will discuss about a new novel approach, in which they co-electrodeposited 3D Cu_2Se with a cauliflower morphology integrated with 2D CuS nanosheets.[100] This unique composite facilitated a large number of active sites and achieved a specific capacitance of 2727 F g^{-1} at a specific current of 2.5 mA cm^{-2}. Fig. 8(d) displays the comparison of GCD profiles of the synthesised composite with its individual materials Cu_2Se (1925 F g^{-1}) and CuS (1156 F g^{-1}).

This emphasizes the superior performance of the uniquely designed composite. This enhanced performance is mainly due to the high number of active sites, optimised diffusion of ions and efficient electron transfer facilitated by the composite structure. In addition, the co-deposition of the element on the Ni foam substrate facilitated the uniform growth of composites and acted like an ion buffering reservoir to enhance the rapid ion transport. After 8000 charge–discharge cycles, the device showed 70.2% of capacity retention. This research showcases the efficiency of the co-electrodeposition combined with binder-free synthesis approach.

The development of bimetallic $CuMnSe_2$/MWCNTs composites[101] represents a significant breakthrough in redox-active electrode materials for hybrid supercapacitors, providing a strong synergy of elevated energy storage capacity, rapid power delivery, and extended cycle life. The $Cu_{0.50}Mn_{0.50}Se_2$/MWCNTs composite demonstrates exceptional electrochemical performance. It achieved a specific capacitance of 1437.4 C g^{-1} (5 mV s^{-1}) and 1365.3 C g^{-1} (1 A g^{-1}). The comparative CV profile is shown in Fig. 8(e). This boosted performance is due to the materials high SSA of 331.79 m^2 g^{-1}, which promoted efficient electrolyte-ion diffusion. An asymmetric hybrid supercapacitor was fabricated with $Cu_{0.50}Mn_{0.50}Se_2$/MWCNTs as anode and AC as cathode. It delivered an impressive E_D of 68.3 Wh kg^{-1} at a P_D of 8.5 kW kg^{-1}, and it retained 82.3% of its initial specific capacitance after 8000 cycles, demonstrating its practical applicability, which makes it a potential candidate for supercapacitor applications.

The novel CuSe composite[102] presented in this research addresses the advancement in multifunctional materials for EMI shielding and energy storage applications. They integrated a CuSe hollow microsphere with graphene oxide GO nanosheets, which creates heterodimensional architecture. It exhibits a remarkable electrochemical capacitance of 930 F g^{-1} at a current density of 1 A g^{-1}. The peak specific capacitance was achieved for 20% GO loading with CuSe (CG20). From the EIS studies displayed in Fig. 8(f), it is evident that the integration of GO improved the electrochemical performance along with the improved stability and durability for long-term use.

A study by Ahmad *et al.* on ZnS–$CuSe_2$ nanocomposites[103] emphasizes the synergistic effect of the composite. This combination of ZnS–$CuSe_2$ enhanced the conductivity, superior redox activity and better structural integrity. The study revealed that it is mixed with cubic and orthorhombic phases, which supports its high crystallinity and purity. The CV and EIS study points out the distinct redox peaks contributed by the faradaic redox reaction and also enables the rapid charge–discharge ability. It also significantly reduced charge transfer resistance and promoted efficient ion and electron transport. When integrated into a hybrid asymmetric supercapacitor (HASC) with activated carbon (AC). Fig. 8(g) displays the comparative CV graphs of $CuSe_2$, ZnS and $CuSe_2$//ZnS, it shows that the ZnS–$CuSe_2$ electrode achieves a high operating voltage of 1.7 V, a C_s of 95 F g^{-1}, and an E_D value of 38 Wh kg^{-1}, alongside an exceptional P_D value of 3927 W kg^{-1}. It also achieved a significant durability by retaining 81.8% of initial capacitance even after 8000 charge–discharge cycles. From this study, we can consider its potential for future applications.

In this research potassium copper selenide (KCu_4Se_8) nanowires[104] developed *via* a modified composite-hydroxide mediated (M-CHM). The electrochemical studies displayed that at 5 mV s^{-1} scan rate, it delivered a specific capacitance of 25.3 F g^{-1}. This capacitance is a combination of both EDLC and pseudocapacitive behaviour of the material, which is evident from the CV profile shown in Fig. 8(h). When KCu_4Se_8 is coated with V_2O_5 it significantly boosted the specific capacitance to 93.7 F g^{-1}. This is attributed to the synergistic effect of KCu_4Se_8//V_2O_5.

This study provides a critical in-depth exploration of the electrochemical functionalities of nickel–copper selenide (NiCuSe) and nickel–cobalt selenide (NiCoSe) and nickel–cobalt selenide (NiCoSe)[105] as electrode materials for HSCs. NiCuSe and NiCoSe demonstrated promising electrochemical performance by achieving a specific capacitance of 127.2 mAh g^{-1} and 177.2 mAh g^{-1}, respectively, at a specific current density of 3 A g^{-1}. NiCoSe exhibited a superior charge storage capability, highlighting its strong charge storage capabilities. The GCD profiles are showcased in Fig. 8(i). This boosted performance is primarily due to its unique morphology, which possesses a mesoporous structure with SSA of 43 m^2 g^{-1} (NiCuSe) and 45 m^2 g^{-1} (NiCoSe). This structure promotes the redox activity, improves the electrochemical stability and also facilitates

efficient ion transport and charge storage. Further studies on the hybrid device developed using NiCuSe//modified activated carbon (MAC) and NiCoSe//MAC configurations. It delivered impressive E_D values of 26.56 Wh kg^{-1} and 28.78 Wh kg^{-1}. Its corresponding P_D are 2732 W kg^{-1} and 2571 W kg^{-1}, respectively. It is noted that NiCuSe exhibits superior conductivity, along with high-rate capability and provides better cyclic stability at elevated current densities. These findings emphasize the potential applicability of bimetallic selenides for sustainable energy solutions.

This research studied the composite of copper selenide ($CuSe_2$) and reduced graphene oxide (rGO),[106] synthesised *via* a SILAR method. The composite yielded a high electrochemical capacitance of 612 F g^{-1}. This is the result of the high surface area provided by the composite 84 m^2 g^{-1}, which enhanced the charge storage and ion transport. The fabricated flexible ACS device showcased an excellent durability of 89% of its initial capacitance even when it was bent at an angle of 165°. This is due to the layered $CuSe_2$@rGO composite, which retains its structure and performance under deformation. Apart from that, the ACS device demonstrated an exceptional E_D of 28.3 Wh kg^{-1} at a P_D of 1538 W kg^{-1}. In adiition, the self-discharging property was studied, which showed that the device retained 293 mV after 166 minutes of open circuit discharge. This is attributed to the minimal internal leakage, and these results emphasize the practical applicability in portable electronics.

This research presents a high-performance composite material of CuSe/NiVSe, which is integrated with an AC for developing a hybrid supercapacitor.[107] These composites are synthesised *via* a hydrothermal method followed by calcination, which will enhance the structural property and optimize the electrochemical properties. The introduction of selenium significantly boosted the areal (236.1 μAh cm^{-2}) and specific capacitance (94.4 mAh g^{-1}). It also maintained an excellent stability of 103.8%. Furthermore, they emphasized the use of ammonium fluoride (NH_4F) which used to promote the development of nanostructure with enlarged surface area. The manufactured device achieved an impressive ED of 40.7 Wh kg^{-1} at a P_D of 3040.4 W kg^{-1}. Further the EIS studies also confirmed its long-term operational stability. These findings showcase its potential as an effective electrode material for SC application.

In a previous study, $CoSe_2$ nanorods and CuSe polyhedrons anchored on graphene oxide (CCS@GO)[108] demonstrated exceptional electrochemical performance for hybrid supercapacitor application. This is primarily due to its high mesoporosity, which facilitated efficient electron and ion transport pathways. Moreover, this enhanced charge storage is due to the synergy of $CoSe_2$ and CuSe, which resulted in a C_s of 192.8 F g^{-1} (1 A g^{-1}). The developed composite CCS@GO electrode achieved a remarkable E_D of 54.6 Wh kg^{-1} at a P_D of 700 W kg^{-1}. Along with the performance it also demonstrated its stability by maintaining 82.5% of its initial capacitance after 10 000 cycles. These results underscore its suitability for long term applications. These studies highlight the significance of composite integration with CuSe. The results reveal that by optimising the morphology and composition will enhance the performance of the material, and when integrating it with a suitable composite it further boosts the performance.

2.4 Copper tellurides

Copper telluride exhibits more metallic-like properties compared to the other members of copper chalcogenides. Due to the larger atomic size and less electronegativity, it weakens the Cu–Te bond and exhibits delocalised electronic states, promoting the overlapping of orbitals, which facilitates a quasi-metallic conduction. Due to the higher intrinsic conductivity, it facilitates ultrafast electron transport across the electrode–electrolyte interface. Copper telluride belongs to the *Cmcm* space group and has an orthorhombic crystal structure. CuTe is intrinsically associated with copper vacancies, which act as reversible redox-active sites by facilitating a pseudocapacitive charge storage.[25] However, this quasi-metallic conductivity is observed in the bulk CuTe. When it is reduced to the nanoscale, the quantum confinement effect emerges and drastically alters the bandgap (bulk → 1.0 eV–1.5 eV & nanostructures → 2.9 eV–3.2 eV).[109,110] Additionally, the large atomic size and weak CuTe bond make it structurally unstable; often, it is a challenge to synthesise a pristine CuTe because it is prone to oxidation and phase degradation. To overcome these challenges, various composite strategies have been employed to improve the stability. CuTe, with its unique combination of properties, can be tuned to offer high energy density or high power density, as per the energy application requirements.[111] In this section, we will discuss about the impact of morphology, integration of composites and hybridisation with other metals on the electrochemical properties of copper tellurides.

In this study CuTe nanoparticles with a mesoporous structure are synthesised by the hydrothermal method.[112] When the material was tested at a specific current of 1 A g^{-1} it achieved an electrochemical capacitance of 248 F g^{-1}. The BET analysis showed its SSA as 8.0 m^2 g^{-1}. The porous structure provided by the material favours the charge storage, and facilitates electrolyte-ion mobility. This structure facilitated with hierarchical pores, with the dimensions of 3 nm–12 nm. It possesses a pore volume of 0.10 cm^3 g^{-1}. This mesoporous structure provides efficient diffusion of ions and facilitates the faradaic redox reaction. In the other study where $Cu_{2-x}Te$ nanoparticles were developed *via* hydrothermal method by the researcher[113] and examined extensively; the results revealed its potential as an efficient material. When the synthesised nanoparticle was studied at a potential sweep rate of 2 mV s^{-1} it yielded a remarkable charge storage capacity of 381 F g^{-1}. The cyclic voltammetry graph displayed in Fig. 9(a) shows its superior performance, like efficient charge storage due to the intrinsically high number of redox-active sites, and it also facilitated rapid electrochemical kinetics, primarily due to its intrinsic high conductivity. A solid-state supercapacitor is fabricated, with the gel type electrolyte PVA-$LiClO_4$, expecting the enhancement of the performance. The device delivered an energy density of 11 Wh kg^{-1} and also delivered a remarkable power density of 800 W kg^{-1}. Along with its high performance, the device exhibited a remarkable stability with 71.5%

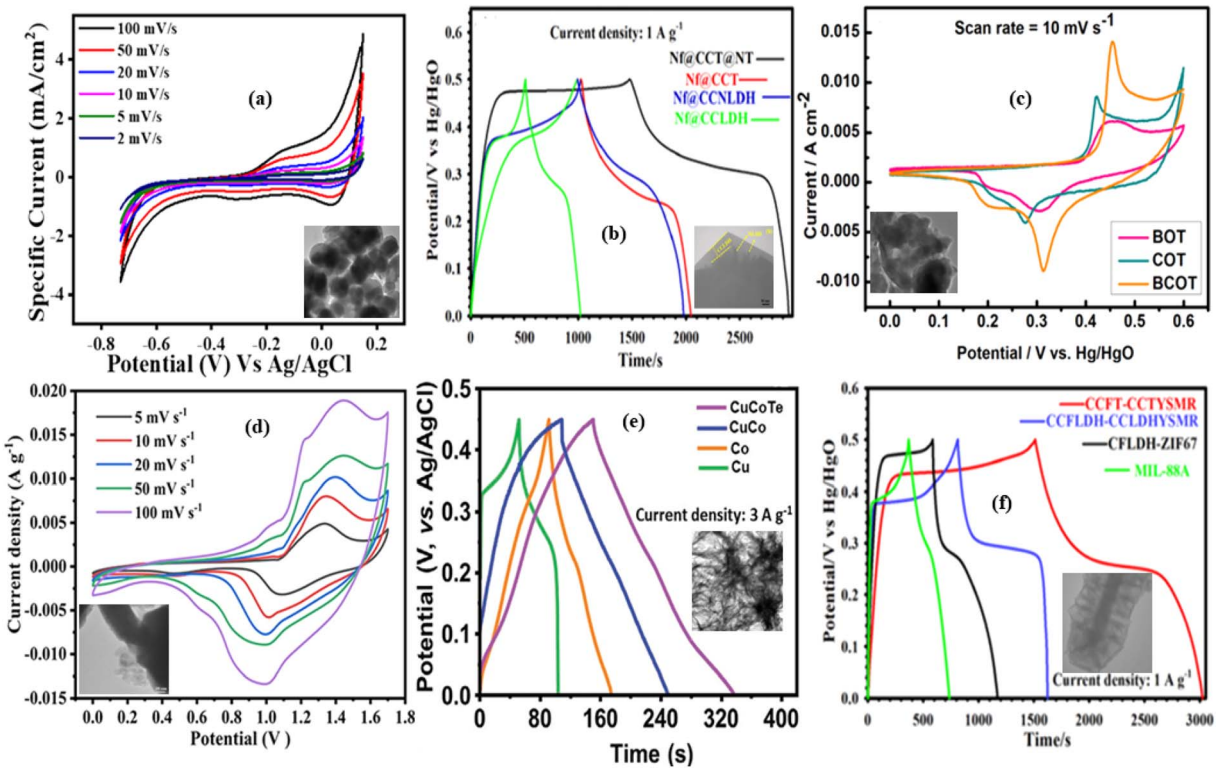

Fig. 9 (a) $Cu_{2-x}Te$/SS electrode in 2 M KCl, inset is the TEM image of $Cu_{2-x}Te$ nanoparticles. Reproduced with permission.[113] Copyright 2024, Elsevier. (b) Galvanostatic charge–discharge (GCD) plots of Nf@CCLDH, Nf@CCNLDH, Nf@CCT, and Nf@CCT@NT at current density of 1 Ag^{-1}; inset shows the TEM image of CCNLDH. Reproduced with permission.[118] Copyright 2025, Elsevier. (c) Comparative CV graphs of BOT, COT, and BCOT at 10 mV s^{-1}; inset shows the TEM image of BCOT. Reproduced with permission.[115] Copyright 2024, American Chemical Society. (d) CV curve of Cu_xTe_y//Cu_xTe- device; inset shows the TEM image of Cu_xTe_y. Reproduced with permission.[116] Copyright 2024, Springer Nature. (e) Comparative GCD graph of Cu, Co, CuCo, CuCoTe; inset is the TEM image of CTC. Reproduced with permission.[119] Copyright 2021, Wiley. (f) GCD curves of the CCFT-CCTYSMR, CCFLDH-CCLDHYSMR, CFLDH-ZIF67, and MIL-88A electrodes and inset shows the TEM images of the CCFT-CCTYSMR. Reproduced with permission.[117] Copyright 2024, Royal Society of Chemistry.

capacitance retention after 3000 cycles. This study not only shows the deep understanding of the material but also shows that how efficient copper tellurides can be used for supercapacitor application.

In another study conducted on copper oxytellurides Cu_3TeO_6,[114] the nanoparticles are synthesised by a coprecipitation method. The synthesised material, when tested at 1 A g^{-1}, exhibited an exceptional electrochemical capacitance of 1157 F g^{-1}. Even at a higher specific current of 150 A g^{-1}, it still demonstrated a remarkable charge storage capacity of 221 F g^{-1}. These results showcase its superior rate capability. Not only that, it also maintained an excellent stability of retaining 100% of initial capacitance even after a continuous 40 000 charge–discharge cycles. The results display the extraordinary stability and reliability of the material. This stability can be attributed to the intrinsic architecture of the material, which is composed of a 3D spin-web-like structure. This structure also facilitates the electron transport in a more efficient way. This exceptional performance can be due to the Synergistics effect of the Cu_3TeO_6 phase. The impedance studies also revealed its low charge transfer resistance, which improved the ion diffusion and redox kinetics. They fabricated an asymmetric supercapacitor (Cu_3TeO_6//AC), and the electrochemical studies revealed that, it delivered an E_D of 5.4 Wh kg^{-1} and an outstanding P_D of 7505 W kg^{-1}. The studies showcased that Cu_3TeO_6 nanoparticles can be an excellent candidate, which can fulfill the requirement of excellent cyclic stability and power density. A comparison study conducted between copper oxytellurides (COT), bismuth oxytellurides (BOT) and bismuth copper oxytelluride (BCOT) revealed that BCOT showed better performance than COT.[115] The comparative cyclic voltammetry (CV) curve at a scan rate of 10 mV s^{-1} is shown in Fig. 9(c), from which we can confirm the better performance of BCOT. The specific capacitance of all three has been calculated; among the three, BCOT showed a higher specific capacitance of 323 F g^{-1}, while the others can achieve only BOT (95 F g^{-1}) and COT (158 F g^{-1}). This enhanced performance can be owing to the cumulative synergy of Bi, Cu, O and Te. Also, BCOT exhibited an excellent cyclic stability, retaining 90.5% of its capacity after 5000 cycles. From this study, we can understand that this enhanced performance can be resulting from the structural advantage and synergy mechanism. Which provided by the microwave-assisted method, helped to achieve a nanosheet layered architecture, which improved the ion diffusion.

The electrochemical performance of Cu_xTe_y[116] as an anode material was studied. From the electrochemical studies we calculated the specific capacitance, and it achieved 709 mAh g^{-1}. Further studies showed that a mesoporous structure, with

an SSA of 2.0775 $m^2 g^{-1}$ and a pore size of 25.2 nm, facilitates the diffusion of electrolytic ions into the active site more efficiently. The stability of the material was also studied, and it revealed about 72.3% of capacity retention over 1000 consecutive charge discharge cycles. A symmetry supercapacitor is fabricated with Cu_xTe_y. Further the electrochemical studies of the device achieved an excellent E_D of 73 Wh kg^{-1}, which is coupled with impressive P_D 3056 W kg^{-1}. The cyclic voltammetry (CV) of Cu_xTe_y//Cu_xTe_y symmetric devise shown in Fig. 9(d) confirms its excellent behaviour. This exceptional performance is facilitated by the synergy of the material, combined with the mesoporous structural advantage, which makes them a potential candidate for supercapacitor application. The above-mentioned studies reveal that copper tellurides can be a good candidate due to its high conductivity and rich redox activity. But the pristine CuTe has its own limitations like instability and limited surface area. To mitigate these challenges, strategies like modifying its compositions like $Cu_{2-x}Te$ and introducing other elements, like Cu_3TeO_6 resulted in an excellent boost in performance and stability. However, still synthesising a pure phase and maintaining its stability remain challenges.

2.4.1 Copper telluride composites. Copper telluride is an outstanding candidate for supercapacitor applications, because of its intrinsic properties with high redox activity and high electronic conductivity. However, it possesses a few challenges, including the limited accessible surface area, structural integrity and phase stability in its pristine phase. To overcome these challenges, researchers shifted their focus towards strategically introducing secondary metal ions and hybridising with various composites to modify the intrinsic band structure and structural properties of pristine CuTe. This compositional tuning by integrating with various materials, is expected to boost the accessibility of electrochemically active sites and the synergy of copper binary and ternary tellurides, which will increase the charge carrier density and improve structural integrity. In the following, we will discuss about the experimental results that highlight the interplay between the materials and its electrochemical performance.

In this research, Jayababu and team synthesised CuCo layered double hydroxide (LDH)-coated CuCoTe honeycomb-like nanosheets (CTC HLSsNF)[119] and studied them in detail. The studies displayed that at a high specific current of 7 A g^{-1} it achieved an electrochemical capacitance of 399 mAh g^{-1}. It reveals that even at a higher current density, it exhibits exceptional performance, and the GCD profiles are also displayed in Fig. 9(e). It also maintained 81.3% of durability over 3000 cycles. This extraordinary performance is mainly due to the honeycomb-like nanosheet structure, which offered a rich electroactive site, provided an effective ion diffusion pathway, and enhanced charge storage and the fast redox reaction kinetics. In this, the electrochemically active sites were increased by metal hydroxide layers, and the nickel foam (NF) with irregularly oriented canes allows the passage of electrolytes and provides good pathways for charge-carrier transport. The vertically grown nanosheets enable more electrochemically active site availability to the electrolyte, providing enhanced pathways for the charge carriers. A hybrid supercapacitor (HSC) was developed using AC, and further studies demonstrated its exceptional performance, achieving an energy density of 214.7 Wh kg^{-1} at a high-power density of 40 kW kg^{-1}. This reveals its extraordinary suitability for a hybrid supercapacitor. When the bimetallic tellurides are hybridised, they surpass the binary chalcogenides by providing high redox activity and improved electronic conductivity.

In this study, two types of yolk-shelled microrods were synthesized CuCoFeTe-CuCoTe (CCFT-CCTYSMRs) and CoFe–CuCo layered hydroxides (CCFLDH-CCLDHYSMRs) and their properties were comparatively evaluated.[117] The study reveals that CCFT-CCTYSMRs delivered an exceptional specific capacitance of 1512 C g^{-1}, which is nearly double the amount of CCFLDH-CCLDHYSMRs (812 C g^{-1}). In Fig. 9(f), the GCD profile of CCFT-CCTYSMR is displayed. This remarkable performance is the complementary effect of this innovative architecture. The distinct design and the presence of tellurium have significantly increased the electronic conductivity, SSA, and enriched the surface with redox reactive sites. It exhibited a cycling stability of 88.95% over 10 000 cycles which is mainly associated with the innovative structure. The fabricated hybrid supercapacitor exhibited an exceptional performance by delivering an ED of 63.46 Wh kg^{-1} and a P_D of 803.80 W kg^{-1}. These results clearly indicate the potential of the ternary copper telluride and the hybridisation of copper chalcogenides.

This study discusses about the fabrication of hybrid supercapacitor from the synthesised material CuTe–CoTe nanosheet, which is decorated with $NiTe_2$ nanoflowers.[118] It revealed that this mixed metal telluride approach has significantly increased the performance, which we can be seen from the GCD profiles shown in Fig. 9(b). The electrochemical capacitance of the electrode was 1481.25 C g^{-1}, following which the fabricated device delivered an astonishing ED of 60.88 Wh kg^{-1} and PD of 801.08 W kg^{-1}. It also displayed a cycling stability of around 92.15%. Furthermore, the electrode demonstrated excellent stability and performance at higher current density of 62 A g^{-1}. This shows its outstanding rate performance. This enhanced performance can be associated with the distinct hierarchical architecture and the collaborative effect of Te and the mixed metal tellurides, which enabled rich redox activity and also provided an enhanced structural stability. From the above discussion on various composite strategies, we can understand the limitation of pristine CuTe. To overcome these limitations, integrating the pristine material with a secondary composite and hierarchical architecture enables achieving high-performance electrode materials. The ternary copper tellurides and composite materials provide a new direction towards developing a high-performance supercapacitor electrode.

The overall discussion about the copper chalcogenide class of materials indicates that their intrinsic properties such as rich redox activity, stability, facile synthesis, various morphologies and composition make them an excellent candidate for supercapacitor application. Among these materials, CuS exhibits high theoretical capacitance, CuSe offers superior electronic conductivity, and CuTe combines quasi-metallic conductivity with rich redox activity. Their performance can be further

Table 2 Comparison of the electrochemical performances of copper chalcogenides

Electrode material	Nanostructure	Synthesis method	Electrolyte	Specific capacitance (current density/scan rate)	Cyclic stability (number of cycles)	References
CuS	Nanoparticle	Wet chemical, hydrothermal method, and dual solvent method	1 M Na_2SO_4	CuS CLNTs 275 F g^{-1} (0.5 A g^{-1})	CuS HCs 99% (500 cycles)	41
	Nanotubes			CuS NTs 95 F g^{-1} (0.5 A g^{-1})	CuS NTs 94% (500 cycles)	
	Hexagonal coins			CuS NPs 70 F g^{-1} (0.5 A g^{-1})	CuS NPs 92% (500 cycles)	
	Cross-linked nanotubes			CuS HCs 57 F g^{-1} (0.5 A g^{-1})	CuS CLNTs 87% (500 cycles)	
	Nanoworms			CuS NWs 34 F g^{-1} (0.5 A g^{-1})	CuS NWs 60% (500 cycles)	
CuS	Microspheres	PVP-assisted reflux method	2 M KOH	1960 F g^{-1} (10 mA cm^{-2})	89% (10 000 cycles)	42
CuS	Hierarchically nanostructured flower-like	Chemical solution immersion method	1 M KOH	1.35 F cm^{-2} (2 m A cm^{-2})	93.2% (20 000 cycles)	43
CuS	Nano-hollow spheres	Hydrothermal method	6 M KOH	948 F g^{-1} (1 A g^{-1})	95.5% (5000 cycles)	44
CuS	Nanospheres	Hydrothermal method	6 M KOH	814 F g^{-1} (1 A g^{-1})	90.5% (2000 cycles)	45
CuS	Double-shell nanocages	Anion exchange method	2 M KOH	843 F g^{-1} (1 A g^{-1})	89.2% (4000 cycles)	46
CuS	Nanosheets	One-step solvothermal method	6 M KOH	833.3 F g^{-1} (1 A g^{-1})	70.1% (500 cycles)	47
CuS	3D hierarchical microspheres	Solvothermal method	2 M KOH	237 F g^{-1} (0.5 A g^{-1})	~88% (4000 cycles)	48
CuS	Nanoplatelets	Chemical bath deposition	1 M $LiClO_4$	55.55 F g^{-1} (3 A g^{-1})	86.09% (100 cycles)	49
CuS	Flower like	Hydrothermal method	1 M KOH	10.04 mF cm^{-2} (0.1 mA cm^{-2})	94% (2000 cycles)	139
CuS	Nanowire	Chemical route at neutral pH	1 M Na_2SO_4	380 F g^{-1} (1 A g^{-1})	35% (5000 cycles)	50
CuS	Marigold flower-like	Hydrothermal method	2 M KOH	631.2 F g^{-1} (1 A g^{-1})	82% (2500 cycles)	51
Ni:CuS	Nanoflakes	Hydrothermal method	2 M KOH	1485.35 F g^{-1} (1.0 A g^{-1})	92.96% (5000 cycles)	52
Fe:CuS	Mesoporous spherical	Hydrothermal method	2 M KOH	516.39 F g^{-1} (5 mV s^{-1})	—	53
La:CuS	Nanospheres	Microwave irradiation method	1 M KOH	1325 F g^{-1} (2 mA g^{-1})	91% (1000 cycles)	54
Co:CuS	Nanoflower	Hydrothermal method	2 M KOH	586.45 F g^{-1} (5 mV s^{-1})	—	55
Ni:CuS	Nanocube	Hydrothermal method	2 M KOH	753 F g^{-1} (5 mA cm^{-2})	—	56
Zn:CuS	Nanoflower	Hydrothermal method	2 M KOH	826.31 F g^{-1} (5 mA cm^{-2})	—	57
Cu_4SnS_4	Spherical interconnected nanoparticles	SILAR method	1 M NaOH	704 F g^{-1} (mA cm^{-2})	81% (2000 cycles)	58
$CuCo_2S_4$	Nanosheet array	Hydrothermal method (sequential ion-exchange method)	3 M KOH	3132.7 F g^{-1} (1 A g^{-1})	70.8% (4000 cycles)	61
CuWS	Nanorod nanoplate	Hydrothermal method	1 M $LiSO_4$	2666.6 F g^{-1} (10 mA g^{-1})	92.15% (10 000 cycles)	60
Cu_3SbS_4	Nanowires	Microwave-irradiation method	1 M LiOH	835.24 mAh g^{-1} (2.5 mA cm^{-2})	96.7% (1000 cycles)	59
$CuFeS_2$	Microflower	Hydrothermal method	1 M LiOH	95.28 F g^{-1} (5 mV s^{-1})	94.38% (2000 cycles)	62
CuS/Cu_2S	Nanoparticles	Hydrothermal method	2 M KOH	CuS/Cu_2S 356 mAh g^{-1} (1 A g^{-1})	96% (5000 cycles)	63
MWCNT/CuS/Cu_2S				MWCNT/CuS/Cu_2S 427.38 mAh g^{-1} (1 A g^{-1})		
g-CuS/Cc	Nanosheet	Galvanostatic electrodeposition	PVA-KOH gel polymer electrolyte	4676 mF cm^{-2} (2 mA cm^{-2})	89.8% (10 000 cycles)	64
CuS/CNT	3D hierarchical flower-like microspheres	Refluxing method assisted by PVP	2 M KOH	1960 F g^{-1} (10 mA cm^{-2})	89% (10 000 cycles)	65

Table 2 (*Contd.*)

Electrode material	Nanostructure	Synthesis method	Electrolyte	Specific capacitance (current density/scan rate)	Cyclic stability (number of cycles)	References
PIM/CuS@CNT CuS@CNT	Uniform hexagonal platelets	Solvothermal method and dip coating	2 M KOH	PIM/CuS@CNT 1.51 F cm^{-2} (5 mA cm^{-2}) CuS@CNT 0.833 F cm^{-2} (5 mA cm^{-2})	PIM/CuS//CNT 92% (1000 cycles) CuS//CNT 83% (1000 cycles)	66
Ti_3C_2/CuS composites	Multilayer Ti_3C_2 with CuS nanoparticles forming a sandwich-like structure	Hydrothermal method	1 M KOH	169.5 C g^{-1} (1 A g^{-1})	82.4% (5000 cycles)	67
CuS quantum dots// RGO nanocomposite	Nanowires	Hydrothermal method	2 M KOH	3058 F g^{-1} (1 A g^{-1})	~60.3% (1000 cycles)	68
CuS Ni–CuS nanocomposite	Hierarchical flower	Reflux synthesis method	1 M KOH	CuS 132.89 F g^{-1} (2 A g^{-1}) Ni–CuS 464.03 F g^{-1} (2 A g^{-1})	—	69
CuS//rGO	Crosslinked nanosheet/ nanoparticle composite	*In situ* chemical reaction method	6 M KOH	256 mF cm^{-2} (2 mA cm^{-2})	74% (10 000 cycles)	70
CuS@MnS	Cone-shaped nanostructure	One-step hydrothermal method	3 M KOH	89.77 mAh g^{-1} (1 A g^{-1})	95.9% (3000 cycles)	71
CuS/CoS	Nanopetal-like architecture	Two-step hydrothermal method	3 M KOH	138.75 mAh g^{-1} (1 A g^{-1})	87.56% (4000 cycles)	72
$CuFeS_2$/CNT	Microflowers	Single-step hydrothermal method	1 M Na_2SO_4	667 F g^{-1} (15 A g^{-1})	100% (3000 cycles)	73
CuFeS2@FeSe2	Hollow spheres	Binder-free hydrothermal method	3 M KOH	1306 F g^{-1} (2 A g^{-1})	91.03% (3000 cycles)	74
CTS-rGO/NF	Nanospikes structure	Electrodeposition method	1 M KOH	820.83 F g^{-1} (5 mA cm^{-2})	92.70% (1000 cycles)	75
$Cu_{2-x}Se$	Mesoporous hexagonal nanoplates	Solvothermal method	6 M KOH	495.6 F g^{-1} (1 A g^{-1})	~81.3% (2000 cycles)	78
$CuSe_2$	Nanoneedles	Hydrothermal method	1 M NaOH	1037.5 F g^{-1} (0.25 mA cm^{-2})	118% (1000 cycles)	79
Cu_2Se	Nanodendrites	Electrodeposition	1 M Na_2SO_4	688 F g^{-1} (5 mV s^{-1})	92% (4000 cycles)	80
CuSe	Nanosheets	Hydrothermal method	1 M $NaSO_3CF_3$ in diglyme (DGM)	236 mAh g^{-1} (5 A g^{-1})	91.2% (3300 cycles)	81
CuSe	Hexagonal nanosheets	One-pot colloidal synthesis	2.5 M NaOH	272 F g^{-1} (1 A g^{-1})	96% (3500 cycles)	82
CuSe	Vertically oriented nanosheets	Electrodeposition method	1 M Na2SO_4	209 F g^{-1} (0.2 A g^{-1})	~90% (10 000 cycles)	83
CuSe	Micro-flower like structure	Wet-chemical synthesis	1 M NaOH	490 F g^{-1} (1.5 A g^{-1})	88% (11 090 cycles)	84
Cu_3Se_2	Mesoporous structure	Chemical bath deposition	1 M KOH	1285 F g^{-1} (0.5 A g^{-1})	92% (3000 cycles)	85
Cu_3Se_2	Nanosheet	Chemical bath deposition	1 M KOH	928 F cm^{-2} (2 mV s^{-1})	87% (5000 cycles)	86
Cu_3SbS_4 Cu_3SbSe_4 Cu_9S_5 $Cu_{2-x}Se$	Nanoparticles	Solution-based synthesis method	1 M KOH	Cu_3SbS_4 397 F g^{-1} (5 mV s^{-1}) Cu_3SbSe_4 313 F g^{-1} (5 mV s^{-1}) Cu_9S_5 84 F g^{-1} (5 mV s^{-1}) $Cu_{2-x}Se$ 59 F g^{-1} (5 mV s^{-1})	—	87
CuCoSe (CCS)	Hollow spheres	Self-templated synthesis followed by selenisation process	6 M KOH	1680.9 F g^{-1} (3 A g^{-1})	94.7% (10 000 cycles)	88
CuCoSe	Nanowires	Hydrothermal method	Solid polyester resin with ionic liquid ($EMIMBF_4$) and lithium salt (LiTf)	28.63 F g^{-1} (0.2 A g^{-1})	96.5% (2000 cycles)	89

Table 2 (*Contd.*)

Electrode material	Nanostructure	Synthesis method	Electrolyte	Specific capacitance (current density/scan rate)	Cyclic stability (number of cycles)	References
CCSe	Microsphere	Two step solvothermal method	3 M KOH	562 C g^{-1} (2 A g^{-1})	94.5% (5000 cycles)	90
Cu_xFe_ySe	3D micro-cage/flower-like structures	Oil bath chemical deposition method	3 M KOH	186.1 mAh g^{-1} (1 A g^{-1})	91.3% (8000 cycles)	91
$CuMn_2Se_4$	Petal-like lawn structure	Binder free hydrothermal method	Polyvinyl alcohol-potassium hydroxide (PVA-KOH)	3140 F g^{-1} (3 A g^{-1})	96.5% (10 000 cycles)	92
$Cu_xFe_{3-x}Se_4$	Needle-like and flower-like clusters	Chronoamperometric (potentiostatic) electrodeposition method	3 M KOH	317 mAh g^{-1} (1 A g^{-1})	89.6% (10 000 cycles)	93
Cu_2NiBiX_4 (X = S, Se)	Cu_2NiBiS_4 aggregated particles $Cu_2NiBiSe_4$ well-dispersed sphere-like nanoparticles	Solvothermal method	1 M KOH	Cu_2NiBiS_4 1221 F g^{-1} (2.5 A g^{-1}) $Cu_2NiBiSe_4$ 1443 F g^{-1} (2.5 A g^{-1})	$Cu_2NiBiSe_4$ 98% (100 cycles)	94
$CuCo_2Se_4$ (YS-CCS)	Yolk-shelled microsphere	Two-step hydrothermal method	3 M KOH	512 F g^{-1} (1 A g^{-1})	~83.7% (6000 cycles)	95
$NiSe_2$–CuSe	Combination of cubic $NiSe_2$ and tiny CuSe nanoparticles	Wet-chemical synthesis followed by hydrothermal method	3 M KOH	376 C g^{-1} (1 A g^{-1})	91.7% (10 000 cycles)	96
TiO_2/CuSe	Aggregated arrays of TiO_2 and nanoparticle-like morphology of CuSe	Wet chemical synthesis method	3 M KOH	184 F g^{-1} (2 A g^{-1})	90% (20 000 cycles)	97
CdO–CuSe	Nanoparticle	Wet chemical assisted synthesis and hydrothermal method	3 M KOH	385 C g^{-1} (1 A g^{-1})	94.8% (9000 cycles)	98
$Cu_2Se@Co_3Se_4$	Hexagonal nanosheets (Cu_2Se) nanospheres (Co_3Se_4)	Two-step hydrothermal method	2 M KOH	1005 F g^{-1} (1 A g^{-1})	94.2% (10 000 cycles)	99
Cu_2Se/CuS	3D nanocauliflower structure (Cu_2Se) with randomly deposited 2D nanosheets (CuS)	Co-electrodeposition method	Polyvinyl alcohol (PVA)-KOH gel	2727 F g^{-1} (2.5 mA cm^{-2})	70.2% (8000 cycles)	100
$Cu_{0.50}Mn_{0.50}Se_2$/MWCNTs	Nanocomposite with cubic crystalline structure	Hydrothermal method	1 M KOH	1365.3 C g^{-1} (1 A g^{-1})	82.3% (8000 cycles)	101
CuSe/GO nanosheet	Nanorod-assembled hollow microspheres with GO nanosheets	Simple template method followed by an electrostatic adsorption process	6 M KOH	930 F g^{-1} (CG20) (1 A g^{-1})	—	102
ZnS–$CuSe_2$	Combined morphology of flakes like and aggregated nanoparticles	Sonochemical-assisted synthesis and chemical precipitation techniques	3 M KOH	640 F g^{-1} (1 A g^{-1})	81.8% (8000 cycles)	103
KCu_4Se_8	Nanowires	Modified composite-hydroxide mediated (M-CHM) method	LiCl/PVA	25.3 F g^{-1} (5 mV s^{-1})	112% (5000 cycles)	104
NiCuSe//NiCoSe	Porous structure with interconnected nanoflakes	MOF (metal–organic framework) template synthesis followed by selenization	3 M KOH	NiCuSe 127.2 mAh g^{-1} (3 A g^{-1})	—	105

Table 2 (*Contd.*)

Electrode material	Nanostructure	Synthesis method	Electrolyte	Specific capacitance (current density/scan rate)	Cyclic stability (number of cycles)	References
$CuSe_2$@rGO	Nanospheres anchored in rGO	Successive ionic layer adsorption and reaction (SILAR)	PVA-KOH	612 F g^{-1} (2 mV s^{-1})	~89% (1000 cycles)	106
CuSe/NiVSe	Mixed morphology (nanoparticles rooted on nanosheets)	Hydrothermal synthesis followed by selenization	1 M KOH	94.4 mAh g^{-1} (1 mA cm^{-2})	103.8% (8000 cycles)	107
CCS@GO	$CoSe_2$ nanorods and CuSe polyhedrons agglomerated and anchored on graphene oxide sheets	Facile hydrothermal method	3 M KOH	192.8 F g^{-1} (1 A g^{-1})	82.5% (10 000 cycles)	108
Cu_2Te	Nearly spherical nanoparticles with orthorhombic structure	Hydrothermal method	2 M KOH	248 F g^{-1} (1 A g^{-1})	—	112
($Cu_{2-x}Te$)	Nanoparticles	Hydrothermal method	2 M KCl	381 F g^{-1} (2 mV s^{-1})	85% (5000 cycles)	113
Cu_3TeO_6	Cubic nanostructure	Coprecipitation method	2 M KOH	1157 F g^{-1} (1 A g^{-1})	98% (8000 cycles)	114
Copper oxytelluride (COT)	Nanosheet-like structures	Microwave-assisted synthesis	2 M KOH	158 F g^{-1} (2 A g^{-1})	88.8% (5000 cycles)	115
Cu_xTe_y	Lamellar arrangement with attached massive particles	Microwave-assisted synthesis	6 M KOH	708 mAh g^{-1} (1 A g^{-1})	71.3% (1000 cycles)	116
CuCo LDHs//CuCoTe	Honeycomb-like nanosheets	Modified liquid-phase precipitation (MLPP), dip-coating, and electrochemical deposition (ECD)	1 M KOH	399 mAh g^{-1} (7 A g^{-1})	81.3% (3000 cycles)	119
CuCoFeTe–CuCoTe	Yolk-shelled hierarchical microrod structure	Conversion methodology involving metal–organic frameworks (MOFs) and tellurization reactions	6 M KOH	1512 C g^{-1} (1 A g^{-1})	91.86% (10 000 cycles)	117
CuTe–CoTe–$NiTe_2$	Hybrid heterostructure	Hydrothermal synthesis followed by tellurization	6 M KOH	1481.25 C g^{-1} (1 A g^{-1})	92.15% (10 000 cycles)	118

enhanced through elemental doping, morphology engineering, and integration with suitable composites. However, they have their own limitations hindering their practical applicability. Apart from these limitations, copper chalcogenides are a promising family of materials for next-generation supercapacitors.

A comparative analysis of the electrode materials, highlighting their influence on composition, morphology and synergistic combination on electrochemical performance, is summarized and displayed in Table 2. These inputs provide insights to emphasize the tunability of copper chalcogenides to enhance charge storage for future advancements in developing a high-performance supercapacitor.

3. Advanced methods for maximising SC performance – various engineering methods to maximise SC performance

3.1 Binder free synthesis

A breakthrough in the synthesis of copper chalcogenide-based electrodes is the development of a binder-free synthesis techniques, which offers a superior methodology over binder-reliant ones. Although binders provide structural advantage, they introduce many performance-affecting factors. Usually electrode manufacturing depends on the type of binders used; most commonly used are polymeric binders like PVDF or PTFE. By hindering charge transfer routes, these binders increase internal resistance and function as inactive mass, reducing effective energy and power densities. Above all, they degrade electrodes due to their chemical instability, which is an outcome of prolonged electrochemical cycling and lowers long-term performance. This approach overcomes these limitations by removing unnecessary material and directly anchoring the active material on the current collector. This led to a drastic improvement in charge transport. It enhanced electron transport and reduced the loss of resistance associated with the presence of a binder by forming a direct link between current collector and the active material. For instance, compared to binder-based alternatives, $CuSe_2$ nanostructures without a binder exhibit superior electrochemical performance with a charge storage capacitance of 1037.5 F g^{-1}. The lack of insulating polymer matrices provides maximum utilization of the active material, enabling the electrode to approach its theoretical electrochemical limits. When the focus is on long-term stability applications, the integral parameters of supercapacitor electrodes that should be considered are structural integrity and durability. A strong physical or chemical adhesion between the active material and the current collector is provided by binder-free structures, which results in avoiding structural damage upon repeated charge–discharge cycles. This structural stability ensures long-term electrochemical performance, as in the case of hierarchical $CuSe_2$ nanoneedles prepared by binder-free methods, which show excellent capacitance retention over prolonged cycling.

Likewise, copper telluride ($Cu_{2-x}Te$) nanoparticles that were hydrothermally synthesized and had a mean diameter of 38 nm and delivered a charge storage capacity of 381 F g^{-1} (163 mF cm^{-2}). On combining with a PVA-$LiClO_4$ gel type electrolyte, an E_D of 11 Wh kg^{-1} and a P_D of 800 W kg^{-1} were obtained, which was a result of the crystalline nature of the electrolyte enabling efficient charge storage and rapid redox activity. Furthermore, long-term stability achieved through binder-free synthesis was demonstrated by showcasing a capacitance retention of 71.5% after 3000 cycles. Structural control of nanostructured electrodes is achieved by binder-free synthesis, which helps to create nanostructures with a large surface area and better electrolyte accessibility. These morphological benefits are seen in micro flower-like copper sulphide (CuS) on carbon cloth (CuS@CC)[120] that are synthesized by hydrothermal synthesis, where optimizing reaction time (15 hours) results in micro flowers (diameter ~3.08 nm) and nanosheets (thickness ~34.68 nm). Ion diffusion pathways are decreased considerably while maximizing the electroactive surface area, which is a result of the hierarchical morphology, further resulting in an impressive charge storage capacity of 149 F g^{-1} at 1 A g^{-1}. Charge storage kinetics are enhanced significantly by the interlinked nanosheet architecture, which facilitates continuous electron transport channels, further ensuring quick ion diffusion and high rate capability.

Rather than just improving the electrochemical performance, avoiding the use of polymeric binders lays a path towards a sustainable approach to energy storage solutions. Environmentally hazardous solvents like *N*-methyl-2-pyrrolidone (NMP), that are usually associated with the conventional binder-based fabrication, raise challenges related to environmental sustainability and industrial scalability. Whereas microwave-assisted hydrothermal methods are environmentally friendly and affordable by reducing reaction time significantly while still allowing fine control over material morphology and crystallinity. In the production of high-performance supercapacitor electrodes, binder-free synthesis represents a breakthrough by overcoming intrinsic limitations. Binder-free copper chalcogenides serve as a significant foundation for the advancement of future power storage technologies because of improved charge transport, better electrochemical stability, optimal nano-structuring, and sustainable fabrication. Research in the future should be focused on altering synthesis conditions, which includes the precursor concentration and reaction conditions, towards further optimisation of electrochemical behaviour.[121] Furthermore, combining binder-free architectures with flexible substrates and hybrid energy storage systems might open up new avenues for use in portable electronic device, EVs, and sustainable energy storage. With further innovation, binder-free approaches have the potential to redefine supercapacitor technology, propelling the industry toward more efficient, robust, and eco-friendly energy storage solutions.

3.2 Surface engineering

Surface engineering is quite an interesting approach which mainly focuses on the electrode's surface. We are all aware that surface of an electrode material can directly influence its

electrochemical performance. The electrode material surface directly affects charge storage mechanism, electrolyte interaction and the stability. By altering the surface parameters such as surface roughness, porosity, and specific surface area, researcher can influence the redox activity, by enhancing the ion accessibility to the active site. There are a few techniques, including chemical etching, plasma treatment, and atomic layer deposition can modify the surface of an electrode, to enhance its functionality, facilitate effective ion diffusion, improve wettability and tailor its surface chemistry. Surface engineering not only improves the charge storage capacity and rate capability but also helps the electrode maintain its structural integrity, by mitigating volumetric expiation during extensive charge–discharge cycles. Which eventually enhances the life span of the supercapacitor.[122]

Surface engineering possesses a great advantage in that it will eventually boost the electrode–electrolyte interface, which facilitates rapid ion diffusion, effective for the ions to access the redox active sites. It will eventually prevent unwanted side reactions that occur while the SC is operating. This will enable the electrode material to deliver high energy density and power density. Along with this boosted performance, the stability of the electrode is crucial. At the same time, surface modifications enable hierarchically structured frameworks, that provide additional support to buffer the structural degradation during consecutive charge–discharge cycles. There are a few factors such as the presence of high surface energy, that can reduce the performance of the electrode by increasing its reactivity and leading to structural degradation. This can be overcome by surface engineering techniques, which will eventually improve the functional life span of the supercapacitor.

In brief, surface engineering will eventually boost electrochemical performance and enhance structural integrity. It improves performance by activating the electrode surface by regulating the charge transfer kinetics. This improved kinetics will enhances the charge storage capacity, energy density and power density. This approach will help to fabricate a high performing supercapacitor better structural stability by overcoming the hurdles such as chemical reactivity, degradation and mechanical instability.[123]

3.3 Defect engineering

Defect engineering serves as one of the successful approaches employed in improving the electrode material's electrochemical performance, and it is a new breakthrough technology for supercapacitor electrode improvement. By the controlled and intentional introduction of structural defects such as vacancies, dislocations, and dopants, researchers can influence the electronic, ionic, and structural properties at the atomic level. When we introduce a defect in the crystal structure will have an impact on the intrinsic properties of copper chalcogenides such as electronic structure, electrical conductivity, ion transportation pathways, energy and power densities, and cycling stability. When a defect caused by the absence of chalcogen atom it will form some intermediate states, called as metal-induced gap states and defect induced gap states. These states can promote the electrode's electrical conductivity. This conductivity increase happens because these two intermediate states reduce the contact resistance by increasing the electron mobility.

Chalcogen or metal vacancy introduction enables the creation of additional sites for ion adsorption as well as electron mobility, thereby the enhancing capacitance and total charge storage. At the same time this defect can influence the electronic configuration of the material. Copper belongs to the d-block element, where it consists of partially filled d-orbitals. These orbitals can be influenced by the defects and can increase the ion adsorption behaviour of the material. This will improve the capacitance by increasing the catalytic activity.

Metal doping, when strategically used, modulates the electronic structure by redistributing electron spin density and charges, thereby enhancing electrical conductivity, a factor critical for the minimizing of internal resistance and maximizing of the energy efficiency in supercapacitors.[124]

This method can alter the surface area or the interlayer gaps present in the material. Copper chalcogenides possess a layered structure, which will enable the material to host the electrolyte ions in a more efficient manner. This structure also facilitates a reversible redox reaction, which will eventually increase the charge storage capacity. The presence of defects lowers energy barriers for ion migration, which in turn boosts the reaction kinetics and overall rate capability of supercapacitors. Atomic layer deposition (ALD) allows the precise tuning of defect dispersion, surface area and structural integrity. This defect optimization not only enhances electrochemical properties, but also reinforces mechanical strength, prevents material degradation and enhances the stability of the electrode material.

From the research outcomes we can observe that these defect-engineered materials revealed an enhanced charge storage mechanism, high energy density, better cyclic stability which shows the significant advantages of defect engineering, and its potential for future energy storage systems.[125]

3.3.1 Vacancy engineering. Vacancy engineering distinguishes itself as a powerful technique for fine-tuning the electrochemical behaviour and maximizing the performance of supercapacitor electrodes, particularly copper chalcogenides. Vacancy engineering signifies that by strategically introducing vacancies into the crystal structure, electrode materials electronic and electrochemical properties can be tuned in a fine manner, which introduces the potential for future advancement for efficient energy storage.[126] These vacancies provide new active sites, significantly increasing the surface area. Facilitating increased charge storage and rapid ion adsorption, which plays a crucial part in enhancing the overall charge storage capacitance of supercapacitors.

Vacancy engineering has a significant effect on modulating electrical conductivity. Charge carrier mobility is improved largely, and internal resistance is reduced significantly these improvements can be attributed to the presence of vacancies such as chalcogen or metal vacancies.

In recent research it is evident that the developed vacancies display better performance than their counterparts without defect. This synergy led to an increase in the number of active sites, optimized charge transport pathways, and improved

surface reactivity, contributing to the higher capacitance retention over prolonged cycling stability. These notable improvements emphasise the significance of vacancy engineering in material design, and also offer an approach to overcome the intrinsic limitations.

In addition, with vacancy engineering, when it's combined with other strategies such as defect engineering, and heteroatom doping, it can further enhance the structural integrity and electrochemical activity. By adopting these techniques electrochemical activity of an electrode can be pushed to its boundaries, which breaks new ground for next-generation supercapacitor technology.[127]

3.3.2 Doping. One of the most well-known and widely used approaches by researchers is doping. It is a vital method that is potentially applied to promote better electrochemical activity of copper chalcogenides. This can greatly improve their energy storage capability as active materials in supercapacitor devices. The heteroatom doping into the copper chalcogenide lattice enables tuning electronic conductivity, optimization of charge kinetics, and enhancement of structural stability. When we introduce a heteroatom into the lattice, it significantly impacts few parameters like ion diffusion kinetics, density of active sites, and redox activity. These are the parameters that mainly influence the charge storage performance. By introducing dopants, we can enhance the electrode's specific capacitance, rate capability, and cycling stability. From the literature, we found that various transition metals, rare earth elements, and hybrid dopants were studied, and the results showed that they significantly enhanced the chemical and physical properties of copper chalcogenides.

When a dopant is introduced, it alters the electronic structure and defects by introducing various valence states into the Fermi level of the material. This will result in a rise in redox reaction and reduce the charge transfer resistance thereby increasing the overall performance. CuS-based materials doped with heteroatoms have increased conductivity through mixed valency, which enhances electron mobility. Doping also creates structural changes such as increased porosity and controlled morphological changes, which enhance ion conduction and facilitate electrolyte penetration. These are crucial for the operational efficiency of supercapacitors.[52]

In addition, the introduction of dopants can increase the stability of the CuS crystal structure, which eventually suppresses undesirable phase transitions during electrochemical cycling. This enhancement results in improved cyclic stability and a longer lifespan for the electrode.[53] The synergistic effects of two-element doping (co-doping) provide additional benefits by combining complementary functions *e.g.*, optimization of active sites, pore structure, and suppression of structural deterioration. The choice of dopant species and their content determines the extent of these enhancements, as different elements offer different degrees of contribution to electrochemical properties.[54]

Besides this, doped CuS nanostructures have improved properties that are morphology-sensitive, where nanostructured morphologies such as mesoporous, flake-like, flower-like, and cube-shaped architectures, show significant improvements in capacitance and charge storage. The structural modification, achieved through controlled doping processes, leads to improved accessibility of surface areas, electrolyte penetration, and redox processes, all of which are critical parameters for the improvement of overall supercapacitor electrode performance.[55–57]

4. Practical application of copper-based chalcogenides in energy storage

Supercapacitors or ultracapacitors are energy storage device that closes the gap between typical capacitors and batteries. With their exceptional power delivery, excellent cycling stability, and swift charging and discharging response capabilities make them highly suitable for different kinds of applications, including consumer electronics, electric transportation, and renewable energy systems. This section provides an overview about the practical application of supercapacitors, following that highlighting the practical demonstrations where they have been used to power up the electronic devises including LED bulbs, motor fans, digital stopwatches *etc.* In automotive sector supercapacitors plays one of the most impactful utilizations such as regenerative braking systems for electric and hybrid vehicles, which reduces the battery strain and significantly improves the energy efficiency. Furthermore, supercapacitors facilitate rapid charging, and it is incorporated as auxiliary power storage and emergency energy storage system in railways and aerospace sectors. The quick power burst of supercapacitors helps to start vehicle engines and stabilize electrical loads. From the experiments we are aware about the SCs low power capabilities and applications. It has been showcased in experiments about its small-scale application by powering up electronic devices like LEDs, fans, stopwatch *etc.* The integration of SC into portable and consumer electronics has been increased, it has been widely used in memory back up, sensors, smart watches, *etc.*, which benefits from its rapid charge capability and IoT-enabled devices utilize supercapacitors for efficient power management to ensure its stable operation during power fluctuations.

Supercapacitor's intrinsic property to charge and discharge energy instantaneously make them suitable for micro grid application. Supercapacitors also play a crucial role in stabilizing electrical grids by mitigating power fluctuations associated with intermittent sustainable energy sources like solar and wind. In remote or off-grid locations, they can effectively complement battery storage systems by enhancing overall energy efficiency and extending battery lifespan.

It is also well suited for defence and industrial applications; they are integrated in robotics which require the instant power burst. In military applications it's used to power radar, electromagnetic launcher, and communication device which operates at high frequency range.

Recent advancements in compact, micro supercapacitors have opened new doors to innovative uses in biomedical applications. Medical implants like pacemakers, neurostimulators and biosensors can utilize supercapacitors

effectively for energy storage and wireless energy transfer. Which paves new way for next generation healthcare applications.

From the literature, researchers have demonstrated the practical applicability of their fabricated supercapacitors, as illustrated in Fig. 10. A test was conducted to assess its real-time performance of the fabricated hybrid supercapacitor, as shown in Fig. 10(a–c).[107] In the other application, they installed a self-charging unit by connecting a solar panel with an output voltage of about 3.1 V in series with the developed HSC device. In Fig. 10(a and b) presents the visuals of an electric circuit containing two hybrid supercapacitors connected in a series manner along with that two solar panels connected as a charging unit (Fig. 10(a)). Then those HSC devices were serially connected to assess their integrated output and utilised to operate a small clock, which operated for 10 min (Fig. 10(b)). After it was once again charged with the help of solar panels and ran a digital timer, which lasted for 2 min (Fig. 10(c)).

Fig. 10(d and e) depict the photographs assessing the practicality of the developed ASC made up of $Ni_3Se_2/NiSe_2$@CC// CFS-1.5@CC. Two ASCs were fabricated and connected in series so as to obtain a voltage that is approximately ~3.2 V. Later serially coupled ACS device was connected with a mini motor and a digital timer. Fig. 10(d) shows the functioning of digital timer for 2 min and Fig. 10(e) displays the operation of mini motor for quite a long time. The Fig. 10(f–h), shows photographs of fabricated asymmetric supercapacitor with g-CuS/Cc-SC at different bending angles demonstrate[64] its mechanical flexibility, demonstrating its potential utility in real-world applications, particularly in flexible energy storage technologies. ASC devices and yolk-shelled $CuCo_2Se_4$ (YS-CCS) microspheres,[95] were put together in sequence (Fig. 10(f–k)). This system demonstrated its high specific capacitance by successfully lighting yellow, green, and blue light-emitting diodes (LEDs) in tandem for over 40 minutes. All of these experimental setups showcased above have demonstrated the

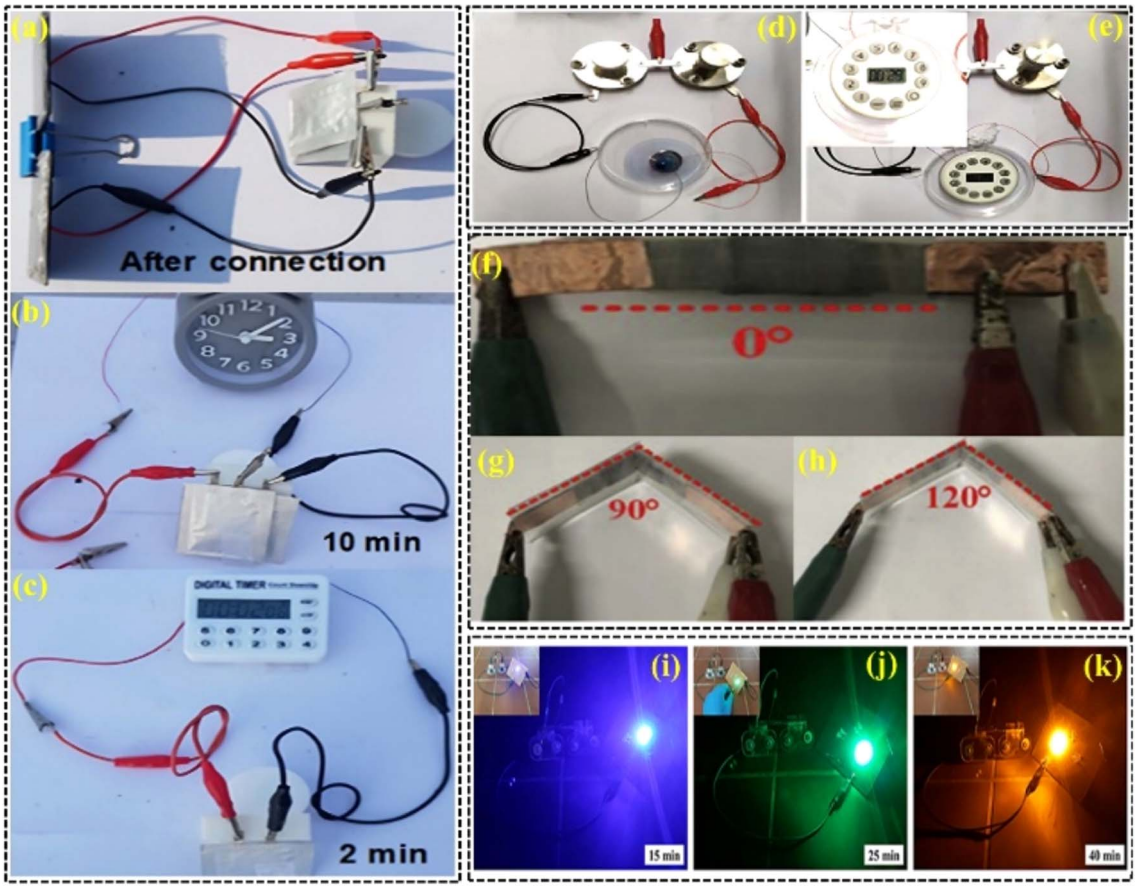

Fig. 10 (a) CuSe/NiVSe//AC HSC charging using a solar cell. Reproduced with permission.[107] Copyright 2023, Elsevier. (b) CuSe/NiVSe//AC HSC powered a clock for 10 min. Reproduced with permission.[107] Copyright 2023, Elsevier. (c) CuSe/NiVSe//AC HSC-powered digital timer for 2 min. Reproduced with permission.[107] Copyright 2023, Elsevier. (d) $Ni_3Se_2/NiSe_2$@CC//CFS-1.5@CC ASC device-powered motor fan. Reproduced with permission.[93] Copyright 2023, Elsevier. (e) $Ni_3Se_2/NiSe_2$@CC//CFS-1.5@CC ASC device powered a digital clock. Reproduced with permission.[93] Copyright 2023, Elsevier. (f) Photographs of g-CuS/Cc-SC at a bending angle of 0°. Reproduced with permission.[64] Copyright 2019, Elsevier. (g) Photographs of g-CuS/Cc-SC at a bending angle of 90°. Reproduced with permission.[64] Copyright 2023, Elsevier. (h) Photographs of g-CuS/Cc-SC demonstrating its flexibility by bending at 120°. Reproduced with permission.[64] Copyright 2023, Elsevier. (i) ASC devices (YS-CCS) lighting a blue LED. Reproduced with permission.[95] Copyright 2024, American Chemical Society. (j) ASC devices (YS-CCS) lighting a green LED. Reproduced with permission.[95] Copyright 2024, American Chemical Society. (k) ASC devices (YS-CCS) lighting a yellow LED. Reproduced with permission.[95] Copyright 2024, American Chemical Society.

ability of supercapacitors to power electric motors, LEDs, and other small electronic devices for short durations, reinforcing their suitability for high-power, pulse-energy applications.

5. Machine learning approach for SC performance predictions

A huge reformation has been brought up by Machine learning (ML) in our understanding and optimization of energy storage systems, especially in prediction and optimization of supercapacitor. Supercapacitors that are known for their rapid charging and discharging ability has widely been used from smartphones to electric vehicles. Nevertheless, their performance varies depending on factors such as material structure, electrode geometry, and operating conditions. ML comes to play here by processing large data sets that helps scientists to find patterns and make very accurate predictions on the performance of supercapacitor.[128] ML algorithms such as Regression Trees (RT) and XGBoost are apt for predicting the capacitance with highly correlated coefficients (R) of up to 0.997 says recent studies and that too where the predicted results are way too impossible to distinguish from reality.[129] The entire potential of ML in supercapacitor prediction can only be attained through a systematic process that involves three major steps: data collection, feature extraction, and model deployment, and all of this are mandatory to guarantee correct and reliable predictions. Fig. 11(a) depicts a schematic workflow of machine learning.

5.1. Data collection and data cleaning

The key and base element to any ML model is a clean and varied dataset. Supercapacitor performance prediction data are collected from open-access libraries like ChEMBL, ICSD, OQMD, and COD, and reported experimental data. Vital information concerning the material properties, synthesis, and electrochemical properties are contained from these datasets. The preprocessing of the data is important to remove the errors, to interpolate the missing values and to standardize the unit as raw data are incomplete and inconsistent. A quality large dataset gives the ML model good generalization capability and gives useful information instead of overfitting to a small number of experimental conditions.

5.2. Feature selection

To predict accurate supercapacitor performance the selection of the valid input features is necessary. Studies have shown that certain factors including specific surface area (SSA), pore size (PS), nitrogen doping concentration, pore volume (PV), and I_D/I_G ratio, electrolyte, synthesis method of material and the type of electrode system (2 or 3 electrode system) considerably affect the specific capacitance. Amongst, SSA having a direct impact on charge storage capacity be considered the most important factor. ML techniques enable us to dwell into complex relationships between features and electrochemical characteristics, which helps researchers to design material properties for improved energy storage.

5.3. ML models

The specific capacitance and total supercapacitance performance can be predicted effectively using various ML models if properly organized dataset and input features are set. Some of the best methods are Decision tree (DT), Random Forest (RF), Support Vector Machines (SVM), Artificial Neural Networks (ANNs), the Levenberg–Marquardt Back-Propagation (LM-BP) algorithm, Recurrent Neural Network (RNN) *etc.* have demonstrated to be very accurate in specific capacitance value prediction. SVM,[130] if combined with Grey Wolf Optimization (GWO), show a strong potential to effectively detect complex non-linear correlations between electrochemical performance and material characteristics. In the following we will discuss briefly about the major algorithms.

5.4. Artificial neural network (ANN)

Among the various algorithms, ANN is a simulation that functions like the neural networks present in human brain. This neural network is made up of numerous simple nodes which interact with each other through a complex interconnection. ANN is mainly function through three layers namely: input layer, hidden layer and output layer. These three layers will have its unique functions where the first layer receives the data or signal from the external sources. The following layer is the hidden layer, in which the neurons will learn by varying the weights and capturing the complex and difficult patterns from the input data. The results are provided by the output layer. The process of data is carried out with the help of activation functions required for nonlinear transformation, in which the data will go through each layer after layer in the hidden layer region and in the end the predicted results were generated by the output layer neurons. To make sure the accuracy of the results, the real label is compared to accurately calculate the errors occurred during the process. This comparison is calculated in reverse from the output layer to the input layer with the help of back propagation algorithm. These steps are carried out to optimize the algorithm by reducing the errors present in the results until it attains the criteria which should be lower than the threshold which is already set.[131]

5.5. Support vector machine (SVM)

Structural risk minimisation is the key principle based on which this learning algorithm support vector machine works, and it will be supervised. It is used for the analysis of regression and classification. Fig. 11(d) shows the way of finding an ideal separating line (optimal hyperplane). Along with the hyperplane, support vectors will be present on either of it. The data present on the support vectors are the closest data to the hyperplane. These close points decide the direction of hyperplane. With the use of Kernel function, SVM can map the nonlinear data to a higher dimension and can be separated linearly which shows its nonlinear data handling capability, regression and classification further helping to reduce the memory storage space along with reducing the computation.

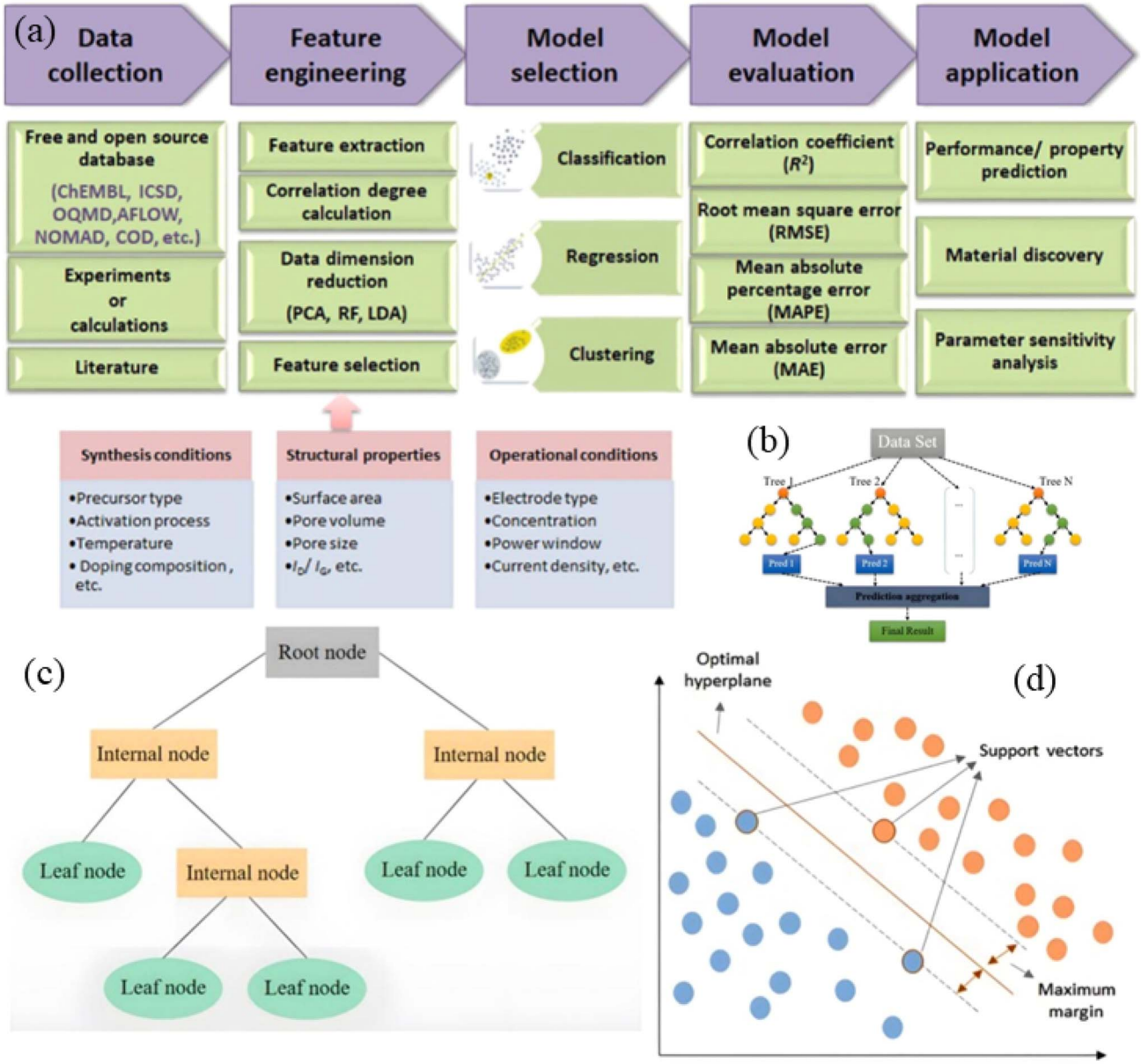

Fig. 11 (a) Systematic framework for predicting supercapacitor performance using ML. Reproduced with permission.[134] Copyright 2024, Elsevier. (b) Schematic of random forest. Reproduced with permission.[130] Copyright 2025, Elsevier. (c) Schematic representation of decision tree. Reproduced with permission.[130] Copyright 2025, Elsevier. (d) Schematic representation of SVM. Reproduced with permission.[130] Copyright 2025, Elsevier.

SVM will work well with the small dataset whereas it shows complications in computation for larger the data.

5.6. Decision tree (DT)

DT is a supervised learning algorithm mainly used for regression and classification of the data. DT performs the classification and regression by repeatedly splitting the input data sets into various subsets. From the Fig. 11(c), it can find that the algorithm looks like a tree in which nodes will be present. Each node will be representing a feature along with there will be an edge signifying a decision rule, and the output will be indicated by the leaf nodes. The initial point will be the root node and the conditions to test will be represented by the internal nodes whereas the result will be represented by the leaf nodes. DT construction includes three steps such as feature selection, node splitting and recursive portioning. When the algorithm begins from the root and choose the best feature to split the data, according to the feature selected the data will be divided into various subsets which will be continuously repeated until a predefined stopping rule is triggered. This algorithm is easy to understand but at the same time it is prone to less accurate results.[132]

Random Forest (RF)[133] is an ensemble learning method that considers numerous decision tree along with which predicts the

results which is depicted in the Fig. 11(b). So, in this algorithm the datasets are randomly sampled, and DTs are trained with that. This method helps to overcome the overfitting and improves the ability to generalise the new data. In this algorithm, DT act as the building blocks with model based on classification of data or regression data. RF uses bagging method to create various training data sets which is obtained through random sampling. As the RF algorithms constructed with various DT training data sets which implements randomness in the training datasets. RF is a powerful learning algorithm which is made up of different DT and combining with that it forecast the results, one of the advantages of RF is it can handle datasets of large amount, high-dimensional data and also can do the complex problems.

Multi-Layer Perceptron (MLP) is a powerful neural network design that can identify subtle patterns in high-dimensional data. If such models are implemented in a systematic way, then the scientists will be able to predict supercapacitor performances with much greater accuracy that can reduce our dependence on time-consuming experimental trials. This data-driven approach not only accelerates material discovery but also optimizes the electrode design for real-world applications.[134]

Different ML methods have their own upper hand in supercapacitor research. For example, ANNs are better employed to identify complex correlations between data compared to conventional methods such as Linear Regression (LR) and Lasso. By identifying a minute detail and improving prediction outcomes, advanced techniques such as hybrid models like CNNs and Long Short-Term Memory (LSTM) networks extend these capabilities. The perpetual learning property to get better by responding to new data can be considered as a distinct capability of ML-based models. The incorporation of ML in the study of supercapacitors considerably improves the identification of materials with better performance and the optimization of energy storage devices with unparalleled efficiency and accuracy. This collaboration between technological innovation and materials science brings out more efficient, durable, and sustainable energy solutions for emerging applications.

Literature have shown that ML have the capacity to significantly improve predictions of copper-based sulphide photocathode performance, and among the most accurate analytical models is the RF model which shown to have an 96.7% accuracy when it was applied to the test dataset, thereby proving its capacity to identify complex data structures. The synthesis procedures, thickness of layer, grain diameter, and acidity level which are known to have great influence on the photocathode efficiency were noted as input parameters. The model gives valuable takeaways on how material properties play a vital role in overall photocurrent density, there by facilitating more efficient photocathode design development.[135] By varying the input parameters of supercapacitor, the same ML model may be used in predicting the supercapacitance performance of the chalcogenide based materials to make it suitable for energy storage. Rather than highlighting the properties suitable for photocathodes, the model would highlight properties related to electrode composition, surface area, porosity, electrolyte type, and redox-active sites. Fig. 11(a) illustrates the framework to predict the SC performance. By training a ML model represented by RF on a dataset (from the literature) with the aforementioned properties related to supercapacitors, researchers can likely to make highly accurate predictions of supercapacitance performance. More than just speeding up the whole discovery of supercapacitor materials with superior performance, this approach would also optimize their design based on trial and error. By combining various disciplines in the area of energy research, ML is increasingly becoming a wonderful tool in the development of sustainable energy technologies. While machine learning has achieved great success in predicting the properties of carbon-based supercapacitors, its use for pseudocapacitive materials remains limited. This is largely due to the lack of quantitative data available in the literature.[136] To address this issue, future research could use available materials databases like the Materials Project, AFLOW, and OQMD.[137]

Fig. 12 Challenges hindering the practical application of copper chalcogenide-based supercapacitors: a schematic view.

These databases offer computed structural and electronic descriptors, such as band gaps, redox-active states, and ion migration barriers, which can be linked to the performance of pseudocapacitors. Using these alternative descriptors, along with transfer learning and physics-informed ML, could greatly improve predictive ability in pseudo capacitor research.[138]

6. Challenges

From the literature we can see that copper chalcogenides have the capability to develop into a promising electroactive material for supercapacitor application. At the same time, we can see that, there are few challenges we have to overcome. We will briefly discuss about the challenges below, by which we can utilize copper chalcogenides as an efficient electrode material. A schematic representation of the challenges is depicted in Fig. 12.

6.1 Stoichiometric control and phase purity

Copper chalcogenides exist in different stoichiometric ratio, which shows that the stoichiometric ratio have a huge effect on the electrochemical performance. But the existing synthesis processes are unable to provide strict compositional control, which results in the formation of different phase mixtures that affect performance consistency. A synthesis process that provides more control over the phase formation and it should be scalable, need to be developed.

6.2 Structural instability and volume expansion

Over a long period and upon repeated charge–discharge cycles copper sulphides and selenides undergo severe volume expansion and phase changes, in turn causing electrode degradation and capacity loss. Structural reinforcement *via* composite formation and buffer layer integration must be attempted.

6.3 Material dissolution and electrolyte compatibility

Electrochemical stability is lowered for several copper chalcogenides materials as they dissolve in aqueous electrolytes with time. To enhance their longevity protective surface modifications and electrolyte compositions should be developed.

6.4 Complex and expensive fabrication

For copper chalcogenide-based nanostructures, current fabrication methods ought to be multi-step, high-temperature, and energy-intensive, making them not scalable. Studies on green, scalable, and affordable synthesis processes like electrochemical deposition and microwave-assisted synthesis are required.

6.5 Integration with next-generation energy storage devices

Amidst the fact copper chalcogenides have showcased superior supercapacitor behaviour, their integration into hybrid energy storage devices like battery-supercapacitor hybrid devices and multi-functional energy storage platforms is unknown. Elaborating their compatibility and combined effects in such devices is a significant research prospect.

7. Conclusion and future outlook

The review reveals that among all the three copper chalcogenides, CuS is the most extensively studied material, due to its rich redox chemistry, stability and abundance. Among copper chalcogenide materials, CuS has the high theoretical capacitance which is primarily due to its layered structure and multiple oxidation states. From the studies, it is evident that its performance can be influenced by tuning the morphology such as nanosheets, nanocages, hollow spheres, and cross-linked nanotubes. Among all these morphologies, nanosheets have demonstrated an excellent performance due to high specific surface area thereby it gives more active sites. Upon comparison, CuSe is less explored but a promising electrode material due to its high intrinsic electrical conductivity and rate capability than CuS. This high intrinsic conductivity is due to the delocalised 4p orbitals of Se. However, copper selenides are less stable than the sulphides. In the case of CuTe, it provides the highest conductivity among the other copper chalcogenides. This is primarily due to the quasi metallic like bonding. But this high conductivity is for bulk CuTe, when it comes to the nanostructure the quantum confinement effect widens the bandgap and significantly reduces the conductivity. Apart from these CuTe faces major challenges in retaining its stability and synthesising pristine material is quite challenging. The intrinsic properties of the copper chalcogenide family make it stands out from the other class of materials like metal oxides, hydroxides and MXenes. When compared to the carbon-based material which is well established and commercialized, copper chalcogenides provide significantly high energy density due to the faradaic redox reaction. Even though the transition metal oxides and hydroxides exhibit better conductivity and high-rate capability, when it comes to the synthesis and stability copper chalcogenides have its advantages like ease to synthesis, structural tunability and stability. When compared to MXene class of materials copper chalcogenides exhibits superior performance, primarily due to its structural diversity, rich redox chemistry, high electronic conductivity and structural integrity.

The analysis of copper chalcogenides for supercapacitor application reveals that, this family of materials (CuS, CuSe, CuTe) have emerged as a promising candidate for high performing electrode for supercapacitor applications. The overall intrinsic properties such as presence of multiple oxidation states of copper (Cu^{+}/Cu^{2+}) and participation of the chalcogens (S, Se and Te) in the redox activity, layered structure, structural tunability, ease to synthesise, cost-effectiveness, abundance and environment-friendliness.

The analysis reveals that the ternary and quaternary copper chalcogenides demonstrate better performance than the binary copper chalcogenides. Among the ternary material $CuMn_2Se_4$ with a specific capacitance of 3140 F g^{-1} and $CuCo_2S_4$ achieved a specific capacitance of 3132.7 F g^{-1}, sets a significant benchmark and represents the current state of the art. This remarkable electrochemical performance is due to the synergy

of multiple metal composition and unique morphology an array of nanosheet grown on Ni foam by a binder-free approach. This combined all strategy enhanced the electronic conductivity, redox activity and provided a superior structural integrity. Among the other materials, Cu_3TeO_6 displayed an exceptional cyclic stability by retaining 100% of its initial capacitance even after 40 000 cycles, and this eventually did set a new benchmark for stability, which is one of the critical challenges in supercapacitor applications. From the analysis, we can also see that the tailoring of the morphology significantly boosts the overall performance. Among the nanostructures hierarchical hollow architecture consistently delivers the superior performance. The analysis from simple nanoparticles to complex nanostructures like crosslinked nanotubes, hollow nanocages, microflowers and hollow spheres clearly indicates the progress in morphology engineering with an understanding of the relationship between the structure and performance. Whereas these specific unique structures facilitate high specific surface area, improved ion accessibility and efficient electron pathways. The binder-free approach has also emerged as an excellent strategy to further enhance the performance by providing the direct contact with the current collector. The studies on introduction of heteroatoms into the lattice reveal an excellent strategy to optimise the performance. The transition metals like Ni, Co and Mn, when doped in the crystal lattice it not only introduces new redox active sites but also tailors the internal band structure, which facilitates efficient charge transfer kinetics. These findings highlight that exploring various dopants and its concentration is an excellent strategy to tailor the properties of copper chalcogenides. The analysis on the composite strategy clearly indicates the limitations of pure copper chalcogenides. The intrinsic limitations like moderate electrical conductivity and structural instability over prolonged charging and discharging cycles indicates the requirement of integration with other materials. The integration of carbon-based material like, graphene, carbon nanotubes, metal oxides and MXenes with copper chalcogenides exhibited a significant improvement in the performance. This composite strategy provides a clear understanding of the synergistic effect of composite materials and provides insights to synthesis advanced composite architectures.

Copper sulphides (CuS), selenides (CuSe), and tellurides (CuTe) have each been shown to provide a unique set of benefits allowing them a feasible choice to integrate with ASC with increased energy density. Their integration with materials based on carbon, intrinsic conducting polymers, and other transition metal chalcogenides has greatly improved electrochemical stability, facilitated more efficient charge transport, and enhanced long-term cycling durability. Creation of hierarchical nanostructures which includes hollow spheres, nanorods, and nanosheets considerably improved charge storage capacity by reducing the resistance of ion diffusion and also providing high electroactive surface area, are some of the recent advancements in the past years. Also, composite materials with copper chalcogenides and graphene, carbon nanotubes (CNTs), and MXenes have shown significant improvement in conductivity and stability and hence can be considered to be potential alternatives to traditional electrode materials. Several challenges still remain for the commercialization of copper chalcogenide-based supercapacitors. The stoichiometric control, structural decay during cycling, and material instability across various electrolytes need to be resolved so as to attain long-term reliability and high efficiency in energy storage. In addition to that, the synthesis routes should be of cost-effective, up scalable, and strategically designed to enable commercialization of these materials in supercapacitor technology. In order to gain greater clarity on the charge storage mechanism in the future, it is impotant to optimise synthesis methods for the

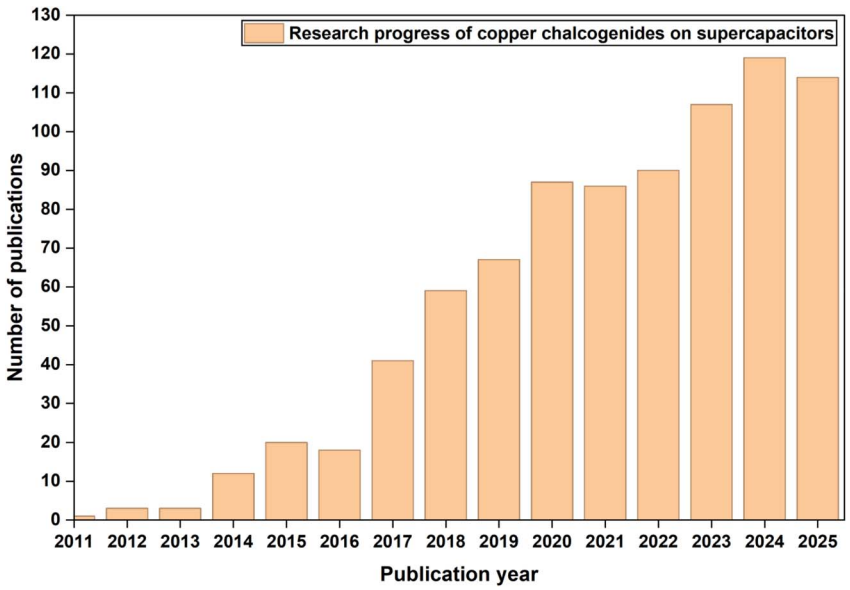

Fig. 13 Research progress in copper chalcogenides for supercapacitor application (source: https://www.scopus.com/home.uri).

materials, explore new hybrid architectures and focus on developing a theoretical models. Apart from this the integration of solid-state and flexible supercapacitor into wearable electronics and automotive applications is an attractive path for next-generation energy storage. Copper chalcogenides have emerged as desirable materials with significant contributions to the advancement of sustainable energy systems which results in continuous development in electrochemical energy studies. The consecutive increase in research progress over the years in the field of copper chalcogenides for supercapacitor, displayed in Fig. 13, demonstrates its potential to be an excellent material for next-generation supercapacitors.

In order to improve mechanical stability, conductivity, and electrochemical efficiency, future developments in copper chalcogenide-based supercapacitors will concentrate on creating high-performance hybrid and composite materials by combining MXenes, metal–organic frameworks (MOFs), and conductive polymers. The development of wearable and flexible supercapacitors using copper chalcogenide electrodes will make it possible to use them in biomedical devices, wearable sensors, and smart fabrics. Furthermore, the fabrication of solid-state supercapacitors using asymmetric/hybrid designs and solid electrolytes would increase energy densities and improve safety for real-world applications by widening the working voltage window. *In situ* characterisation combined with theoretical and computational modelling will yield deeper mechanistic insights into charge storage processes, directing the logical design of next-generation materials. In order to promote the commercial use of copper chalcogenide-based supercapacitors, future research must also focus on sustainable and scalable manufacturing methodologies, combining low-cost precursors, environmentally friendly synthesis procedures, and industrially feasible fabrication methods.

Conflicts of interest

There is no conflict of interest to declare by all the authors.

Data availability

No data were used in this article.

Acknowledgements

MRM acknowledges Manipal Academy of Higher Education for providing Dr TMA Pai doctoral fellowship.

References

1 S. Reenu, L. Phor, A. Kumar and S. Chahal, Electrode materials for supercapacitors: A comprehensive review of advancements and performance, *J. Energy Storage*, 2024, **84**, 110698, DOI: 10.1016/j.est.2024.110698.
2 P. Lamba, *et al.*, Recent advancements in supercapacitors based on different electrode materials: Classifications, synthesis methods and comparative performance, *J. Energy Storage*, 2022, **48**, 103871, DOI: 10.1016/j.est.2021.103871.
3 M. Yaseen, *et al.*, A Review of Supercapacitors: Materials Design, Modification, and Applications, *Energies*, 2021, **14**(22), 7779, DOI: 10.3390/en14227779.
4 X. Zhu, X. Zhang, Y. Li and Y. Liu, Exploring transition metal oxide-based oxygen vacancy supercapacitors: A review, *J. Energy Storage*, 2024, **80**, 110350, DOI: 10.1016/j.est.2023.110350.
5 W. Raza, *et al.*, Recent advancements in supercapacitor technology, *Nano Energy*, 2018, **52**, 441–473, DOI: 10.1016/j.nanoen.2018.08.013.
6 Poonam, K. Sharma, A. Arora and S. K. Tripathi, Review of supercapacitors: Materials and devices, *J. Energy Storage*, 2019, **21**, 801–825, DOI: 10.1016/j.est.2019.01.010.
7 A. Choubey and A. Yadav, MXene and transition metal chalcogenides-based 2D nanomaterials for next-generation supercapacitors, *J. Energy Storage*, 2024, **79**, 110131, DOI: 10.1016/j.est.2023.110131.
8 S. Mohapatra, H. T. Das, B. C. Tripathy and N. Das, Recent Developments in Electrodeposition of Transition Metal Chalcogenides-Based Electrode Materials for Advance Supercapacitor Applications: A Review, *Chem. Rec.*, 2024, **24**(1), e202300220, DOI: 10.1002/tcr.202300220.
9 D. V. Chernysheva, N. V. Smirnova and V. P. Ananikov, Recent Trends in Supercapacitor Research: Sustainability in Energy and Materials, *ChemSusChem*, 2024, **17**(5), e202301367, DOI: 10.1002/cssc.202301367.
10 J. Huang, K. Yuan and Y. Chen, Wide Voltage Aqueous Asymmetric Supercapacitors: Advances, Strategies, and Challenges, *Adv. Funct. Mater.*, 2022, **32**(4), 2108107, DOI: 10.1002/adfm.202108107.
11 D. Majumdar, Recent progress in copper sulfide based nanomaterials for high energy supercapacitor applications, *J. Electroanal. Chem.*, 2021, **880**, 114825, DOI: 10.1016/j.jelechem.2020.114825.
12 J. Sun, B. Luo and H. Li, A Review on the Conventional Capacitors, Supercapacitors, and Emerging Hybrid Ion Capacitors: Past, Present, and Future, *Adv. Energy Sustainability Res.*, 2022, **3**(6), 2100191, DOI: 10.1002/aesr.202100191.
13 J. Hong, *et al.*, Chalcogenide solution-mediated activation protocol for scalable and ultrafast synthesis of single-crystalline 1-D copper sulfide for supercapacitors, *J. Mater. Chem. A*, 2019, **7**(6), 2529–2535, DOI: 10.1039/C8TA10743B.
14 K. Ramasamy, R. K. Gupta, S. Palchoudhury, S. Ivanov and A. Gupta, Layer-Structured Copper Antimony Chalcogenides ($CuSbSe_xS_{2-x}$): Stable Electrode Materials for Supercapacitors, *Chem. Mater.*, 2015, **27**(1), 379–386, DOI: 10.1021/cm5041166.
15 J. Theerthagiri, *et al.*, Recent Advances in Metal Chalcogenides (MX; X = S, Se) Nanostructures for Electrochemical Supercapacitor Applications: A Brief Review, *Nanomaterials*, 2018, **8**(4), 256, DOI: 10.3390/nano8040256.

16 J. Lu, *et al.*, Application of Copper–Sulfur Compound Electrode Materials in Supercapacitors, *Molecules*, 2024, **29**(5), 977, DOI: 10.3390/molecules29050977.
17 M. Ashan, *et al.*, Electrochemical investigation of CuSe nanoparticles decorated over g-CN nanosheet for supercapacitor applications, *J. Alloys Compd.*, 2025, **1016**, 178673, DOI: 10.1016/j.jallcom.2025.178673.
18 G. Wang, L. Zhang and J. Zhang, A review of electrode materials for electrochemical supercapacitors, *Chem. Soc. Rev.*, 2012, **41**(2), 797–828, DOI: 10.1039/C1CS15060J.
19 A. R. Shojaei, Electrical conductivity plus probability of superconductivity in α-CuSe/klockmannite; bulk and nano-layers, *J. Alloys Compd.*, 2015, **632**, 568–574, DOI: 10.1016/j.jallcom.2015.01.146.
20 H. Arabdashti, A. M. Zardkhoshoui, A. Sadeghi and S. S. H. Davarani, Integration of CuTe-CoTe nanosheets with NiTe2 nanoflowers for hybrid supercapacitor, *J. Alloys Compd.*, 2025, **1011**, 178427, DOI: 10.1016/j.jallcom.2024.178427.
21 L. Lin, W. Lei, S. Zhang, Y. Liu, G. G. Wallace and J. Chen, Two-dimensional transition metal dichalcogenides in supercapacitors and secondary batteries, *Energy Storage Mater.*, 2019, **19**, 408–423, DOI: 10.1016/j.ensm.2019.02.023.
22 M. Ahmad, *et al.*, Evolution of Metal Tellurides for Energy Storage/Conversion: From Synthesis to Applications, *Small*, 2024, **20**(28), 2310099, DOI: 10.1002/smll.202310099.
23 A. Jain, *et al.*, Commentary: The Materials Project: A materials genome approach to accelerating materials innovation, *APL Mater.*, 2013, **1**(1), 011002, DOI: 10.1063/1.4812323.
24 K. Momma and F. Izumi, *VESTA 3* for three-dimensional visualization of crystal, volumetric and morphology data, *J. Appl. Crystallogr.*, 2011, **44**(6), 1272–1276, DOI: 10.1107/S0021889811038970.
25 S. Faraji, B. Wang, H. O. Valencia and G. Frapper, Computational discovery of two-dimensional copper chalcogenides Cu X (X = S, Se, Te), *Phys. Rev. Mater.*, 2021, **5**(12), 124007, DOI: 10.1103/PhysRevMaterials.5.124007.
26 T. Willhammar, *et al.*, Structure and vacancy distribution in copper telluride nanoparticles influence plasmonic activity in the near-infrared, *Nat. Commun.*, 2017, **8**(1), 14925, DOI: 10.1038/ncomms14925.
27 E. H. Robinson, K. M. Dwyer, A. C. Koziel, A. Y. Nuriye and J. E. Macdonald, Synthesis of vulcanite (CuTe) and metastable Cu1.5 Te nanocrystals using a dialkyl ditelluride precursor, *Nanoscale*, 2020, **12**(45), 23036–23041, DOI: 10.1039/D0NR06910H.
28 H. Arabdashti, A. M. Zardkhoshoui, A. Sadeghi and S. S. H. Davarani, Integration of CuTe-CoTe nanosheets with NiTe2 nanoflowers for hybrid supercapacitor, *J. Alloys Compd.*, 2025, **1011**, 178427, DOI: 10.1016/j.jallcom.2024.178427.
29 R. A. D. Pattrick, *et al.*, The structure of amorphous copper sulfide precipitates: An X-ray absorption study, *Geochim. Cosmochim. Acta*, 1997, **61**(10), 2023–2036, DOI: 10.1016/S0016-7037(97)00061-6.
30 G. B. Sakr, I. S. Yahia, M. Fadel, S. S. Fouad and N. Romčević, Optical spectroscopy, optical conductivity, dielectric properties and new methods for determining the gap states of CuSe thin films, *J. Alloys Compd.*, 2010, **507**(2), 557–562, DOI: 10.1016/j.jallcom.2010.08.022.
31 N. Elgrishi, K. J. Rountree, B. D. McCarthy, E. S. Rountree, T. T. Eisenhart and J. L. Dempsey, A Practical Beginner's Guide to Cyclic Voltammetry, *J. Chem. Educ.*, 2018, **95**(2), 197–206, DOI: 10.1021/acs.jchemed.7b00361.
32 L. E. Helseth, Comparison of methods for finding the capacitance of a supercapacitor, *J. Energy Storage*, 2021, **35**, 102304, DOI: 10.1016/j.est.2021.102304.
33 M. F. Dupont, A. F. Hollenkamp and S. W. Donne, Large Amplitude Electrochemical Impedance Spectroscopy for Characterizing the Performance of Electrochemical Capacitors, *J. Electrochem. Soc.*, 2014, **161**(4), A648–A656, DOI: 10.1149/2.098404jes.
34 L. A. Santa-Cruz, *et al.*, Electrochemical impedance spectroscopy: from breakthroughs to functional utility in supercapacitors and batteries – a comprehensive assessment, *Phys. Chem. Chem. Phys.*, 2024, **26**(40), 25748–25761, DOI: 10.1039/D4CP02148G.
35 A. Morales-García, A. L. Soares, E. C. Dos Santos, H. A. De Abreu and H. A. Duarte, First-Principles Calculations and Electron Density Topological Analysis of Covellite (CuS), *J. Phys. Chem. A*, 2014, **118**(31), 5823–5831, DOI: 10.1021/jp4114706.
36 Z. Stević and M. Rajčić-Vujasinović, Chalcocite as a potential material for supercapacitors, *J. Power Sources*, 2006, **160**(2), 1511–1517, DOI: 10.1016/j.jpowsour.2006.03.014.
37 S. Shaikh and M. K. Rabinal, Rapid ambient growth of copper sulfide microstructures: Binder free electrodes for supercapacitor, *J. Energy Storage*, 2020, **28**, 101288, DOI: 10.1016/j.est.2020.101288.
38 P. Kumar and R. Nagarajan, An Elegant Room Temperature Procedure for the Precise Control of Composition in the Cu–S System, *Inorg. Chem.*, 2011, **50**(19), 9204–9206, DOI: 10.1021/ic201133a.
39 Y. Gu, *et al.*, Copper sulfide nanostructures and their sodium storage properties, *CrystEngComm*, 2020, **22**(42), 7082–7089, DOI: 10.1039/D0CE01059F.
40 L.-W. Wang, High Chalcocite Cu 2 S : A Solid-Liquid Hybrid Phase, *Phys. Rev. Lett.*, 2012, **108**(8), 085703, DOI: 10.1103/PhysRevLett.108.085703.
41 M. Goswami, *et al.*, Morphology Variations in Copper Sulfide Nanostructures as Anode Materials for Na-Ion Capacitors, *ACS Appl. Nano Mater.*, 2023, **6**(17), 15498–15509, DOI: 10.1021/acsanm.3c02131.
42 Y. Liu, Z. Zhou, S. Zhang, W. Luo and G. Zhang, Controllable synthesis of CuS hollow microflowers hierarchical structures for asymmetric supercapacitors, *Appl. Surf. Sci.*, 2018, **442**, 711–719, DOI: 10.1016/j.apsusc.2018.02.220.

43 W. J. Kim, S. Cho, J. Hong and J. P. Hong, Hierarchically nanostructured 1D-2D flowerlike copper sulfide electrode for high-performance supercapacitor application by one-pot synthetic procedure, *Appl. Surf. Sci.*, 2022, **578**, 152086, DOI: 10.1016/j.apsusc.2021.152086.

44 H. Heydari, S. E. Moosavifard, S. Elyasi and M. Shahraki, Nanoporous CuS nano-hollow spheres as advanced material for high-performance supercapacitors, *Appl. Surf. Sci.*, 2017, **394**, 425–430, DOI: 10.1016/j.apsusc.2016.10.138.

45 H. Heydari, S. E. Moosavifard, M. Shahraki and S. Elyasi, Facile synthesis of nanoporous CuS nanospheres for high-performance supercapacitor electrodes, *J. Energy Chem.*, 2017, **26**(4), 762–767, DOI: 10.1016/j.jechem.2017.03.007.

46 J. Guo, X. Zhang, Y. Sun, X. Zhang, L. Tang and X. Zhang, Double-shell CuS nanocages as advanced supercapacitor electrode materials, *J. Power Sources*, 2017, **355**, 31–35, DOI: 10.1016/j.jpowsour.2017.04.052.

47 K.-J. Huang, J.-Z. Zhang and Y. Fan, One-step solvothermal synthesis of different morphologies CuS nanosheets compared as supercapacitor electrode materials, *J. Alloys Compd.*, 2015, **625**, 158–163, DOI: 10.1016/j.jallcom.2014.11.137.

48 J. Zhang, *et al.*, Solvothermal Synthesis of Three-Dimensional Hierarchical CuS Microspheres from a Cu-Based Ionic Liquid Precursor for High-Performance Asymmetric Supercapacitors, *ACS Appl. Mater. Interfaces*, 2015, **7**(39), 21735–21744, DOI: 10.1021/acsami.5b04452.

49 C. Justin Raj, B. C. Kim, W.-J. Cho, W.-G. Lee, Y. Seo and K.-H. Yu, Electrochemical capacitor behavior of copper sulfide (CuS) nanoplatelets, *J. Alloys Compd.*, 2014, **586**, 191–196, DOI: 10.1016/j.jallcom.2013.10.056.

50 M. Goswami, *et al.*, Self-supported, additive-, and binder-free CuS nanowire array for high performing Na-ion capacitor, *J. Energy Storage*, 2023, **72**, 108546, DOI: 10.1016/j.est.2023.108546.

51 K. Samdhyan, P. Chand and H. Anand, Fabrication of high-performance asymmetric supercapacitor device based on CuS with marigold flower like framework, *J. Energy Storage*, 2025, **106**, 114719, DOI: 10.1016/j.est.2024.114719.

52 B. Qasim, *et al.*, Effect of Ni dopant on the capacitive behavior of CuS for supercapacitor application, *J. Mater. Sci.:Mater. Electron.*, 2024, **35**(6), 445, DOI: 10.1007/s10854-024-12235-x.

53 J. W. Brown, P. S. Ramesh and D. Geetha, Fabrication of mesoporous iron (Fe) doped copper sulfide (CuS) nanocomposite in the presence of a cationic surfactant via mild hydrothermal method for supercapacitors, *Mater. Res. Express*, 2018, **5**(2), 024007, DOI: 10.1088/2053-1591/aaad55.

54 K. Jeyabanu, P. Devendran, A. Manikandan, R. Packiaraj, K. Ramesh and N. Nallamuthu, Preparation and characterization studies of La doped CuS nanospheres by microwave irradiation for high performance supercapacitors, *Phys. B*, 2019, **573**, 92–101, DOI: 10.1016/j.physb.2019.08.028.

55 S. Podili, D. Geetha and P. S. Ramesh, One-pot synthesis of CTAB stabilized mesoporous cobalt doped CuS nano flower with enhanced pseudocapacitive behavior, *J. Mater. Sci.:Mater. Electron.*, 2017, **28**(20), 15387–15397, DOI: 10.1007/s10854-017-7424-2.

56 S. Podili, D. Geetha and P. S. Ramesh, Electrochemical studies on Ni doped CuS nanostructures with cationic surfactant synthesized through a hydrothermal route, *J. Mater. Sci.:Mater. Electron.*, 2018, **29**(13), 11167–11177, DOI: 10.1007/s10854-018-9202-1.

57 S. Podili, D. Geetha and P. S. Ramesh, Tuning the dopant (Zn2+) composition for uniform mesoporous Zn–CuS nanoflower via hydrothermal approach as a novel electrode material for high-rate supercapacitor, *SN Appl. Sci.*, 2020, **2**(6), 1023, DOI: 10.1007/s42452-020-2668-5.

58 A. C. Lokhande, *et al.*, Binder-free novel Cu4SnS4 electrode for high-performance supercapacitors, *Electrochim. Acta*, 2018, **284**, 80–88, DOI: 10.1016/j.electacta.2018.07.170.

59 V. K. Mariappan, K. Krishnamoorthy, P. Pazhamalai, S. Sahoo, S. S. Nardekar and S.-J. Kim, Nanostructured ternary metal chalcogenide-based binder-free electrodes for high energy density asymmetric supercapacitors, *Nano Energy*, 2019, **57**, 307–316, DOI: 10.1016/j.nanoen.2018.12.031.

60 P. Pazhamalai, K. Krishnamoorthy, S. Sahoo, V. K. Mariappan and S.-J. Kim, Copper tungsten sulfide anchored on Ni-foam as a high-performance binder free negative electrode for asymmetric supercapacitor, *Chem. Eng. J.*, 2019, **359**, 409–418, DOI: 10.1016/j.cej.2018.11.153.

61 L.-Q. Fan, *et al.*, Synthesis of CuCo2S4 nanosheet arrays on Ni foam as binder-free electrode for asymmetric supercapacitor, *Int. J. Hydrogen Energy*, 2018, **43**(52), 23372–23381, DOI: 10.1016/j.ijhydene.2018.10.190.

62 S. Sahoo, P. Pazhamalai, V. K. Mariappan, G. K. Veerasubramani, N.-J. Kim and S.-J. Kim, Hydrothermally synthesized chalcopyrite platelets as an electrode material for symmetric supercapacitors, *Inorg. Chem. Front.*, 2020, **7**(7), 1492–1502, DOI: 10.1039/C9QI01335K.

63 L. Rani and J. I. Han, Fabrication of CuS/Cu2S nanoparticles integrated with multi-walled carbon nanotubes for advanced energy storage applications, *J. Energy Storage*, 2024, **82**, 110533, DOI: 10.1016/j.est.2024.110533.

64 K. Jin, *et al.*, Electrodeposited CuS nanosheets on carbonized cotton fabric as flexible supercapacitor electrode for high energy storage, *Electrochim. Acta*, 2019, **295**, 668–676, DOI: 10.1016/j.electacta.2018.10.182.

65 Y. Lu, *et al.*, Hierarchical, porous CuS microspheres integrated with carbon nanotubes for high-performance supercapacitors, *Sci. Rep.*, 2015, **5**(1), 16584, DOI: 10.1038/srep16584.

66 S. Ravi, C. V. V. M. Gopi and H. J. Kim, Enhanced electrochemical capacitance of polyimidazole coated covellite CuS dispersed CNT composite materials for application in supercapacitors, *Dalton Trans.*, 2016, **45**(31), 12362–12371, DOI: 10.1039/C6DT01664B.

67 Z. Pan, F. Cao, X. Hu and X. Ji, A facile method for synthesizing CuS decorated Ti3 C2 MXene with enhanced

performance for asymmetric supercapacitors, *J. Mater. Chem. A*, 2019, 7(15), 8984–8992, DOI: 10.1039/C9TA00085B.

68 K. Ghosh and S. K. Srivastava, Enhanced Supercapacitor Performance and Electromagnetic Interference Shielding Effectiveness of CuS Quantum Dots Grown on Reduced Graphene Oxide Sheets, *ACS Omega*, 2021, **6**(7), 4582–4596, DOI: 10.1021/acsomega.0c05034.

69 C. Behera, R. Samal, A. K. Panda, C. S. Rout and S. L. Samal, Synthesis of flower and biconcave shape CuS: Enhancement of super-capacitance properties via Ni–CuS nanocomposite formation, *Solid State Sci.*, 2021, **117**, 106631, DOI: 10.1016/j.solidstatesciences.2021.106631.

70 J. Lu, *et al.*, Three-Dimensional Crosslinked Nanosheet/Nanoparticle Composite CuS Electrode for Supercapacitors, *ACS Appl. Nano Mater.*, 2024, **7**(19), 22474–22486, DOI: 10.1021/acsanm.4c01890.

71 P. Himasree, *et al.*, One-step hydrothermal synthesis of CuS@MnS on Ni foam for high performance supercapacitor electrode material, *Electrochim. Acta*, 2019, **305**, 467–473, DOI: 10.1016/j.electacta.2019.03.041.

72 K. V. G. Raghavendra, K. M. Rao and N. T. U. Kumar, Hydrothermal synthesis of CuS/CoS nano composite as an efficient electrode for the supercapattery applications, *J. Energy Storage*, 2021, **40**, 102749, DOI: 10.1016/j.est.2021.102749.

73 A. C. Lokhande, *et al.*, Chalcopyrite based carbon composite electrodes for high performance symmetric supercapacitor, *Chem. Eng. J.*, 2020, **399**, 125711, DOI: 10.1016/j.cej.2020.125711.

74 T. N. Amirabad and A. A. Ensafi, Spherical CuFeS2 @FeSe2 structure as a binder-free electrode and its performance in asymmetric supercapacitors, *React. Chem. Eng.*, 2024, **9**(12), 3267–3276, DOI: 10.1039/D4RE00144C.

75 E. K. Feyie, L. T. Tufa, J. Lee, A. Tadesse and E. A. Zereffa, Electrodeposited Copper Tin Sulfide/Reduced Graphene Oxide Nanospikes for a High-Performance Supercapacitor Electrode, *ACS Omega*, 2024, **9**(8), 9452–9462, DOI: 10.1021/acsomega.3c09008.

76 D. Arif, *et al.*, High-performance ZnO–CuSe nanocomposites as advanced electrode materials for energy storage applications, *J. Mater. Res. Technol.*, 2025, **37**, 1725–1736, DOI: 10.1016/j.jmrt.2025.06.137.

77 D. B. Malavekar, S. B. Kale, V. C. Lokhande, U. M. Patil, J. H. Kim and C. D. Lokhande, Chemically Synthesized Cu3 Se2 Film Based Flexible Solid-State Symmetric Supercapacitor: Effect of Reaction Bath Temperature, *J. Phys. Chem. C*, 2020, **124**(52), 28395–28406, DOI: 10.1021/acs.jpcc.0c08454.

78 H. Yu, J. Liu, X. Wu, R. Li, R. Jin and G. Zhou, Construction of mesocrystal Cu2-xSe nanoplates with high infiltration for enhanced electrochemical performance in lithium ion batteries and electrochemical supercapacitors, *Appl. Surf. Sci.*, 2024, **655**, 159530, DOI: 10.1016/j.apsusc.2024.159530.

79 P. Pazhamalai, K. Krishnamoorthy and S. J. Kim, Hierarchical copper selenide nanoneedles grown on copper foil as a binder free electrode for supercapacitors, *Int. J. Hydrogen Energy*, 2016, **41**(33), 14830–14835, DOI: 10.1016/j.ijhydene.2016.05.157.

80 S. K. Shinde, *et al.*, Electrochemical synthesis: Monoclinic Cu 2 Se nano-dendrites with high performance for supercapacitors, *J. Taiwan Inst. Chem. Eng.*, 2017, **75**, 271–279, DOI: 10.1016/j.jtice.2017.01.028.

81 C. Chen, *et al.*, A facile synthesis of CuSe nanosheets for high-performance sodium-ion hybrid capacitors, *RSC Adv.*, 2022, **12**(33), 21558–21566, DOI: 10.1039/D2RA03206F.

82 G. P. Patil, C. D. Jadhav, S. Lyssenko, A. Borenstein and R. Minnes, Exploring one-pot colloidal synthesis of klockmannite CuSe nanosheet electrode for symmetric solid-state supercapacitor device, *J. Mater. Chem. C*, 2024, **12**(36), 14404–14420, DOI: 10.1039/D4TC02727B.

83 L. Li, *et al.*, Vertically Oriented and Interpenetrating CuSe Nanosheet Films with Open Channels for Flexible All-Solid-State Supercapacitors, *ACS Omega*, 2017, **2**(3), 1089–1096, DOI: 10.1021/acsomega.6b00535.

84 M. Sajjad, *et al.*, Low-temperature synthesis of 3D copper selenide micro-flowers for high-performance supercapacitors, *Mater. Lett.*, 2022, **314**, 131857, DOI: 10.1016/j.matlet.2022.131857.

85 D. B. Malavekar, S. B. Kale, V. C. Lokhande, U. M. Patil, J. H. Kim and C. D. Lokhande, Chemically Synthesized Cu3 Se2 Film Based Flexible Solid-State Symmetric Supercapacitor: Effect of Reaction Bath Temperature, *J. Phys. Chem. C*, 2020, **124**(52), 28395–28406, DOI: 10.1021/acs.jpcc.0c08454.

86 D. B. Malavekar, M. A. Gaikwad, K. D. Patil, S. Jang, S. W. Park and J. H. Kim, Nanoarchitectonics of self-grown copper selenide on copper for solid-state asymmetric supercapacitor, *J. Energy Storage*, 2023, **68**, 107675, DOI: 10.1016/j.est.2023.107675.

87 H. N. Sumedha, J. N. Hausmann, S. Kalra, R. Viswanatha, P. W. Menezes and M. S. Santosh, Symmetric supercapacitors based on copper–antimony chalcogenides: A trade-off between S and Se, *Ceram. Int.*, 2023, **49**(2), 1756–1763, DOI: 10.1016/j.ceramint.2022.09.139.

88 A. M. Zardkhoshoui and S. S. H. Davarani, Construction of complex copper-cobalt selenide hollow structures as an attractive battery-type electrode material for hybrid supercapacitors, *Chem. Eng. J.*, 2020, **402**, 126241, DOI: 10.1016/j.cej.2020.126241.

89 B. K. Deka, *et al.*, Bimetallic copper cobalt selenide nanowire-anchored woven carbon fiber-based structural supercapacitors, *Chem. Eng. J.*, 2019, **355**, 551–559, DOI: 10.1016/j.cej.2018.08.172.

90 S. E. Moosavifard, F. Saleki, A. Mohammadi, A. Hafizi and M. R. Rahimpour, Construction of hierarchical nanoporous bimetallic copper-cobalt selenide hollow spheres for hybrid supercapacitor, *J. Electroanal. Chem.*, 2020, **871**, 114295, DOI: 10.1016/j.jelechem.2020.114295.

91 D. Khalafallah, M. Zhi and Z. Hong, Rational engineering of hierarchical mesoporous CuxFeySe battery-type electrodes for asymmetric hybrid supercapacitors, *Ceram. Int.*, 2021, **47**(20), 29081–29090, DOI: 10.1016/j.ceramint.2021.07.069.

92 M. V. Paranjape, E. G. Shankar, M. Punnarao and J. S. Yu, Enhanced electrochemical energy storage of binder-free ternary copper manganese selenide nanocomposite electrodes via polydopamine coating for quasi-solid-state hybrid supercapacitors, *J. Energy Storage*, 2025, **105**, 114801, DOI: 10.1016/j.est.2024.114801.

93 A. K. Das, E. G. Shankar, B. Ramulu and J. S. Yu, Electrodeposited CuxFe3-xSe4 nanoheterostructure arrays on carbon cloth as a binder-free faradaic negative electrode for asymmetric supercapacitors, *Composites, Part B*, 2023, **258**, 110705, DOI: 10.1016/j.compositesb.2023.110705.

94 M. Umer, *et al.*, Facile synthesis of novel Cu2 NiBiX4 (X = Se, S) chalcogenides as bifunctional electrocatalysts for oxygen evolution reaction (OER) and supercapacitive performance, *Sustainable Energy Fuels*, 2023, **7**(22), 5409–5421, DOI: 10.1039/D3SE01062G.

95 F. Tavakoli, B. Rezaei, A. R. Taghipour Jahromi and A. A. Ensafi, Facile Synthesis of Yolk-Shelled CuCo2 Se4 Microspheres as a Novel Electrode Material for Supercapacitor Application, *ACS Appl. Mater. Interfaces*, 2020, **12**(1), 418–427, DOI: 10.1021/acsami.9b12805.

96 M. Hayat, *et al.*, Exploring the electrochemical properties of CuSe-decorated NiSe2 nanocubes for battery-supercapacitor hybrid devices, *Chemosphere*, 2023, **340**, 139720, DOI: 10.1016/j.chemosphere.2023.139720.

97 M. Z. Ullah Shah, *et al.*, A novel TiO2/CuSe based nanocomposite for high-voltage asymmetric supercapacitors, *J. Sci.:Adv. Mater. Devices*, 2022, **7**(2), 100418, DOI: 10.1016/j.jsamd.2022.100418.

98 A. U. Khan, *et al.*, A new cadmium oxide (CdO) and copper selenide (CuSe) nanocomposite: An energy-efficient electrode for wide-voltage hybrid supercapacitors, *Colloids Surf., A*, 2023, **656**, 130327, DOI: 10.1016/j.colsurfa.2022.130327.

99 A. Li, M. Zhai, M. Luan and J. Hu, Mixed Cu2 Se Hexagonal Nanosheets@Co3 Se4 Nanospheres for High-Performance Asymmetric Supercapacitors, *Chem.–Eur. J.*, 2021, **27**(39), 10134–10141, DOI: 10.1002/chem.202100857.

100 T. D. Raju, A. Gopalakrishnan and S. Badhulika, Facile synthesis of 3D/2D Cu2Se cauliflower/CuS nanosheets composite as a binder-free electrode for high-performance asymmetric solid-state supercapacitors, *J. Alloys Compd.*, 2020, **845**, 156241, DOI: 10.1016/j.jallcom.2020.156241.

101 R. Ullah, *et al.*, Elucidating bimetallic CuMnSe2/MWCNTs composite as redox-active electrode material for hybrid supercapacitors, *J. Energy Storage*, 2025, **109**, 115124, DOI: 10.1016/j.est.2024.115124.

102 J.-Q. Wang, Q. Zheng, W.-Q. Cao, H.-Z. Zhai and M.-S. Cao, Heterodimensional hybrids assembled with multiple-dimensional copper selenide hollow microspheres and graphene oxide nanosheets for electromagnetic energy conversion and electrochemical energy storage, *Adv. Compos. Hybrid Mater.*, 2024, **7**(1), 14, DOI: 10.1007/s42114-023-00813-2.

103 S. A. Ahmad, *et al.*, High power aqueous hybrid asymmetric supercapacitor based on zero-dimensional ZnS nanoparticles with two-dimensional nanoflakes CuSe2 nanostructures, *Ceram. Int.*, 2023, **49**(12), 20007–20016, DOI: 10.1016/j.ceramint.2023.03.122.

104 K. Zhang, *et al.*, Synthesis and structure determination of potassium copper selenide nanowires and solid-state supercapacitor application, *J. Power Sources*, 2014, **268**, 522–532, DOI: 10.1016/j.jpowsour.2014.06.079.

105 K. K. Garlapati, A. R. Nath, A. M. Arjun, A. Vijayan and N. Sandhyarani, The rational investigation of bimetallic selenides as electrode materials for hybrid supercapacitors, *Electrochim. Acta*, 2022, **424**, 140627, DOI: 10.1016/j.electacta.2022.140627.

106 D. B. Malavekar, R. N. Bulakhe, S. B. Kale, U. M. Patil, I. In and C. D. Lokhande, Synthesis of layered copper selenide on reduced graphene oxide sheets via SILAR method for flexible asymmetric solid-state supercapacitor, *J. Alloys Compd.*, 2021, **869**, 159198, DOI: 10.1016/j.jallcom.2021.159198.

107 M. Nagaraju, B. Ramulu, S. J. Arbaz and J. S. Yu, Multiphase Cu-Ni selenide nanocomposite electrode materials for high-performance hybrid supercapacitors, *Appl. Surf. Sci.*, 2023, **622**, 156952, DOI: 10.1016/j.apsusc.2023.156952.

108 K. Karuppasamy, *et al.*, Unveiling a binary metal selenide composite of CuSe polyhedrons/CoSe2 nanorods decorated graphene oxide as an active electrode material for high-performance hybrid supercapacitors, *Chem. Eng. J.*, 2022, **427**, 131535, DOI: 10.1016/j.cej.2021.131535.

109 K. Kabra, S. Arora, K. B. Joshi and G. Sharma, DFT investigation of mechanical and vibrational properties of CuTe, *Phys. B*, 2021, **620**, 413214, DOI: 10.1016/j.physb.2021.413214.

110 J. Park, J. Seo, J.-H. Lim and B. Yoo, Synthesis of Copper Telluride Thin Films by Electrodeposition and Their Electrical and Thermoelectric Properties, *Front. Chem.*, 2022, **10**, 799305, DOI: 10.3389/fchem.2022.799305.

111 E. H. Robinson, K. M. Dwyer, A. C. Koziel, A. Y. Nuriye and J. E. Macdonald, Synthesis of vulcanite (CuTe) and metastable Cu1.5 Te nanocrystals using a dialkyl ditelluride precursor, *Nanoscale*, 2020, **12**(45), 23036–23041, DOI: 10.1039/D0NR06910H.

112 Rohit and R. K. Dutta, Hydrothermal synthesis of multifunctional Cu2Te nanoparticles as photocatalyst and as supercapacitor electrode, *Inorg. Chem. Commun.*, 2024, **166**, 112532, DOI: 10.1016/j.inoche.2024.112532.

113 G. P. Patil, C. D. Jadhav, S. Lyssenko and R. Minnes, Hydrothermally synthesized copper telluride nanoparticles: First approach to flexible solid-state symmetric supercapacitor, *Chem. Eng. J.*, 2024, **498**, 155284, DOI: 10.1016/j.cej.2024.155284.

114 S. Thangriyal, M. L. Aparna and R. R. Gangavarapu, Charge Storage Performance of Cubic Cu3 TeO6 Nanoparticles for Supercapattery Application, *ACS Appl. Nano Mater.*, 2024, **7**(16), 18420–18434, DOI: 10.1021/acsanm.3c04101.

115 P. C. Kumar, A. A. Nechikott, P. K. Nayak, D. Alagarasan and R. Naik, Superior Performance of 2D Layered Bimetallic Bismuth and Copper Oxytellurides for Supercapacitor

Applications, *ACS Appl. Energy Mater.*, 2024, **7**(19), 8478–8488, DOI: **10.1021/acsaem.4c01420**.

116 Y. Kang, H. Li, N. Lv and J. Luo, Microwave-assisted synthesis of CuxTey as an anode material for supercapacitors, *Ionics*, 2024, **30**(6), 3553–3561, DOI: **10.1007/s11581-024-05518-0**.

117 D. Dehghanpour Farashah, M. Abdollahi, A. Mohammadi Zardkhoshoui and S. S. Hosseiny Davarani, Exploring the potential of CuCoFeTe@CuCoTe yolk-shelled microrods in supercapacitor applications, *Nanoscale*, 2024, **16**(17), 8650–8660, DOI: **10.1039/D4NR00076E**.

118 H. Arabdashti, A. M. Zardkhoshoui, A. Sadeghi and S. S. H. Davarani, Integration of CuTe-CoTe nanosheets with NiTe2 nanoflowers for hybrid supercapacitor, *J. Alloys Compd.*, 2025, **1011**, 178427, DOI: **10.1016/j.jallcom.2024.178427**.

119 N. Jayababu and D. Kim, CuCo LDHs Coated CuCoTe Honeycomb-Like Nanosheets as a Novel Anode Material for Hybrid Supercapacitors, *Small*, 2021, **17**(36), 2102369, DOI: **10.1002/smll.202102369**.

120 S. Pavithra, A. Sakunthala, S. Vinofia, K. Pramoda, V. Kathirvel and R. S. Keri, Superior performance of hierarchical 3D microflower CuS grown on carbon cloth as binder free electrode for supercapacitor applications, *Mater. Res. Bull.*, 2024, **180**, 113010, DOI: **10.1016/j.materresbull.2024.113010**.

121 O. Gerard, A. Numan, S. Krishnan, M. Khalid, R. Subramaniam and R. Kasi, A review on the recent advances in binder-free electrodes for electrochemical energy storage application, *J. Energy Storage*, 2022, **50**, 104283, DOI: **10.1016/j.est.2022.104283**.

122 Y. Wu, *et al.*, Implementation of structural and surface engineering strategies to copper sulfide for enhanced sodium-ion storage, *J. Alloys Compd.*, 2022, **923**, 166308, DOI: **10.1016/j.jallcom.2022.166308**.

123 C. Xing, *et al.*, Thermoelectric Performance of Surface-Engineered Cu 1.5– *x* Te–Cu2 Se Nanocomposites, *ACS Nano*, 2023, **17**(9), 8442–8452, DOI: **10.1021/acsnano.3c00495**.

124 L. Wang, J. Wu, X. Wang and S. Fu, Defect engineering of MoS2-based materials as supercapacitors electrode: A mini review, *J. Alloys Compd.*, 2023, **959**, 170548, DOI: **10.1016/j.jallcom.2023.170548**.

125 T. Gao, *et al.*, Application of Defect Engineering via ALD in Supercapacitors, *Batteries*, 2024, **10**(12), 438, DOI: **10.3390/batteries10120438**.

126 Y. Jiang, *et al.*, Vacancy Engineering in 2D Transition Metal Chalcogenide Photocatalyst: Structure Modulation, Function and Synergy Application, *Small*, 2024, **20**(34), 2310396, DOI: **10.1002/smll.202310396**.

127 Z. Wu, Y. Zhao, W. Jin, B. Jia, J. Wang and T. Ma, Recent Progress of Vacancy Engineering for Electrochemical Energy Conversion Related Applications, *Adv. Funct. Mater.*, 2021, **31**(9), 2009070, DOI: **10.1002/adfm.202009070**.

128 T. Wang, *et al.*, Machine-learning-assisted material discovery of oxygen-rich highly porous carbon active materials for aqueous supercapacitors, *Nat. Commun.*, 2023, **14**(1), 4607, DOI: **10.1038/s41467-023-40282-1**.

129 A. Emad-Eldeen, M. A. Azim, M. Abdelsattar and A. AbdelMoety, Utilizing machine learning and deep learning for enhanced supercapacitor performance prediction, *J. Energy Storage*, 2024, **100**, 113556, DOI: **10.1016/j.est.2024.113556**.

130 K. Li, H. Du, L. Liu, H. Yang, J. Fang and D. Li, Research progress of machine learning in the field of photocatalysis applications, *J. Ind. Eng. Chem.*, 2025, S1226086X25002746, DOI: **10.1016/j.jiec.2025.04.039**.

131 N. V. Muravyev, G. Luciano, H. L. Ornaghi, R. Svoboda and S. Vyazovkin, Artificial Neural Networks for Pyrolysis, Thermal Analysis, and Thermokinetic Studies: The Status Quo, *Molecules*, 2021, **26**(12), 3727, DOI: **10.3390/molecules26123727**.

132 T. Soleimani, D. L. Ferber, G. Junqua and M. L. Ferber, An approach for modular environmental life cycle assessment of effluent treatment: Configuration of effluent treatment modules based on decision tree tailored to best available techniques, *Environ. Impact Assess. Rev.*, 2025, **112**, 107782, DOI: **10.1016/j.eiar.2024.107782**.

133 F. Bagherzadeh, M.-J. Mehrani, M. Basirifard and J. Roostaei, Comparative study on total nitrogen prediction in wastewater treatment plant and effect of various feature selection methods on machine learning algorithms performance, *J. Water Process Eng.*, 2021, **41**, 102033, DOI: **10.1016/j.jwpe.2021.102033**.

134 V. Sawant, R. Deshmukh and C. Awati, Machine learning techniques for prediction of capacitance and remaining useful life of supercapacitors: A comprehensive review, *J. Energy Chem.*, 2023, **77**, 438–451, DOI: **10.1016/j.jechem.2022.11.012**.

135 Y. Cao, *et al.*, Machine learning aided design of high performance copper-based sulfide photocathodes, *J. Mater. Chem. A*, 2024, **12**(47), 33125–33132, DOI: **10.1039/D4TA06128D**.

136 S. A. Tawfik and S. P. Russo, Naturally-meaningful and efficient descriptors: machine learning of material properties based on robust one-shot ab initio descriptors, *J. Cheminf.*, 2022, **14**(1), 78, DOI: **10.1186/s13321-022-00658-9**.

137 W. Ye, C. Chen, S. Dwaraknath, A. Jain, S. P. Ong and K. A. Persson, Harnessing the Materials Project for machine-learning and accelerated discovery, *MRS Bull.*, 2018, **43**(9), 664–669, DOI: **10.1557/mrs.2018.202**.

138 H. Adamu, S. I. Abba, P. B. Anyin, Y. Sani and M. Qamar, Artificial intelligence-navigated development of high-performance electrochemical energy storage systems through feature engineering of multiple descriptor families of materials, *Energy Adv.*, 2023, **2**(5), 615–645, DOI: **10.1039/D3YA00104K**.

139 T. Marimuthu, N. Anandhan, R. Panneerselvam, K. P. Ganesan and A. A. Roselin, Synthesis and characterization of copper sulfide thin films for quantum dot sensitized solar cell and supercapacitor applications, *Nano-Struct. Nano-Objects*, 2019, **17**, 138–147, DOI: **10.1016/j.nanoso.2018.12.004**.